Studies on modulators of platelet (hem)ITAM signaling and platelet production in genetically modified mice

• • •

Untersuchungen an Modulatoren des thrombozytären (hem)ITAM-Signalwegs und der Thrombozytenbildung in genetisch veränderten Mäusen

Doctoral thesis for a doctoral degree
at the Graduate School of Life Sciences,
Julius-Maximilians-Universität Würzburg,
Section Biomedicine

submitted by

Deya Cherpokova

from Plovdiv, Bulgaria

Würzburg, 2015

Submitted on: _____

Office stamp

Members of the *Promotionskomitee*:

Chairperson: **Prof. Dr. Thomas Dandekar**

Primary Supervisor: **Prof. Dr. Bernhard Nieswandt**

Supervisor (Second):   **Prof. Dr. Alma Zernecke-Madsen**

Supervisor (Third):   **Prof. Dr. Georg Krohne**

Date of Public Defense: _____

Date of Receipt of Certificates: _____

Table of contents

Summary

Platelet activation and aggregation at sites of vascular injury is critical to prevent excessive blood loss, but may also lead to life-threatening ischemic disease states, such as myocardial infarction and stroke. *Glycoprotein* (GP) VI and *C-type lectin-like receptor 2* (CLEC-2) are essential platelet activating receptors in hemostasis and thrombo-inflammatory disease which signal through a (hem)*immunoreceptor tyrosine-based activation motif* (ITAM)-dependent pathway. The adapter molecules *Src-like adapter protein* (SLAP) and SLAP2 are involved in the regulation of immune cell receptor surface expression and signaling, but their function in platelets is unknown. As revealed in this thesis, single deficiency of SLAP or SLAP2 in mice had only moderate effects on platelet function, while SLAP/SLAP2 double deficiency resulted in markedly increased signal transduction, integrin activation, granule release, aggregation, procoagulant activity and thrombin generation following (hem)ITAM-coupled, but not G protein-coupled receptor activation. $Slap^{-/-}/Slap2^{-/-}$ mice displayed accelerated occlusive arterial thrombus formation and a dramatically worsened outcome after focal cerebral ischemia. These results establish SLAP and SLAP2 as critical inhibitors of platelet (hem)ITAM signaling in the setting of arterial thrombosis and ischemic stroke.

GPVI has emerged as a promising novel pharmacological target for treatment of thrombotic and inflammatory disease states, but the exact mechanisms of its immunodepletion *in vivo* are incompletely understood. It was hypothesized that SLAP and SLAP2 may be involved in the control of GPVI down-regulation because of their role in the internalization of immune cell receptors. As demonstrated in the second part of the thesis, SLAP and SLAP2 were dispensable for antibody-induced GPVI down-regulation, but anti-GPVI treatment resulted in prolonged strong thrombocytopenia in $Slap^{-/-}/Slap2^{-/-}$ mice. The profound thrombocytopenia likely resulted from the powerful platelet activation which the anti-GPVI antibody induced in $Slap^{-/-}/Slap2^{-/-}$ platelets, but importantly, not in wild-type platelets. These data indicate that the expression and activation state of key modulators of the GPVI signaling cascade may have important implications for the safety profile and efficacy of anti-GPVI agents.

Small GTPases of the Rho family, such as RhoA and Cdc42, are critically involved in the regulation of cytoskeletal rearrangements during platelet activation, but little is known about the specific roles and functional redundancy of both proteins in platelet biogenesis. As shown in the final part of the thesis, combined deficiency of RhoA and Cdc42 led to marked alterations in megakaryocyte morphology and the generation of platelets of heterogeneous size and granule content. Despite severe hemostatic defects and profound thrombo-cytopenia, circulating $RhoA^{-/-}/Cdc42^{-/-}$ platelets were still capable of granule secretion and the formation of occlusive thrombi. These results implicate the existence of both distinct and overlapping roles of RhoA and Cdc42 in platelet production and function.

Zusammenfassung

Die Aktivierung und Aggregation von Thrombozyten nach einer Gefäßverletzung ist entscheidend, um einen starken Blutverlust zu vermeiden. Diese Prozesse können aber auch zu lebensbedrohlichen ischämischen Erkrankungen führen, wie beispielsweise Myokardinfarkt und Schlaganfall. Die aktivatorischen Thrombozytenrezeptoren Glykoprotein (GP) VI und *C-type lectin-like receptor 2* (CLEC-2) spielen eine wichtige Rolle im Prozess der Hämostase und Thrombo-Inflammation. Die Aktivierung beider Rezeptoren leitet eine (hem)*immunoreceptor tyrosine-based activation motif* (ITAM)-abhängige Signalkaskade ein. Die Adapterproteine *Src-like adapter protein* (SLAP) und SLAP2 sind an der Regulation der Oberflächenexpression von Immunzellrezeptoren und der Steuerung nachgeschalteter Signalwege beteiligt, aber ihre Funktion in Thrombozyten ist unbekannt. In dieser Arbeit wurde gezeigt, dass die Einzeldefizienz von SLAP oder SLAP2 in Mäusen einen milden Effekt auf die Thrombozytenfunktion hatte. Hingegen führte das Fehlen beider Proteine zu deutlich verstärkter Signaltransduktion, Integrinaktivierung, Freisetzung von Granula, Aggregation, prokoagulatorischer Aktivität und Thrombingenerierung nach (hem)ITAM-abhängiger, aber nicht G-Protein-gekoppelter Rezeptoraktivierung. Die SLAP/SLAP2-Doppeldefizienz ging mit beschleunigter Bildung okklusiver arterieller Thromben und dramatisch verschlechtertem Zustand nach fokaler zerebraler Ischämie einher. Diese Ergebnisse etablieren SLAP und SLAP2 als essentielle Inhibitoren des (hem)ITAM-Signalwegs in arterieller Thrombose und im ischämischen Schlaganfall.

GPVI wird zunehmend als vielversprechender neuer pharmakologischer Angriffspunkt für die Behandlung von thrombotischen und entzündlichen Erkrankungen betrachtet. Die genauen Mechanismen der Herabregulierung von GPVI nach Antikörper-Gabe *in vivo* sind jedoch unvollständig aufgeklärt. Im Hinblick auf die Rolle von SLAP und SLAP2 in der Internalisierung von Immunzellrezeptoren wurde die Hypothese aufgestellt, dass beide Adapterproteine entscheidend an der Herabregulierung von GPVI beteiligt sein könnten. Im zweiten Teil dieser Dissertation wurde aber gezeigt, dass SLAP und SLAP2 nicht erforderlich sind für die Depletion von GPVI. Dagegen ging die Antikörper-induzierte Herabregulierung von GPVI mit lang anhaltender starker Thrombozytopenie in *Slap$^{-/-}$/Slap2$^{-/-}$* Mäusen einher. Der anti-GPVI-Antikörper induzierte eine starke Aktivierung von *Slap$^{-/-}$/Slap2$^{-/-}$* Thrombo-zyten, nicht aber von Wildtypthrombozyten, was eine mögliche Erklärung für die schwere Thrombozytopenie lieferte. Diese Ergebnisse weisen darauf hin, dass die Expression und der Aktivierungszustand von Molekülen, die die Feinregulierung der GPVI-Signalkaskade steuern, wichtige Auswirkungen auf das Sicherheitsprofil und die Wirksamkeit von an GPVI angreifenden Substanzen haben könnten.

Kleine GTPasen der Rho-Proteinfamilie, wie z.B. RhoA und Cdc42, sind maßgeblich an der Regulation von Umstrukturierungen des Zytoskeletts während der Aktivierung von Thrombozyten beteiligt. Dennoch ist wenig über spezifische und überlappende Funktionen von RhoA und Cdc42 während der Thrombozyten-Biogenese bekannt. Der letzte Teil der Arbeit befasste sich mit den Auswirkungen einer Doppeldefizienz von RhoA und Cdc42 in Megakaryozyten. Das Fehlen beider Proteine führte zu einer dramatisch veränderten Megakaryozytenmorphologie und zur Produktion von Thrombozyten heterogener Größe und Granulainhaltes. Trotz markanter Thrombozytopenie und stark beeinträchtigter Hämostase in den *RhoA$^{-/-}$/Cdc42$^{-/-}$* Mäusen waren zirkulierende Thrombozyten in der Lage, ihre Granula freizusetzen, und die Bildung okklusiver Thromben war weitestgehend unverändert. Diese Ergebnisse implizieren, dass RhoA und Cdc42 sowohl unterschiedliche als auch überlappende Rollen in der Produktion und Funktion von Thrombozyten spielen.

1. Introduction

Platelets are small anucleate discoid-shaped blood cells with a diameter of 3-4 μm in humans and 1-2 μm in mice. Platelets are constantly produced by their bone-marrow resident precursors, the *megakaryocytes* (MKs), to maintain a normal range of circulating platelets (150 x 10^3 – 400 x 10^3 platelets/μl in humans and ~1000 x 10^3 platelets/μl in mice). The life span of platelets is restricted to 10 days in humans and up to 5 days in mice. Aged, dysfunctional or pre-activated platelets are cleared from the circulation by resident macrophages in the spleen and liver.[1] Most of the circulating platelets never undergo adhesion before they are removed from the circulation. However, upon damage to the vessel wall, platelets come into contact with components of the exposed *extracellular matrix* (ECM) which induces their activation, adhesion and aggregation followed by the formation of a thrombus that seals vessels lesions, minimizes blood loss and prevents infection. In pathological conditions, however, uncontrolled thrombus formation can occur that may lead to acute ischemic disease states, such as myocardial infarction and stroke, which currently represent the leading causes of death and permanent disability worldwide.[2] Therefore, platelet activation needs to be tightly regulated by a complex interplay between activating and inhibitory mechanisms in platelets that ensure controlled spatial and temporal responses.

1.1. Platelet activation and thrombus formation

Besides their essential role in primary hemostasis and thrombus formation, platelets are critically involved in several other (patho)physiological processes, including lymphatic development, cancer metastasis, wound healing, angiogenesis and maintenance of the vascular integrity during inflammation. These distinct functions arise from the diverse cargo present in platelet granules. Platelets contain different types of granules, including lysosomes, α-, dense and the recently described t-granules.[3,4] Lysosomes store enzymes necessary for the degradation of proteins, carbohydrates and lipids. Dense granules contain many inorganic substances, including adenine nucleotides, polyphosphates, bioactive amines and Ca^{2+}. α-granules are the most abundant platelet granules. They store adhesion proteins (most notably fibrinogen, P-selectin, *von Willebrand factor* (VWF)), coagulation factors, growth factors and chemokines (e.g. *platelet factor* (PF) 4). In addition, platelets contain a surface-connected or *open canalicular system* (OCS) which provides a membrane source for surface area increase following platelet activation and shape change, a dense tubular system derived from residual endoplasmatic reticulum, mitochondria, peroxisomes,

glycogen stores, an actin-based cytoskeletal network and a peripheral band of microtubule coils.[5]

At sites of vascular injury, several subendothelial matrix components or proteins adsorbed onto exposed tissue, including VWF, fibrillar collagens, fibronectin and laminin, come into contact with the flowing blood which initiates platelet adhesion and activation, eventually leading to thrombus formation, a process which can be subdivided into three major steps: (1) initial contact to the exposed ECM (tethering); (2) cellular activation and release of second-wave mediators; (3) firm adhesion to the ECM and thrombus growth (Figure 1).[6] The initial capture of circulating platelets to exposed components of the ECM at sites of vascular injury is mediated by the interaction of the *glycoprotein* (GP) Ib-V-IX receptor complex with VWF immobilized on collagen.[7] GPIbα-VWF interactions are essential for initial platelet tethering under conditions of high shear flow (> 500 s^{-1}), found e.g. in arterioles or stenotic arteries, but cannot mediate firm adhesion to the ECM and lead instead to rapid deceleration of circulating platelets.[7] Platelet adhesion and aggregation exclusively depend on GPIb-VWF interactions at very high shear rates (> 10,000 s^{-1}).[8-10] Platelet deceleration enables the binding of collagen to GPVI, the central activating platelet collagen receptor.[11] GPVI-collagen interactions initiate a powerful intracellular signaling cascade characterized by a rise in cytosolic Ca^{2+} concentration, surface exposure of negatively charged procoagulant *phosphatidylserine* (PS), cytoskeletal rearrangements, mobilization of α- and dense granules and subsequent release of secondary platelet agonists, including *adenosine diphosphate* (ADP) and *thromboxane A_2* (TxA$_2$).[12,13] Concomitantly, exposed *tissue factor* (TF) triggers thrombin generation that is further enhanced by PS exposure on the platelet surface which provides high-affinity binding sites for coagulation factors and serves as a membrane substrate for the tenase and prothrombinase complexes.[14] In addition, thrombin generation is supported by the release of negatively charged inorganic *polyphosphates* (PolyP) from dense granules that potently activate coagulation *factor* XII (FXII, Hageman factor) – the starting point of the intrinsic coagulation pathway.[15] ADP, TxA$_2$ and locally generated thrombin act in an autocrine and paracrine manner on *G protein-coupled receptors* (GPCRs) and thus reinforce cellular activation and recruit additional circulating platelets to the growing thrombus. Finally, the extra- and intracellular signaling events induce the conformational change of integrin adhesion receptors, most notably αIIbβ3 (GPIIb/IIIa), from a low to a high affinity state, thereby mediating firm platelet adhesion, aggregation and thrombus growth.[6] Besides αIIbβ3, platelets also express the integrins αVβ3, α2β1, α5β1 and α6β1.[16] Integrin αIIbβ3 binding to fibrinogen enables bridging of adjacent cells and thus essentially contributes to thrombus stabilization. In addition, integrin αIIbβ3 plays an important role for firm platelet adhesion to the ECM by binding to a plethora

of ligands, including fibronectin, VWF, thrombospondin and vitronectin, which is further supported by binding of β1-integrins to collagen, laminin and fibronectin.[17]
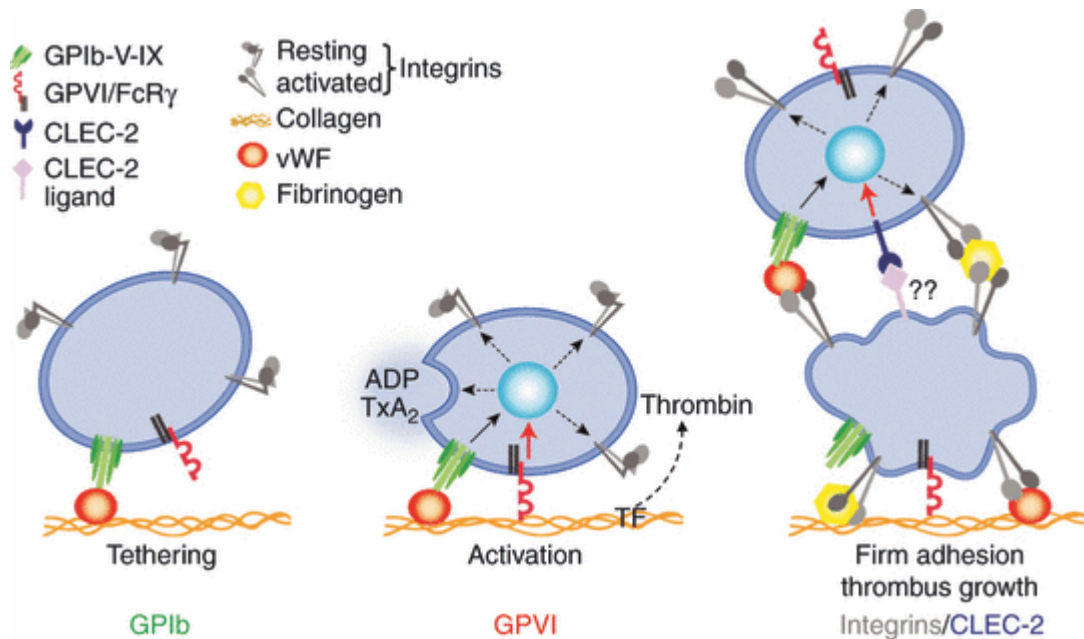
Figure 1. Model of platelet adhesion to the ECM and subsequent thrombus formation. At sites of vascular injury, initial contact (tethering) of platelets with components of the ECM predominantly depends on the interaction between GPIb and VWF. In the next step, GPVI-collagen interactions trigger cellular activation and conversion of integrins to a high-affinity state. Second-wave mediators (such as ADP and TxA$_2$) are released. Tissue factor triggers thrombin generation which also induces cellular activation. Finally, activated platelet integrins facilitate firm platelet adhesion to the ECM. Enhanced release of soluble second-wave agonists amplifies integrin activation on adherent platelets and sustains thrombus growth. ADP, *adenosine diphosphate*; TxA$_2$, *thromboxane A$_2$*, VWF, *von Willebrand factor*; TF, *tissue factor*; GPRC, *G protein-coupled receptors*, CLEC-2: *C-type lectin-like type II*. Taken from: Nieswandt *et al.*, 2011.[12]

Platelet activation can occur through two major pathways, depending on the initial stimulus (Figure 2). As mentioned above, soluble agonists, such as ADP, TxA$_2$ and thrombin, operate via receptors that couple to heterotrimeric G proteins (G$_q$, G$_{12/13}$, G$_i$).[18] The second major route leading to powerful cellular activation involves engagement of (hem)*immunoreceptor tyrosine-based activation motif* (ITAM)-bearing receptors and is introduced in detail in Section 1.2. Both signaling pathways culminate in the activation of *phospholipase C* (PLC) isoforms, leading to hydrolysis of *phosphatidyl-inositol-4,5-bisphosphate* (PIP$_2$) to *inositol-3,4,5-trisphosphate* (IP$_3$) and *diacyl glycerol* (DAG) which results in elevation of cytosolic Ca^{2+} concentration, integrin activation, platelet shape change, aggregation and secretion.
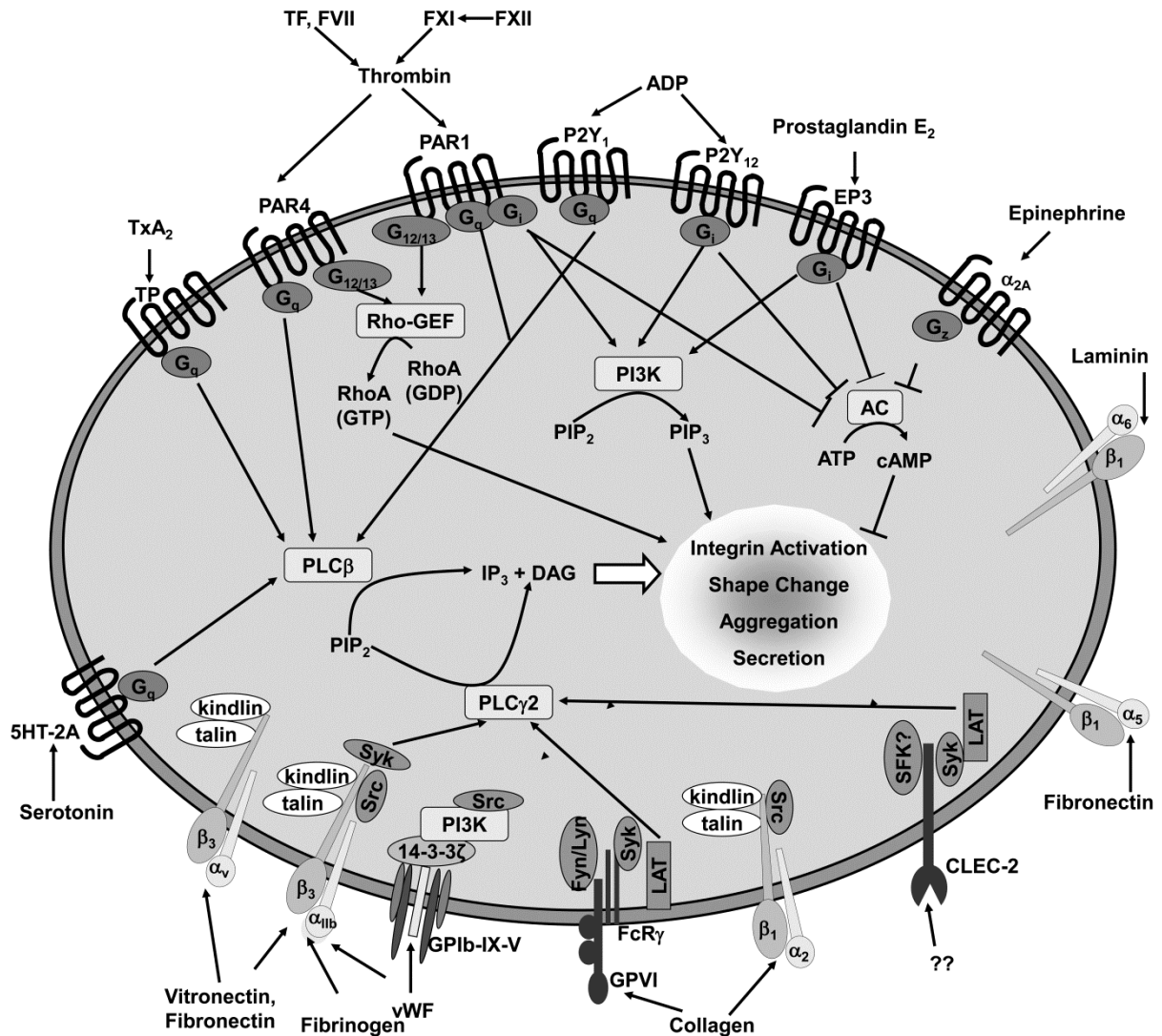
Figure 2. Major signaling pathways in platelets. Soluble agonists, including ADP, TxA_2 and thrombin, mediate effects via receptors that couple to heterotrimeric G proteins (G_q, $G_{12/13}$, G_i) and activate downstream effectors. Adhesion receptors, such as GPVI, CLEC-2 and active integrins, induce PLCγ2 activation upon ligand binding. Both signaling pathways culminate in integrin activation, platelet shape change, aggregation and secretion. PI3K, *phosphatidylinositol-3-kinase*; PIP_2, *phosphatidylinositol-4,5-bisphosphate*; PIP_3, *phosphatidylinositol-3,4,5-trisphosphate*; IP3, *inositol-3,4,5-trisphosphate*; AC, *adenylyl cyclase*; DAG, *diacylglycerol*; PLC, *phospholipase C*; CLEC-2: *C-type lectin-like type II*; PAR, *protease-activated receptor*; ADP, *adenosine diphosphate*; GDP, *guanosine diphosphate*; GTP, *guanosine triphosphate*; GEF, *guanine nucleotide exchange factor*; RhoA, *Ras homolog gene family, member A*; Fg, *fibrinogen*; TF, *tissue factor*; TxA_2, *thromboxane A_2*; VWF, *von Willebrand factor*; LAT, *linker for activation of T cells*; Syk, *spleen tyrosine kinase*; SFK, *Src family kinase*. Taken from: Stegner and Nieswandt, 2010.[19]

1.2. (Hem)ITAM signaling in platelets

An ITAM represents a highly conserved sequence defined by the presence of 2 Yxx(L/I) motifs separated by 6-12 amino acids which can be found in the cytosolic chain of several hematopoietic immunoglobulin receptors, including *Fc receptors* (FcR), *T and B cell receptors* (TCR, BCR) and C-type lectin-like receptors.[20] Ligand-induced receptor activation

initiates the phosphorylation of both tyrosine residues in the ITAM which in turn serves as a starting point for a signaling cascade that consists of a number of kinases, adapter proteins and effector molecules. Human platelets express three ITAM-bearing receptors: GPVI, FcγRIIA and the hemITAM receptor *C-type lectin-like receptor 2* (CLEC-2). Platelet activation through FcγRIIA has important implications in the pathogenesis of several diseases related to immune-mediated thrombocytopenia and thrombosis syndromes. However, mouse platelets lack FcγRIIA. Since the receptor signals through a similar pathway as GPVI, specifically GPVI signaling will be discussed in further detail in the following section.

1.2.1. GPVI

The central activating collagen receptor GPVI is a 62 kDa MK-/platelet-specific type I transmembrane protein that belongs to the Ig superfamily of surface receptors.[21] GPVI is non-covalently associated with the disulphide-linked homodimeric FcRγ-chain through a salt bridge. Each FcRγ-chain contains one copy of a classical ITAM which thereby serves as the signal transducing subunit of the GPVI/FcRγ receptor complex.[11] The FcRγ-chain is indispensable for both GPVI expression and the initiation of downstream signaling.[22] GPVI is expressed at approximately 4000-6000 copies per platelet partially in a monomeric and dimeric form;[23] the latter binds collagen with high affinity.[24] The cytosolic tail of GPVI contains a calmodulin binding motif and a *proline-rich region* (PRR) that is recognized by the *Src homology* 3 (SH3) domain of the *Src family tyrosine kinases* (SFK) Fyn and Lyn.[25,26]

Ligand-induced crosslinking of GPVI leads to phosphorylation of the two tyrosine residues within the ITAM on the FcRγ-chain predominantly by the SFK Lyn.[27,28] Phosphorylation of the FcRγ-chain ITAM is followed by the recruitment, phosphorylation and activation of the SH2 domain-containing *spleen tyrosine kinase* (Syk) which initiates a downstream signaling cascade composed of a series of adapter proteins, including *linker for activation of T cells* (LAT) and *SH2-containing leukocyte protein 76* (SLP-76), that ultimately results in the activation of effector enzymes, including *phosphoinositol* (PI)-3-kinases and PLCγ2 (Figure 3).[29]

GPVI has emerged as an attractive potential target for antithrombotic therapy, as its deficiency, blockade or antibody-induced depletion provides powerful protection from experimental arterial thrombosis without affecting platelet hemostatic functions.[13,30] Similarly, patients with a congenital GPVI deficiency or autoantibody-induced receptor loss suffer from only a mild bleeding disorder, while platelet aggregation following stimulation with collagen is abolished.[13,31] Besides its crucial role in occlusive arterial thrombosis in different animal models, GPVI has been identified as a critical modulator of several (experimental) thrombo-

inflammatory disease states, including ischemic stroke,[32] loss of vascular integrity at sites of inflammation,[33] rheumatoid arthritis,[34] glomerulonephritis[35] and atheroprogression.[36,37]
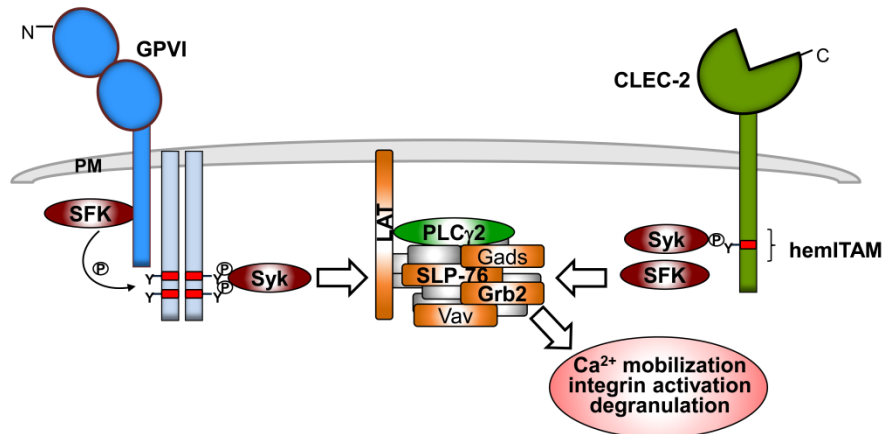
Figure 3. (hem)ITAM signaling in platelets. The type I transmembrane protein GPVI is non-covalently associated with the ITAM-bearing FcRγ-chain. Ligand binding induces phosphorylation of the ITAM by SFKs, followed by the recruitment and activation of Syk. Syk phosphorylation triggers a downstream signaling cascade that consists of kinases, adapter and effector molecules. This pathway culminates in the activation of PLCγ2. The *C-type lectin-like type II* (CLEC-2) contains a single YXXL sequence (hemITAM) in its cytoplasmic tail which is phosphorylated by Syk. Following hemITAM phosphorylation, SFKs and Syk cooperatively modulate a signaling cascade similar to that found downstream of GPVI. SFK, *Src family kinase*; Syk, *spleen tyrosine kinase*; LAT, *linker for activation of T cells*; Grb2, *growth factor receptor-bound protein 2*; Gads, *Grb2-related adapter downstream of Shc*; SLP-76, *SH2-containing leukocyte protein 76*; PLCγ2, *phospholipase C γ2*; PM, *plasma membrane*. Taken from: Stegner *et al.*, 2014.[38]

Current GPVI targeting strategies under development focus on three different approaches. They include blockade of the GPVI-collagen interaction, immunodepletion of GPVI via monoclonal antibodies and interference with key signaling molecules downstream of GPVI, such as the tyrosine kinase Syk.[38] Immunodepletion by monoclonal anti-GPVI antibodies (JAQ1-3) induces specific and irreversible removal of the receptor from the surface of murine platelets, resulting in a GPVI-knockout-like phenotype for at least two weeks which is accompanied only by a short thrombocytopenia.[39,40] The process of antibody-induced GPVI down-regulation *in vivo* is still incompletely understood, but ectodomain shedding by members of the *a disintegrin and metalloproteinase* (ADAM) family and internalization/degradation seem to be the principal mechanisms involved in irreversible removal of GPVI from the surface of circulating platelets.[39,41,42] Both pathways involved in targeted GPVI down-regulation require functional signaling through the ITAM in the FcRγ-chain, but downstream signaling events likely diverge.[41,43]

Despite compelling experimental evidence which documents the potential of GPVI as a promising antithrombotic and anti-inflammatory target, the safety profile of an anti-GPVI therapy has to be carefully assessed. For instance, GPVI immunodepletion severely compromises hemostatic functions in mice deficient in the hemITAM receptor CLEC-2,[33,44] integrin α2β1 or concomitantly treated with acetylsalicylic acid,[45] thus emphasizing the

necessity to evaluate the functional status of other receptors prior to and during GPVI targeting.

1.2.2. CLEC-2

The second (hem)ITAM-containing receptor on mouse platelets CLEC-2 is an ~32 kDa type II transmembrane protein which signals via phosphorylation of a single conserved YxxL motif (hemITAM) in its cytoplasmic tail. CLEC-2 is highly expressed on MKs and platelets (~2000 copies per platelet) and additionally at lower levels on some immune cells.[29,46] CLEC-2 has been identified as the receptor for the powerful platelet activating snake venom toxin rhodocytin[47] and the sialoglycoprotein podoplanin[48] which remains the only currently known endogenous ligand of CLEC-2. Interestingly, however, podoplanin is not expressed on platelets and vascular endothelial cells and therefore, it has been proposed that a hitherto unidentified CLEC-2 ligand may exist which presumably becomes exposed or released at sites of injury or on growing thrombi and thus contributes to CLEC-2-dependent thrombus stabilization.[49]

CLEC-2 is expressed as a homodimer on resting platelets and clustering of the receptor following ligand binding induces powerful cellular activation.[50] Receptor engagement of CLEC-2 triggers a signaling cascade which involves similar molecules downstream of Syk like the GPVI pathway (Figure 3).[29] Importantly, recent studies suggested a significant difference in the proximal events in GPVI and CLEC-2 signaling. As indicated above, phosphorylation of the ITAM on the FcRγ-chain is mediated by SFKs, followed by the recruitment, phosphorylation and activation of Syk, whereas Syk is essential for phosphorylation of the hemITAM, with SFKs being predominantly involved in the regulation of downstream signaling events.[51]

Initial studies on the role of CLEC-2 in thrombosis and hemostasis implicated that the receptor might become a target for antithrombotic therapy.[49,52] Immunodepletion of CLEC-2 from circulating platelets[49] or genetic ablation of the receptor[52] was accompanied by a significant protection of mice in models of occlusive arterial thrombosis, but only by a moderate increase in bleeding times. However, recent studies demonstrated a previously unrecognized functional redundancy of GPVI and CLEC-2 in hemostasis and the maintenance of vascular integrity at sites of inflammation.[33,44] These findings have obvious implications regarding the suitability of the hemITAM receptor as a safe antithrombotic target. Furthermore, CLEC-2 plays a crucial role in a plethora of other (patho)physiological processes, including tumor metastasis, maintenance of the integrity of high endothelial venules, development of lymph nodes and blood/lymph vessel separation.[53-56] Genetic ablation of CLEC-2 leads to embryonic or neonatal lethality associated with blood-filled

lymphatics and severe edema formation,[52,57] a phenotype which strongly resembles that observed during embryonic development in mice lacking key (hem)ITAM-signaling molecules, including Syk, SLP-76 and PLCγ2, and importantly, podoplanin.[54] Recent studies which took advantage of tissue-specific deletion approaches identified that (hem)ITAM-signaling in platelets mediates blood/lymphatic separation and further documented that interactions between platelet CLEC-2 and podoplanin on lymphatic endothelial cells play an essential role in this process.[57,58]

Similar to GPVI, CLEC-2 can be immunodepleted from the surface of murine platelets by a monoclonal antibody (INU1).[44,49,59] Antibody-induced CLEC-2 down-regulation is accompanied by a receptor loss for > 5 days post treatment and a severe thrombocytopenia during the first 24-48 h after antibody administration.[44,49,59] Experimental evidence suggests that the mechanism by which antibody-induced CLEC-2 down-regulation in mice occurs is through SFK-triggered receptor internalization *in vitro* and *in vivo*, whereas the concomitantly occurring thrombocytopenia is, to a large extent, Syk-dependent.[59] Syk blockade thus reveals the possibility to mechanistically uncouple targeted CLEC-2 down-regulation from the therapeutically undesired thrombocytopenia.

1.2.3. Attenuation of (hem)ITAM signaling

Platelet function *in vivo* is negatively regulated by several mechanisms. Bioactive nitric oxide (NO) and prostacyclin (PGI$_2$) produced in endothelial cells support restriction of thrombus growth to the damaged areas and prevent further spreading in healthy vessels.[60] A naturally occurring intrinsic mechanism to dampen tonic signaling through (hem)ITAM receptors involves the action of receptors bearing an *immunoreceptor tyrosine-based inhibitory motif* (ITIM) defined by the consensus sequence L/I/V/SxYxxL/V.[61] ITIM is commonly found in pairs separated by 15 to 30 amino acid residues.[61] In hematopoietic cells, ITIM-bearing receptors inhibit ITAM signaling through recruitment of the tandem *SH2 domain-containing protein tyrosine phosphatases* (SHP), SHP-1 and SHP-2, and the single *SH2 domain-containing inositol 5-phosphatases* (SHIP), SHIP1 and SHIP2.[61] Platelets express a few ITIM-bearing proteins, including *platelet endothelial cell adhesion molecule-1* (PECAM-1), G6b-B, *TREM-like transcript-1* (TLT-1) and *carcino-embryonic antigen-related cell adhesion molecule-1* (CEACAM1) and CEACAM2.[29,62] Some ITIM-containing receptors, e.g. PECAM-1 and G6b-B, bear an *immunoreceptor tyrosine-based switch motif* (ITSM) in their cytoplasmic tail in addition to the ITIM.[63] ITSM is characterized by the consensus TxYxxV/I which can be tyrosine phosphorylated by SFKs and can subsequently bind to SHP-1, SHP-2 and SHIP.[64] PECAM-1, CEACAM1 and CEACAM2 play a minor inhibitory role in (hem)ITAM signaling in murine platelets.[62,65-67] By contrast, TLT-1 is essentially involved in maintenance of vascular

integrity during inflammation by facilitating platelet aggregation and preventing hemorrhage at sites of vascular injury.[68] It has been suggested that G6b-B is a critical negative regulator of ITAM signaling in mature MKs and thus decisively contributes to platelet production and reactivity.[69] Furthermore, studies in G6b-B-deficient mice may help to resolve the question of how MKs remain relatively refractory to the ECM-rich environment, although they are equipped with the same repertoire of receptors as platelets.[69]

1.3. *Src-like adapter proteins* (SLAP)

SLAP and SLAP2 constitute a family of adapter proteins that are expressed in multiple organs and cell types, but their function has been most extensively studied in lymphocytes. Mouse and human *Slap* genes are located on the thyroglobulin gene locus on chromosome 15 D2 and 8q22.3, respectively,[70,71] and code for a protein of 34 kDa. *Slap2* is found on chromosome 2 H1 (mouse) and 20q11.23 (human).[72] Alternative translation initiation of both murine and human *Slap2* determines the expression of 2 protein isoforms of 28 and 25 kDa, with the latter isoform lacking the myristoylation sequence and serine-rich region at the N-terminus.[72-74]

SLAP mRNA is expressed in heart, brain, spleen, thymus, bone marrow, lung, liver, skeletal muscle and kidney.[71,75-77] Likewise, SLAP2 mRNA expression was detected in lymphatic organs, including thymus, lymph nodes and spleen, in a variety of hematopoietic cells of both lymphoid and myeloid lineages in the bone marrow and the peripheral blood, as well as in liver and lung.[73-75] SLAP family members share structural similarities with SFKs which are characterized by the presence of a unique N-terminal region, an SH3-domain and an SH2-domain. The SH3 and the SH2 domain are highly homologous to the SH3 and SH2 domain of Lck, sharing 55% and 50% amino acid sequence identity, respectively.[78] Unlike SFKs, SLAP and SLAP2 lack a C-terminal kinase domain.[75] However, the C-terminal tail has been suggested to facilitate interactions between SLAP and the E3 ubiquitin ligase c-Cbl and thus enable SLAP to participate in the negative regulation of receptor expression and signaling.[79] In addition, the C-terminus of SLAP mediates dimerization of the protein and is essential for the negative regulation of the TCR (see below).[79] SLAP and SLAP2 share substantial amino acid identity between different domains (Figure 4).
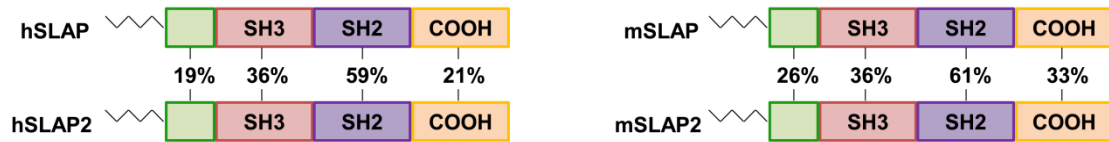
Figure 4. Sequence similarities between members of the *Src-like adapter protein* (SLAP) family. Amino acid identity in percentage found in the N-terminus, SH3 and SH2 domain and the C-terminal region of SLAP and SLAP2 in humans (left panel) and mice (right panel). Modified from: Dragone *et al.*, 2009.[75]

Different pull-down assays identified that SLAP interacts with proximal components of the TCR and BCR complexes, including TCRζ and Igα, as well as with the SFK Lck and the E3 ubiquitin ligase c-Cbl.[78,80-82] Similarly, SLAP2 has been demonstrated to interact with TCRζ, Lck and c-Cbl, but also with the *colony-stimulating factor-1 receptor* (CSF-1R) on macrophages.[73,74,83-85] Pull-down approaches and yeast-two-hybrid screens following overexpression studies identified a plethora of further interacting partners of SLAP/SLAP2, but many of these putative interactions have not been validated in primary cells yet and the functional consequences remain elusive.[75]

Initial experiments in knockout mice demonstrated that SLAP plays and important function in T lymphocyte maturation through regulation of TCR levels during the CD4$^+$CD8$^+$ double positive stage of thymus development.[86] Further mechanistic studies revealed that the negative regulation of TCR levels by SLAP likely occurs through contribution to the degradation of TCRζ and inhibition of the recycling of TCR complex components back to the cell surface.[80] A decisive step in this process is the phosphorylation of the cytoplasmic domain of TCRζ. Lck has been identified as the critical SFK that is required for SLAP to negatively regulate TCR expression levels through interactions with the phosphorylated form of TCRζ[80] or CD3ε.[81] Similarly, overexpression of SLAP2 in Jurkat T cells resulted in decreased surface expression of CD3ε, demonstrating that SLAP2 serves as a negative regulator of TCR levels, presumably through functional cooperation with the ubiquitin ligase c-Cbl.[74] Furthermore, SLAP is critically involved in B cell development, since it essentially contributes to the maintenance of normal BCR levels and intact signaling during B cell maturation.[87] Mechanistically, the fine-tuning of BCR levels during B cell development occurs through the cooperative action of SLAP and c-Cbl, whereby SLAP likely facilitates interactions between c-Cbl and antigen-bound components of the BCR complex.[82] In addition, SLAP modulates the surface expression and stability of receptors which belong to the *receptor tyrosine kinase* (RTK) family, including CSF-1R,[84,85] Flt3[88] and EPHA2.[89] Of note, recent studies indicated that this naturally occurring inhibitory mechanism controlled by SLAP may have important implications in the suppression of tumor development.[88,89]

Little is known about the function of SLAP family members in platelets other than that upon platelet stimulation specifically with the GPVI activating snake venom protein convulxin, SLAP2 co-immunoprecipitates with c-Cbl, Syk and LAT.[90] However, the functional consequences of these putative interactions remained unknown.

1.4. Platelet biogenesis

Platelets are constantly produced by their *bone marrow* (BM) resident precursors, MKs, in a unique and complex process that remains poorly understood.[91] Recent developments in imaging with two-photon microscopy have yielded significant progress in visualization of proplatelet formation *in situ*,[92,93] thereby overcoming one of the obstacles in MK biology research – the inaccessibility of MKs in their natural environment in the BM which is the primary site of thrombopoiesis. Besides the BM, MKs are also found in spleen and lung. Mature MKs reach a diameter of 50-100 μm in humans and up to 50 μm in mice and represent only approximately 0.1‰ of all nucleated cells in the BM.[91]

MKs belong to the myeloid cell lineage and differentiate from pluripotent *hematopoietic stem cells* (HSCs) which give rise to two types of precursor cells: *burst-forming unit* (BFU) cells and *colony-forming unit* (CFU) cells.[94] The development of both cell types culminates in the formation of immediate MK precursor cells (CFU-Meg). The cytokine *thrombopoietin* (Thpo) is the primary regulator of thrombopoiesis.[95] Thpo signals through the c-Mpl receptor on MKs and platelets. Hepatocytes are the major source of Thpo and its production is critically regulated by signaling through the hepatic Ashwell-Morell receptor which recognizes and removes aged platelets.[96] Importantly, however, mice deficient in c-Mpl or Thpo still successfully produce platelets,[97] indicating that MK maturation and platelet biogenesis can occur independently of Thpo and implicating the involvement of additional factors. For instance, the cytokines *interleukin* (IL-) 3, IL-6, IL-11 and, especially during acute platelet needs, IL-1α,[98] *granulocyte macrophage colony-stimulating factor* (GM-CSF) and the chemokines *stromal cell–derived factor-1* (SDF-1) and PF4 have been demonstrated to contribute to MK maturation.[94,99]

MKs undergo a complex maturation process before they obtain the capacity to release platelets. MK development involves nuclear proliferation during which MKs become polyploid through several rounds of endomitosis (cycles of DNA replication without cell division) – a unique process which depends on Thpo.[3] Endomitosis leads to a DNA content of 4n to 128n in a single polylobulated nucleus before final maturation and proplatelet formation can take place. Concomitantly, maturation of MKs includes cytoplasm enlargement, the synthesis of platelet-specific granules and organelles and the formation of a *demarcation membrane*

system (DMS) – an elaborate meshwork of membrane channels containing cisternae and tubules that serve as a membrane reservoir for proplatelet production (Figure 5).[100,101] Subsequently, substantial MK cytoplasm remodeling occurs prior to proplatelet formation and final fission leading to the release of discoid platelets. After proplatelet release, the MK nucleus is extruded and degraded.[3]
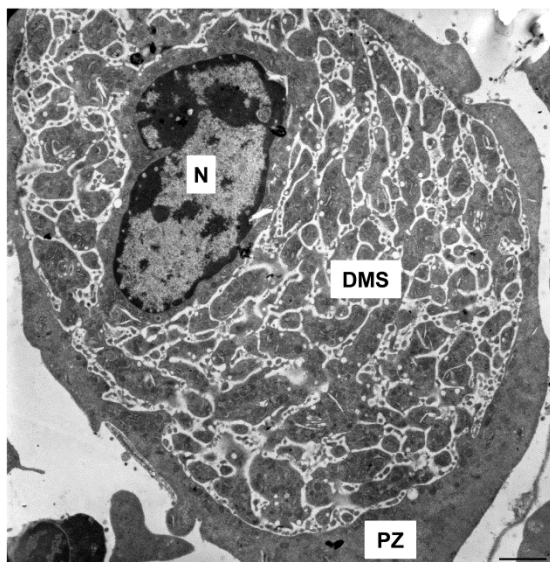
Figure 5. Ultrastructure of a mature BM MK. The ultrastructure of mature MKs in the bone marrow is characterized by the presence of a well-organized *demarcation membrane system* (DMS), as depicted in the transmission electron microscopy image. DMS provides a membrane reservoir for proplatelet formation. The *peripheral zone* (PZ) is devoid of membrane invaginations and organelles and provides the demarcation of the MK from surrounding cells. N, *nucleus*. Bar: 1.7 μm.

The exact mechanisms of platelet generation from MKs are still incompletely understood. However, recent *in vivo* studies provide cumulative evidence in favor of the following model of thrombopoiesis: Mature MKs reside in the vicinity of sinusoidal blood vessels into which they extend and release proplatelets that consist of platelet-sized swellings connected by thin cytoplasmic bridges (shaft).[91] Final shaping and fragmentation of proplatelets into platelets likely occurs through shear forces in the blood stream.[92] The process of proplatelet fragmentation remains enigmatic, but recent work demonstrated that shedding of platelets into the circulation is supported by exposure to a high concentration of sphingosine 1-phosphate.[93]

Proplatelet formation requires substantial cytoskeletal rearrangements. Microtubules which consist of $\alpha\beta$-tubulin dimers are the key components of the machinery that drives proplatelet elongation.[102,103] In addition, microtubules line the proplatelet shaft and enable the transport of organelles and granules into the proplatelets.[104] Proplatelet bending and bifurcation depends on actin polymerization,[105] but otherwise little is known about the role of the actin cytoskeleton during MK maturation. Small GTPases of the Rho family have been established as critical regulators of cytoskeletal rearrangements in various cell types.[106] However, the role of these proteins in the reorganization of the MK actin and tubulin cytoskeleton preceding platelet release is largely unknown.

1.5. Small GTPases of the Rho family

Mammalian Rho GTPases comprise a family of 20 proteins which belong to the Ras superfamily of monomeric 20-25 kDa *guanosine-5'-triphosphate* (GTP-) binding proteins which are best documented for their important functions in the control of cytoskeletal rearrangements (Figure 6).[106] Rho GTPases cycle between a GTP-bound (active) and a *guanosine diphosphate* (GDP-) bound (inactive) state. The switch between both forms is regulated by three sets of proteins: *Guanine nucleotide-exchange factors* (GEFs) promote the exchange of GDP to GTP. *GTPase-activating proteins* (GAPs) accelerate the hydrolysis of GTP to GDP and thus inhibit Rho GTPase activation. *Guanine nucleotide-dissociation inhibitors* (GDIs) sequester GDP-bound Rho GTPases away from regulators and target proteins and thus prevent spontaneous activation.[107] In their active, GTP-bound form, Rho GTPases interact with effector proteins and thus modulate a plethora of processes, including vesicle transport, microtubule dynamics, adhesion and migration.[106,107]
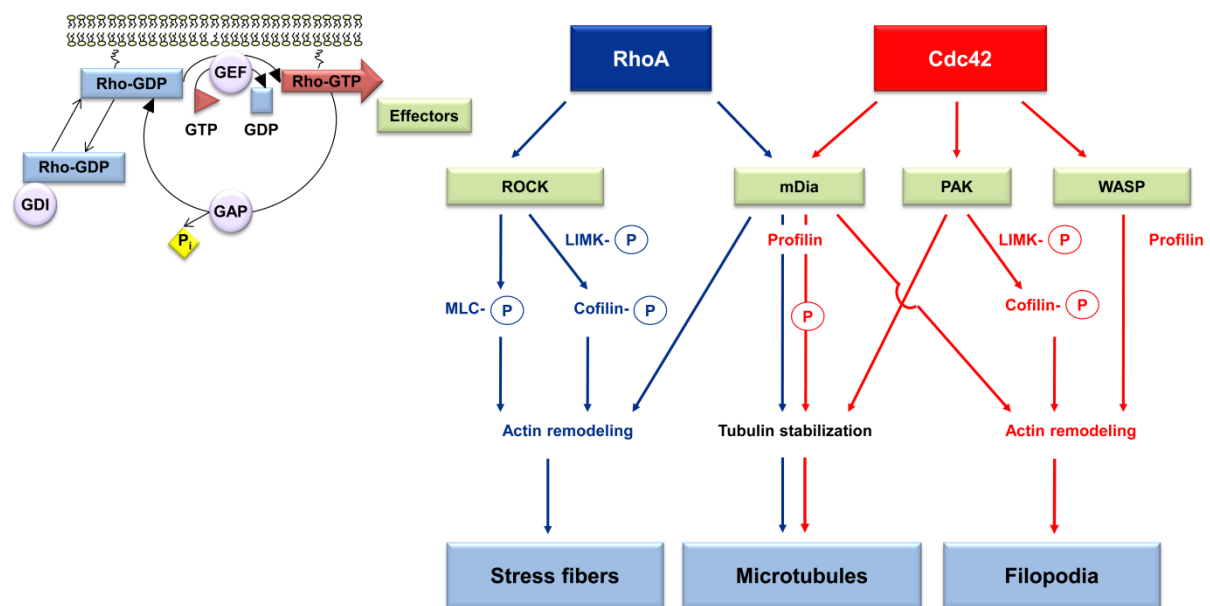
Figure 6. The Rho GTPase cycle and signal transduction pathways. (left panel) Activation and regulation of Rho GTPases. Rho GTPases cycle between an inactive, GDP-bound, and an active, GTP-bound, state in which they can interact with effector molecules. GEFs mediate the exchange of GDP to GTP. GAPs trigger the hydrolysis of Rho GTP to GDP and thus inhibit Rho GTPase activation. GDIs induce sequestering of Rho proteins away from regulators and target proteins and thus prevent interactions. (right panel) Overview of common and diverging signaling pathways of RhoA and Cdc42 in the regulation of cytoskeletal rearrangements. GEFs, *guanine nucleotide-exchange factors*; GAPs, *GTPase-activating proteins*; GDIs, *guanine nucleotide-dissociation inhibitors*; RhoA, *Ras homolog gene family, member A*; Cdc42, *cell division control protein 42 homolog*; ROCK, *Rho-associated protein kinase*; MLC, *myosin light chain*; LIMK, *LIM domain kinase*; PAK, *p21-activated kinase*; mDia, *mammalian diaphanous*; WASP, *Wiskott-Aldrich syndrome protein*. Modified from ref.[106-108]

A substantial body of knowledge about the functions of Rho GTPases in cell biology has been gained by overexpression studies, knockdown approaches or pharmacological inhibition of Rho GTPases or their downstream effector molecules. Many of these studies have yielded contradictory results, likely due to off-target effects of some of these approaches. In recent years, mouse models with tissue- or lineage-specific deletion of Rho GTPase genes have greatly facilitated investigations on the role of Rho GTPases and have provided valuable insights into the functions of these proteins *in vivo*.[109]

1.5.1. Rho GTPases in platelets

RhoA (*Ras homolog gene family, member A*), Cdc42 (*cell division control protein 42 homolog*) and Rac1 (*Ras-related C3 botulinum toxin substrate 1*) are the best characterized Rho GTPases in platelet biology. As mentioned in Section 1.1. (Figure 2), soluble agonists, such as thrombin, ADP and TxA_2, operate via receptors that couple to heterotrimeric G proteins (G_q, $G_{12/13}$, G_i).[18] Upon agonist binding, G_q activates PLCβ isoforms, leading to increased levels of cytoplasmic calcium and activation of the *protein kinase C* (PKC) via formation of IP_3 and DAG, respectively.[18] G_{13} regulates the Rho/Rho-kinase pathway resulting in *myosin light chain* (MLC) phosphorylation and initiation of platelet shape change.[110] RhoA mediates platelet shape change from discoid to spherical following activation.[111,112] GTP-bound RhoA binds to and activates *Rho-associated protein kinase* (ROCK) that induces actin remodeling, ROCK phosphorylation and inactivation of the MLC phosphatase which results in a net increase in MLC phosphorylation.[111] Alternatively, G_q signaling directly stimulates MLC kinase activation and MLC phosphorylation.[111] Studies in MK-/platelet-specific RhoA-deficient mice revealed that RhoA is essential for G_{13}-mediated shape change and contributes to G_{13}/G_q-dependent integrin αIIbβ3 activation, granule release and clot retraction which *in vivo* translates into contribution to arterial thrombus formation and stability.[112]

Cdc42 has been established as a regulator of filopodia formation, exocytosis and secretion.[106,107] Studies in MK-/platelet-specific mice yielded unexpected results, as filopodia formation on fibrinogen was unaltered in Cdc42-deficient platelets.[113] By contrast, Cdc42 deficiency led to decreased filopodia formation on VWF, suggesting a unique role of Cdc42 downstream of GPIb. Unexpectedly, lack of Cdc42 in platelets resulted in increased secretion from α- and dense granules which was associated with enhanced thrombus formation *ex vivo* under flow and *in vivo* in a model of arterial thrombosis.[113] In sharp contrast, Cdc42 excision in all hematopoietic cells introduced by a different approach demonstrated that Cdc42 deficiency results in reduced platelet filopodia formation on fibrinogen.[114]

The findings that platelet Cdc42 is not essential for filopodia formation led to the hypothesis that the newly characterized Rho GTPase Rif (RhoF) might be responsible for filopodia generation.[113] However, Rif was found to be dispensable for filopodia formation and for platelet function in general (Goggs *et al.*, 2013[115] and Sebastian Dütting, unpublished).

The role of Rac1 in platelet biology has been extensively studied. Of note, many initial studies relied on the powerful inhibition of Rac1 by pharmacological substances which have been recently demonstrated to exert profound off-target effects.[116] Rac1 has been established as the Rho GTPase critical for lamellipodia formation in platelets.[117,118] In addition, Rac1 controls the GPVI-PLCγ2 activation axis and thus contributes to GPVI-dependent thrombus formation under flow and in models of experimental arterial thrombosis.[117,118] Likewise, RhoG, the GTPase most closely related to Rac, has been demonstrated to contribute to GPVI signaling and GPVI-mediated thrombus formation *in vivo*.[119,120]

Although Rho GTPases have common binding partners and share similar signaling pathways, little is known about functional cooperation of different Rho GTPases in platelet production and function.

1.5.2. Rho GTPases in megakaryopoiesis and platelet biogenesis

Despite intensive research in recent years, little is known about the mode of action of Rho GTPases in platelet biogenesis. Overexpression experiments using a dominant-negative or constitutively active form of RhoA demonstrated that RhoA activation inhibits *in vitro* proplatelet formation via ROCK, the main effector of RhoA.[121] Likewise, interference with RhoA downstream signaling by inhibition of MLC phosphorylation or deletion of the myosin IIA heavy chain resulted in increased proplatelet formation.[122,123] Importantly, *MYH9* mutations in the motor head domain of myosin IIA lead to macrothrombocytopenia in humans.[124] In line with these findings, mice deficient in PSMC1, an essential subunit of the 26S proteasome, exhibited abolished proplatelet formation *in vitro* and *in situ* and severe thrombocytopenia which was attributed to upregulation and hyperactivity of RhoA.[125] Conversely, inhibition of RhoA or its downstream target ROCK during concomitant proteasome blockade rescued proplatelet formation.[125] Equally, treatment of PSMC1-deficient mice with potent ROCK inhibitors ameliorated the severe thrombocytopenia observed in these animals.[125]

Surprisingly, the moderate thrombocytopenia observed in RhoA-deficient mice[112,126] suggested that RhoA is necessary for platelet production which contradicts results obtained from ovexpression studies or pharmacological approaches blocking RhoA effector

molecules. However, the moderately decreased life span in these mice implied that increased removal of RhoA-deficient platelets from the circulation likely contributes to the observed phenotype. Of note, the impact of genetic ablation of RhoA on MK biology has not been extensively investigated yet and studies utilizing conditional knockout mice only identified a minor shift to higher mean ploidy levels and slightly increased numbers of BM MKs in RhoA-deficient mice.[112,126] Thus, the role of RhoA in platelet biogenesis remains elusive.

Similarly, little is known about the role of other Rho GTPases in platelet production other than that deficiency of Cdc42 leads to a moderate reduction of platelet counts, suggesting that Cdc42 likely plays a role in platelet biogenesis.[113,114] Importantly, more direct evidence for a contribution of Rho GTPases to thrombopoiesis came from a recent study which emphasized a previously unrecognized functional redundancy between Cdc42 and Rac1 in MK development and platelet production.[127] Lack of Rac1 or Cdc42 had no or only a mild effect on circulating platelet counts and morphology, whereas combined deficiency of both proteins resulted in a severe macrothrombocytopenia caused by defective proplatelet formation, markedly altered ultrastructure of MKs and platelets and a striking defect in microtubule structure. These studies support the notion that Rho GTPases are critically involved in platelet biogenesis and may have partially overlapping functions in the control of MK maturation and thrombopoiesis.

1.6. Aim of the study

The (hem)ITAM-containing receptors GPVI and CLEC-2 have been increasingly recognized as essential regulators of hemostasis and thrombo-inflammatory disease states. However, little is known about the contribution of downstream signaling molecules modulating receptor activity. SLAP and SLAP2 are involved in the regulation of immune cell surface expression and signaling, but their function in platelets is unknown. In the first part of this thesis, the contribution of both adapter proteins to platelet activation and their specific role in hemostasis, arterial thrombosis and ischemic stroke was investigated.

GPVI has emerged as a promising antithrombotic target because immunodepletion or blockade of the receptor provides profound protection in different models of experimental thrombosis without affecting hemostatic functions. However, the exact mechanisms underlying targeted GPVI down-regulation and the involvement of downstream signaling molecules remain incompletely understood. Therefore, the role of SLAP and SLAP2 in antibody-induced GPVI down-regulation was investigated in the second part of this thesis.

The Rho GTPases RhoA and Cdc42 have been identified as critical players in platelet physiology, as they have key functions in cytoskeletal rearrangements during cellular activation and degranulation. However, possible overlapping and distinct roles of both Rho GTPases in the regulation of platelet biogenesis and function have remained elusive. Conditional knockout mice with MK-/platelet-specific deficiency in RhoA and Cdc42 were generated and analyzed in the third part of this thesis.

2. Materials and Methods

2.1. Materials

2.1.1. Kits, reagents and cell culture material

Reagent	Company
A23187	AppliChem (Darmstadt, Germany)
Adenosine diphosphate (ADP)	Sigma-Aldrich (Schnelldorf, Germany)
Agarose	Roth (Karlsruhe, Germany)
Amersham® Hyperfilm®, ECL	GE Healthcare (Little Chalfont, UK)
Ammonium persulphate (APS)	Roth (Karlsruhe, Germany)
Apyrase (Grade III)	Sigma-Aldrich (Schnelldorf, Germany)
Bovine serum albumin (BSA)	AppliChem (Darmstadt, Germany)
Bovine serum albumin (BSA), low endotoxin	PAA (Cölbe, Germany)
Brij® O10	Sigma-Aldrich (Schnelldorf, Germany)
Clodronate	Clodronate Liposomes (Haarlem, The Netherlands)
Collagen Horm® suspension + SKF sol.	Takeda (Linz, Austria)
cOmplete, Mini protease inhibitor cocktail (# 11836153001)	Roche Diagnostics (Mannheim, Germany)
Convulxin	Enzo Life Sciences (Lörrach, Germany)
Cryo-Gel	Leica Biosystems (Wetzlar, Germany)
Dade® Innovin (tissue factor)	Siemens Healthcare Diagnostics (Deerfield, IL, USA)
DAPI	Life Technologies (Darmstadt, Germany)
dNTP Mix (10 mM)	Life Technologies (Darmstadt, Germany)
EDTA	AppliChem (Darmstadt, Germany)
Eosin Y solution (# 318906)	Sigma-Aldrich (Schnelldorf, Germany)
Epinephrine	Sigma-Aldrich (Schnelldorf, Germany)
Epon 812	Roth (Karlsruhe, Germany)
Fat-free dry milk	AppliChem (Darmstadt, Germany)
$FeCl_3 \cdot 6\ H_2O$	Roth (Karlsruhe, Germany)
Fentanyl	Janssen-Cilag (Neuss, Germany)
Fibrinogen from human plasma (# F3879)	Sigma-Aldrich (Schnelldorf, Germany)
Fibrinogen from human plasma (# F4883)	Sigma-Aldrich (Schnelldorf, Germany)
Flumazenil	AlleMan Pharma (Pfullingen, Germany)
Fluoroshield™	Sigma-Aldrich (Schnelldorf, Germany)
Fluoroshield™ with DAPI	Sigma-Aldrich (Schnelldorf, Germany)

Reagent	Company
GeneRuler DNA Ladder Mix	Life Technologies (Darmstadt, Germany)
Glutaraldehyde solution (25%)	Science Services (Munich, Germany)
Hematoxylin solution (# MHS32)	Sigma-Aldrich (Schnelldorf, Germany)
Heparin sodium	Ratiopharm (Ulm, Germany)
HEPES (4-(2-hydroxyethyl)-1-piperazine-ethanesulfonic acid)	Life Technologies (Darmstadt, Germany)
Histopaque®-1077	Sigma-Aldrich (Schnelldorf, Germany)
IGEPAL® CA-630	Sigma-Aldrich (Schnelldorf, Germany)
Immobilon-P transfer membrane, PVDF, 0.45 μm	Merck Millipore (Darmstadt, Germany)
Indomethacin	Sigma-Aldrich (Schnelldorf, Germany)
Isofluran CP®	cp-pharma (Burgdorf, Germany)
Medetomidine	Pfizer (Karlsruhe, Germany)
Midazolam	Roche (Grenzach-Wyhlen, Germany)
Midori Green Advanced DNA stain	Nippon Genetics Europe (Düren, Germany)
Mouse Thrombopoietin DuoSet (# DY488)	R&D Systems (Abingdon, UK)
Naloxon	AlleMan Pharma (Pfullingen, Germany)
nProtein A Sepharose 4 Fast Flow	GE Healthcare (Little Chalfont, UK)
NuPAGE® LDS Sample Buffer (4x)	Life Technologies (Darmstadt, Germany)
NuPAGE® Novex® 4-12% Bis-Tris Gels, 1mm, 10 well, 15 well	Life Technologies (Darmstadt, Germany)
PageRuler Prestained Protein Ladder (# 26616, 26619)	Life Technologies (Darmstadt, Germany)
Paraformaldehyde (PFA)	Sigma-Aldrich (Schnelldorf, Germany)
Phenol/chloroform/isoamyl alcohol	Roth (Karlsruhe, Germany)
Phire Hot Start II DNA Polymerase (# F-124S)	Life Technologies (Darmstadt, Germany)
Propidium iodide	Life Technologies (Darmstadt, Germany)
Prostacyclin (PGI_2)	Calbiochem (Bad Soden, Germany)
Protease inhibitor cocktail (# P8340)	Sigma-Aldrich (Schnelldorf, Germany)
Proteinase K, recombinant, PCR grade (20 mg/ml)	Life Technologies (Darmstadt, Germany)
RayBio Mouse PF-4 (CXCL4) ELISA Kit (# ELM-PF4-1)	Raybiotech (Norcross, GA, USA)
Refludan® (Lepirudin)	Bayer Schering Pharma AG (Wuppertal, Germany)
RNase A (# R4875)	Sigma-Aldrich (Schnelldorf, Germany)
Rotiphorese® Gel 30 (37,5:1) acrylamide	Roth (Karlsruhe, Germany)
SeeBlue® Plus2 pre-stained standard	Life Technologies (Darmstadt, Germany)

Reagent	Company
Sodium orthovanadate	Sigma-Aldrich (Schnelldorf, Germany)
Sphero™ AccuCount fluorescent particles	Spherotech (Fulda, Germany)
Streptavidin-HRP (# 016-030-084)	Jackson ImmunoResearch (West Grove, PA, USA)
Taq DNA polymerase (5 U/μl without BSA) (# EP0282)	Life Technologies (Darmstadt, Germany)
TEMED (N,N,N',N'-Tetramethylethylen-ediamine)	Roth (Karlsruhe, Germany)
Thrombin from human plasma (# 10602400001)	Roche Diagnostics (Mannheim, Germany)
TMB substrate reagent set	BD Biosciences (Heidelberg, Germany)
Tween® 20	Roth (Karlsruhe, Germany)
U-46619	Enzo Life Sciences (Lörrach, Germany)
Western Lightning® Plus-ECL	PerkinElmer (Baesweiler, Germany)

Collagen-related peptide was kindly provided by Dr. Steve Watson (University of Birmingham, UK). Rhodocytin was a generous gift from Dr. Johannes Eble (University Hospital, Frankfurt, Germany). All other non-listed chemicals were obtained from AppliChem (Darmstadt, Germany), Roth (Karlsruhe, Germany) or Sigma-Aldrich (Schnelldorf, Germany).

Consumables, cell culture material, kits	Company
12-well cell culture plate	Greiner Bio-One (Frickenhausen, Germany)
18 G x $1^{1/2}$ in., 20 G x $1^{1/2}$ in, 22 G x $1^{1/2}$ in. needles	BD Biosciences (Heidelberg, Germany)
Dynabeads® Untouched™ Mouse CD4	Life Technologies (Darmstadt, Germany)
Fetal calf serum (FSC)	Sigma-Aldrich (Schnelldorf, Germany)
Iscove's Modified Dulbecco's Medium (IMDM)	Life Technologies (Darmstadt, Germany)
Nunc-Immuno™ MediSorp™, F96-Wells	Thermo Scientific (Schwerte, Germany)
MTF; F96-Wells	Hartenstein (Würzburg, Germany)
Penicillin/Streptomycin	Life Technologies (Darmstadt, Germany)
PGA 5-0 prolene sature	Resorba (Nuremberg, Germany)
Phosphate-buffered saline (PBS)	Life Technologies (Darmstadt, Germany)
Syringe filter (0.22 μm and 0.45 μm)	Roth (Karlsruhe, Germany)

Recombinant thrombopoietin was generated as previously described.[128]

2.1.2. Antibodies

2.1.2.1. Purchased primary and secondary antibodies

Antibody	Company
Donkey anti-rat IgG-FITC (# 112095068)	Jackson ImmunoResearch (West Grove, PA, USA)
Donkey anti-rabbit IgG-HRP, MinX (# 711035152)	Jackson ImmunoResearch (West Grove, PA, USA)
Donkey anti-rat IgG-HRP (# 712035153)	Jackson ImmunoResearch (West Grove, PA, USA)
Goat anti-rabbit IgG-HRP (# 7074)	Cell Signaling (Danvers, MA; USA)
Goat anti-rat IgG + IgM (# 112005044)	Jackson ImmunoResearch (West Grove, PA, USA)
Goat anti-SLAP (C-19) (# sc-1215)	Santa Cruz (Heidelberg, Germany)
Hamster anti-mouse/rat CD29 (β1-Integrin)-FITC (clone HMβ1-1) (# 102206)	BioLegend (Fell, Germany)
Mouse anti-Cdc42 (clone 44) (# 610928)	BD Biosciences (Heidelberg, Germany)
Mouse anti-phosphotyrosine (clone 4G10)	Merck Millipore (Darmstadt, Germany)
Mouse anti-RhoA (# ARH03)	Cytoskeleton (Denver, CO, USA)
Mouse anti-α-tubulin Alexa F488 (clone B-5-1-2) (# 322588)	Life Technologies (Darmstadt, Germany)
Phalloidin-Atto647N (# 65906)	Sigma-Aldrich (Schnelldorf, Germany)
Platelet depletion antibody (# R300)	Emfret Analytics (Eibelstadt, Germany)
Polyclonal rabbit anti-human VWF (# A0082)	DAKO (Hamburg, Germany)
Polyclonal rabbit anti-human VWF-HRP (# P0226)	DAKO (Hamburg, Germany)
Rabbit anti-actin (# A2066)	Sigma-Aldrich (Schnelldorf, Germany)
Rabbit anti-GAPDH (# 9545)	Sigma-Aldrich (Schnelldorf, Germany)
Rabbit anti-goat IgG-HRP (# P0449)	DAKO (Hamburg, Germany)
Rabbit anti-mouse IgG-HRP (# P0260)	DAKO (Hamburg, Germany)
Rabbit anti-phospho-PLCγ2 (Y759) (# 3874)	Cell Signaling (Danvers, MA; USA)
Rabbit anti-phospho-Syk (Y525/526) (clone C87C1) (# 2710)	Cell Signaling (Danvers, MA; USA)
Rabbit anti-total-Lyn (clone C13F9) (# 2796)	Cell Signaling (Danvers, MA; USA)
Rabbit anti-total-PLCγ2 (Q-20) (# sc-407)	Santa Cruz (Heidelberg, Germany)
Rabbit anti-total-Syk (clone D1I5Q) (# 12358)	Cell Signaling (Danvers, MA; USA)
Rat anti-mouse CD105 (endoglin) (clone MJ7/18) (# 120402)	BioLegend (San Diego, CA, USA)

Antibody	Company
Rat anti-mouse CD11b (clone M1/70) (# 557394)	BD Biosciences (Heidelberg, Germany)
Rat anti-mouse CD16/CD32 (clone 2.4G2) (# 553142)	BD Biosciences (Heidelberg, Germany)
Rat anti-mouse CD3 molecular complex (clone 17A2) (# 555273)	BD Biosciences (Heidelberg, Germany)
Rat anti-mouse CD45R/B220 (clone RA3-6B2) (# 557390)	BD Biosciences (Heidelberg, Germany)
Rat anti-mouse erythroid cells (clone TER-119) (# 553670)	BD Biosciences (Heidelberg, Germany)
Rat anti-mouse Ly-6G/C (clone RB6-8C5) (# 557445)	BD Biosciences (Heidelberg, Germany)
Rat anti-tubulin (clone YL1/2) (# MAB1864)	Merck Millipore (Darmstadt, Germany)

The polyclonal rabbit anti-SLAP2 antibody was kindly provided by Dr. Jane McGlade (University of Toronto, Canada).[74]

2.1.2.2. Monoclonal rat antibodies generated or modified in our laboratory

Antibody	Clone	Isotype	Antigen	Reference
p0p4	15E2	IgG2b	GPIbα	[129]
p0p3	7A9	IgG2a	GPIbα	[129]
DOM2	89H11	IgG2a	GPV	[130]
p0p6	56F8	IgG2b	GPIX	[130]
JAQ1	98A3	IgG2a	GPVI	[22]
JAQ2	21G10	IgG2a	GPVI	[40]
JAQ3	0E3	IgG2a	GPVI	[40]
INU1	11E9	IgG1	CLEC-2	[49]
ULF1	97H1	IgG2a	CD9	unpublished
LEN1	12C6	IgG2b	α2	[22]
EDL1	57B10	IgG2a	β3	[129]
JON2	14A3	IgG2a	αIIbβ3	[130]
JON/A	4H5	IgG2b	αIIbβ3	[131]
MWReg30	5D7	IgG1	αIIbβ3	[132]
WUG 1.9	5C8	IgG1	P-selectin	[40]

2.1.3. Mice

Slap⁻/⁻, Slap2⁻/⁻, Slap⁻/⁻/Slap2⁻/⁻ mice were generated as previously described[86,133] and have been backcrossed ten generations onto the BALB/c background. BALB/cJRj mice used as recipients in platelet transfer experiments were purchased from Janvier Labs (Saint-Berthevin, France). *Gp6⁻/⁻* mice were generated in our laboratory as previously described[44] and were intercrossed with *Slap⁻/⁻/Slap2⁻/⁻* mice. *Slap⁻/⁻/Slap2⁻/⁻/Gp6⁺/⁻* and litter-matched *Slap⁻/⁻/Slap2⁻/⁻/Gp6⁺/⁺* on a mixed BALB/c/Sv129/C57BL/6 background were used in this study. *Lat⁻/⁻* mice have been described previously.[134] *Syk^{fl/fl}*,[59] *RhoA^{fl/fl}* [135] and *Cdc42^{fl/fl}* [136] mice were intercrossed with mice carrying the platelet factor 4 (PF4)–Cre transgene (*Pf4-Cre⁺/⁻*)[137] to generate animals lacking Syk, RhoA or Cdc42, respectively, specifically in MKs and platelets. If not stated otherwise, 8-to-12-week-old mice of either sex were used in experiments. Animal studies were approved by the district government of Lower Frankonia (Bezirksregierung Unterfranken).

2.1.4. Buffers and media

If not stated otherwise, all buffers were prepared in deionized water obtained from a MilliQ Water Purification System (Millipore, Schwalbach, Germany). pH was adjusted with HCl or NaOH.

Cacodylate buffer, pH 7.2

Sodium cacodylate	0.1 M

CATCH buffer, pH 7.2

HEPES	25 mM
EDTA	3 mM
BSA	3.5%
in PBS	

Coating buffer (ELISA), pH 9.5

$NaHCO_3$	85 mM
Na_2CO_3	15 mM

Decalcification buffer, pH 7.4

EDTA	10%
in PBS	

Fluorescent thrombin substrate (Thrombin generation assay)

Z-GGR-AMC	2.5 mM
HEPES	20 mM
NaCl	140 mM
CaCl$_2$	200 mM
BSA	6%

Karnovsky's fixative

Sodium cacodylate, pH 7.2	0.1 M
Glutaraldehyde	2.5%
PFA	2%

Laemmli sodium dodecyl sulfate (SDS) sample buffer (4x)

Tris-HCl, pH 6.8	200 mM
Glycerol	40%
Bromophenol blue (3',3",5',5"-tetra-bromophenol-sulfonphthalein)	0.04%
SDS	8%
β-mercaptoethanol (reducing conditions)	20%

Laemmli running buffer for SDS-PAGE

Tris	0.25 M
Glycine	1.92 M
SDS	35 mM

Loading dye solution (6x) for analysis of PCR products

Tris buffer (150 mM)	33%
Glycerin	60%
Bromophenol blue (3',3",5',5"-tetra-bromophenol-sulfonphthalein)	0.04%

Lysis buffer for DNA isolation

Tris base	100 mM
EDTA	5 mM
NaCl	200 mM
SDS	0.2%
add Proteinase K (20 mg/ml)	100 μg/ml

Lysis buffer for immunoprecipitation (2x)

NaCl	150 mM
Tris, pH 7.5	20 mM
Brij O10	1%
NaF	10 mM
Na_3VO_4	1 mM
protease inhibitor cocktail	1%

Lysis buffer for platelet lysates, pH 8.0

Tris, pH 7.4	15 mM
NaCl	155 mM
EDTA	1 mM
NaN_3	0.005%
IGEPAL CA-630	1%
protease inhibitor cocktail	1%

Lysis buffer (2x) for tyrosine phosphorylation studies, pH 7.5

NaCl	300 mM
Tris	20 mM
EGTA	2 mM
EDTA	2 mM
NaF	10 mM
Na_3VO_4	4 mM
IGEPAL CA-630	1%
protease inhibitor cocktail	1%

MK differentiation medium

IMDM	
FCS	10%
Penicillin-Streptomycin	1%
recombinant thrombopoietin	50 ng/ml
recombinant hirudin	50 μg/ml

3-(*N*-morpholino)propanesulfonic acid (MOPS) buffer (20x)

MOPS	1 M
Tris base	1 M
SDS	69.3 mM
EDTA	20.5 mM

Phosphate-buffered saline (PBS), pH 7.14

NaCl	137 mM
KCl	2.7 mM
KH_2PO_4	1.5 mM
Na_2HPO_4 x $2H_2O$	8 mM

PBS-T (Wash buffer for ELISA)

PBS (1x)	
Tween® 20	0.1%

PHEM buffer, pH 6.9

PIPES (piperazine-N,N′-bis(2-ethanesulfonic acid))	60 mM
HEPES	25 mM
EGTA	10 mM
MgCl$_2$	2 mM

PRP reagent (Thrombin generation assay)

HEPES	20 mM
NaCl	140 mM
BSA	0.5%
tissue factor (TF)	3 pM

Semi-dry transfer buffer

Tris-Ultra	75 mM
glycine	80 mM
methanol	40%

Separating gel buffer (SDS-PAGE), pH 8.8

Tris-HCl	1.5 M

Sodium citrate, pH 7.0

Sodium citrate	0.129 M

Stacking gel buffer (SDS-PAGE), pH 6.8

Tris-HCl	0.5 M

Stripping buffer ("mild"), pH 2.0

SDS	1%
Glycine	25 mM
in PBS	

TAE buffer (50x)

Tris base	0.2 M
Acetic acid	5.7%
EDTA (0.5 M)	10%

TE buffer

Tris base	10 mM
EDTA	1 mM

Tris-buffered saline (TBS), pH 7.3

Tris-HCl	20 mM
NaCl	137 mM

TBS-T (Wash buffer for Western blotting)

TBS (1x)	
Tween® 20	0.1%

Tyrode-HEPES buffer, pH 7.4

NaCl	134 mM
Na_2HPO_4	0.34 mM
KCl	2.9 mM
$NaHCO_3$	12 mM
HEPES	5 mM
$MgCl_2$	1 mM
glucose	5 mM
BSA	0.35%

2.2. Methods

2.2.1. Isolation of genomic DNA from mouse ears

Ear punches were lysed in 500 µl lysis buffer containing 100 µg/ml Proteinase K. The samples were incubated overnight (o/n) at 56 °C and constantly shaken at 900 rpm (Eppendorf Thermomixer). Phenol/chloroform/isoamyl alcohol mixture (500 µl) was added to each sample. The reaction tubes were shaken well by hand and centrifuged at 10,620 *g* for 10 min at *room temperature* (RT). The upper phase was transferred to reaction tubes containing 500 µl isopropanol and thoroughly shaken by hand. Following a centrifugation step at 18,000 *g* for 10 min at 4 °C, the supernatant was discarded and the DNA pellet was washed with 70% ethanol and centrifuged again at 18,000 *g* for 10 min at 4 °C. The DNA pellet was dried at 37 °C for 30 min and solubilized in 70 µl TE buffer for 30 min at 37 °C under stirring. Genotyping was accomplished by a *polymerase chain reaction* (PCR) using a mixture of primers indicated below.

Pipetting scheme for SLAP WT, SLAP KO and SLAP2 WT PCR (20 µl final volume):

1 µl	DNA template
2 µl	10x Taq buffer (+ KCl, - MgCl$_2$)
2 µl	MgCl$_2$ (stock: 25 mM)
0.5 µl	dNTPs (stock: 10 mM)
2 µl	forward primer (1:10 in H$_2$O, stock: 1 µg/ml)
2 µl	reverse primer (1:10 in H$_2$O, stock: 1 µg/ml)
0.1 µl	*Taq* polymerase (5 U/µl)
10.4 µl	H$_2$O

Primers for genotyping of *Slap$^{-/-}$* mice:

SLAP fwd: 5' – CACTATGCCCTTTACCTTCT – 3'
SLAP WT rev: 5' – ACAGTGGGCTATTACAGGAC – 3'
SLAP NEO rev: 5' – TGGCTACCCGTGATATTGCTGAAGA – 3'

Resulting band sizes:

WT locus: 565 bp (SLAP fwd + SLAP WT rev)
KO locus: 242 bp (SLAP fwd + NEO rev)

Pipetting scheme for SLAP2 KO PCR (20 µl final volume):

1 µl	DNA template
4 µl	5x Phire$^®$ reaction buffer (Thermo Scientific)
0.4 µl	dNTPs (stock: 10 mM)
2 µl	forward primer (stock: 10 µM)
2 µl	reverse primer (stock: 10 µM)
0.6 µl	DMSO (stock: 100 %)
0.4 µl	Phire$^®$ Hot Start II DNA polymerase
9.6 µl	H$_2$O

Primers for genotyping of *Slap2^-/-* mice:

WT allele:

SLAP2 WT fwd: 5' – AGCCGCTGACCATCATCTCT – 3'
SLAP2 WT rev: 5' – CTCTGCCTGAGACTTCCG – 3'

KO allele:

SLAP2 KO fwd: 5' – ACCGAGTACAAGCCCACG – 3'
SLAP2 KO rev: 5' – CAGGCACCGGGCTTGC – 3'

Resulting band sizes:

WT locus: 350 bp (SLAP2 WT fwd + SLAP2 WT rev)
KO locus: 550 bp (SLAP2 KO fwd + SLAP2 KO rev)

Program for SLAP WT, SLAP KO and SLAP2 WT PCRs:

94 °C	7 min	
94 °C	1 min	
55.5 °C	1 min	35 cycles
68 °C	1 min 30 s	
72 °C	10 min	
4 °C	∞	

Program for SLAP2 KO PCR:

98 °C	30 s	
98 °C	5 s	
64.3 °C	5 s	35 cycles
72 °C	7 s	
72 °C	1 min	
4 °C	∞	

Pipetting scheme for LAT PCR (50 μl final volume):

1 μl	DNA template
5 μl	10x Taq buffer (+ KCl, - MgCl$_2$)
5 μl	MgCl$_2$ (stock: 25 mM)
1 μl	dNTPs (stock: 10 mM)
0.5 μl	forward primer (1:10 in H$_2$O, stock: 1 μg/ml)
0.5 μl	reverse primer (1:10 in H$_2$O, stock: 1 μg/ml)
0.5 μl	*Taq* polymerase (5 U/μl)
36.5 μl	H$_2$O

Primers for genotyping of *Lat^-/-* mice:

LAT fwd: 5' – AGCACCTTTCCAGAGCCAACA – 3'
LAT WT rev: 5' – TCATCCAGTTCCGCAAAGCTT – 3'
LAT NEO rev: 5' – GCATCGCCTTCTATCGCCTTC – 3'

Resulting band sizes:

WT locus: 300 bp (LAT fwd + LAT WT rev)
KO locus: 575 bp (LAT fwd + NEO rev)

Program for LAT PCR:

95 ºC	5 min	
95 ºC	1 min	
60 ºC	1 min	35 cycles
72 ºC	2 min	
72 ºC	5 min	
4 ºC	∞	

Pipetting scheme for detection of the *Syk* floxed allele by PCR (25 µl final volume):

1 µl	DNA template
2.5 µl	10x Taq buffer (+ KCl, - MgCl$_2$)
2.5 µl	MgCl$_2$ (stock: 25 mM)
1 µl	dNTPs (stock: 10 mM)
1 µl	forward primer (1:10 in H$_2$O, stock: 100 pmol/µl)
1 µl	reverse primer (1:10 in H$_2$O, stock: 100 pmol/µl)
0.25 µl	*Taq* polymerase (5 U/µl)
15.75 µl	H$_2$O

Primers for genotyping of *Syk*$^{fl/fl}$ mice:

Syk fl fwd: 5' – GGTGCCTACAGGTCTACAGC – 3'
Syk fl rev: 5' – AACCTGGTAATTTCATAACAGC – 3'

Resulting band sizes:

WT locus: 198 bp
Floxed locus: 285 bp

Program for Syk floxed PCR:

96 ºC	3 min	
94 ºC	30 s	
56 ºC	30 s	35 cycles
72 ºC	1 min	
72 ºC	10 min	
4 ºC	∞	

Pipetting scheme for detection of the *Cdc42* floxed allele by PCR (50 μl final volume):

2 μl	DNA template
5 μl	10x Taq buffer (+ KCl, - MgCl$_2$)
5 μl	MgCl$_2$ (stock: 25 mM)
2 μl	dNTPs (stock: 10 mM)
2 μl	forward primer (1:10 in H$_2$O, stock: 1 μg/ml)
2 μl	reverse primer (1:10 in H$_2$O, stock: 1 μg/ml)
0.5 μl	*Taq* polymerase (5 U/μl)
31.5 μl	H$_2$O

Primers for genotyping of *Cdc42$^{fl/fl}$* mice :

Cdc42 fl fwd: 5' - ATGTAGTGTCTGTCCATTGG – 3'
Cdc42 fl rev: 5' – TCTGCCATCTACACATACAC – 3'

Resulting band sizes:

WT locus: 200 bp
Floxed locus: 300 bp

Program for Cdc42 floxed PCR:

95 ºC	2 min	
95 ºC	30 s	
63 ºC	30 s	10 cycles
(-1 °C each cycle)		
72 ºC	45 s	
95 ºC	30 s	
53 ºC	30 s	35 cycles
72 ºC	45 s	
72 ºC	4 min	
4 ºC	∞	

Pipetting scheme for detection of the *RhoA* floxed allele by PCR (20 μl final volume):

2 μl	DNA template
2 μl	10x Taq buffer (+ KCl, - MgCl$_2$)
0.6 μl	MgCl$_2$ (stock: 25 mM)
0.4 μl	dNTPs (stock: 10 mM)
0.2 μl	forward primer (undiluted, stock: 1 μg/ml)
0.2 μl	reverse primer (undiluted, stock: 1 μg/ml)
0.2 μl	*Taq* polymerase (5 U/μl)
14.4 μl	H$_2$O

Primers for genotyping of *RhoA*^{fl/fl} mice:

RhoA fl fwd: 5' - AGCCAGCCTCTTGACCGATTTA – 3'
RhoA fl rev: 5' – TGTGGGATACCGTTTGAGCAT – 3'

Resulting band sizes:

WT locus: 297 bp
Floxed locus: 393 bp

Program for RhoA floxed PCR:

94 ºC	2 min	
94 ºC	30 s	
55 ºC	30 s	35 cycles
72 ºC	30 s	
72 ºC	10 min	
4 ºC	∞	

Pipetting scheme for detection of the PF4-Cre transgene by PCR (25 μl final volume):

1 μl	DNA template
2.5 μl	10x Taq buffer (+ KCl, - MgCl$_2$)
2.5 μl	MgCl$_2$ (stock: 25 mM)
1 μl	dNTPs (stock: 10 mM)
1 μl	forward primer (1:10 in H$_2$O, stock: 1 μg/ml)
1 μl	reverse primer (1:10 in H$_2$O, stock: 1 μg/ml)
0.25 μl	*Taq* polymerase (5 U/μl)
15.75 μl	H$_2$O

Primers:

PF4-Cre fwd: 5' - CCCATACAGCACACCTTTTG – 3'
PF4-Cre rev: 5' – TGCACAGTCAGCAGGTT – 3'

Resulting band sizes:

WT: no band
PF4-Cre+ : 450 bp

Program for PF4-Cre PCR:

95 ºC	5 min	
95 ºC	30 s	
58 ºC	30 s	35 cycles
72 ºC	45 s	
72 ºC	5 min	
4 ºC	∞	

Four µl 6x loading dye solution were added to 20 µl DNA product and the samples were analyzed on a 1.5% agarose gel.

2.2.2. Generation of plasma samples

Capillaries were anti-coagulated with sodium citrate or heparin and 100 µl blood was collected in tubes containing 100 µl heparin or Na-citrate. Samples were centrifuged for 5 min at 700 g, platelet-poor plasma was spun down for 5 min at 18,000 g and erythrocyte- and debris-free supernatants were immediately used for experiments or frozen at -20 °C.

2.2.3. Biochemistry

2.2.3.1. Western blotting (Immunoblotting)

Platelet-rich plasma (PRP) was obtained as described in Section 2.2.4.3. PRP was spun down at 700 g for 5 min and platelet pellets were washed twice in 5 mM EDTA/PBS. Pellets were solubilized in lysis buffer containing 1% IGEPAL CA-630 in a concentration of 1 x 10^6 platelets/µl and were lysed for 1 h on ice. Detergent-insoluble debris was removed by centrifugation at 18,000 g for 10 min, before 4x Laemmli SDS sample buffer was added to the supernatant and samples were boiled for 5 min at 95 °C. Proteins were separated by SDS-PAGE on polyacrylamide gels with a 10% or 12% separating part and a 4% stacking part. A total of 7.5 x 10^6 platelets per sample were loaded onto a gel, run in Laemmli buffer and blotted onto *polyvinylidene difluoride* (PVDF) membranes for 1 h with 0.8 mA/cm^2 membrane using semi-dry transfer systems. To prevent unspecific binding, membranes were blocked for 1 h at RT in 5% non-fat dried milk powder or 5% BSA dissolved in TBS/0.1% Tween$^®$ 20 (TBS-T) and then incubated o/n at 4 °C with primary antibodies. Membranes were washed 3x 15 min in TBS-T and incubated for 1 h at RT with *horseradish peroxidase* (HRP)-conjugated secondary antibodies. Upon extensive washing in TBS-T, membranes were developed using an *enhanced chemiluminescence* (ECL) detection system with autoradiography films or digitally on a Fluorchem™ Q device (Protein Simple, Santa Clara, CA, USA). If HRP-conjugated primary antibodies were used, membranes were incubated with the respective antibody for 1 h at RT. To re-probe a membrane, blots were incubated in stripping buffer for 30 min at RT, washed thoroughly in TBS-T, blocked and subsequently probed with antibodies. Actin, GAPDH or GPIIIa (integrin β3) levels were used as loading control.

2.2.3.2. Tyrosine phosphorylation studies

For identification of tyrosine phosphorylated proteins in platelets, washed platelets in suspension (1.4×10^8 platelets) were used. Platelets were prepared as described in Section 2.2.3.1. To avoid protein dephosphorylation by phosphatases present in certain preparations of BSA, platelets were washed once with Tyrode's buffer with BSA and all subsequent washing steps were carried out in Tyrode's buffer without BSA. To prevent aggregation, 2 U/mL apyrase, 5 mM EDTA and 10 μM indomethacin were added to the platelet suspension. Platelets were stimulated with convulxin or rhodocytin under stirring. Reaction was stopped at different time points by the addition of ice-cold 2x lysis buffer and samples were lysed for 30 min on ice. Cell debris was removed by centrifugation at 18,000 *g*. NuPAGE® 4x LDS buffer supplemented with β-mercaptoethanol was added to the supernatant. Samples were incubated at 70 ºC for 10 min and separated by SDS-PAGE on NuPAGE® 4-12% Bis-Tris gradient gels (Invitrogen) under reducing conditions. Gels were run in 1x MOPS buffer at 4 °C and proteins subsequently transferred onto a PVDF membrane. Membranes were blocked for 1 h at RT and then incubated o/n at 4 ºC with anti-phosphotyrosine antibody, clone 4G10, or with phospho-specific antibodies detecting anti-phospho-PLCγ2 (Y759) and anti-phospho-Syk (Y525/526). Rabbit anti-mouse immunoglobulins-HRP or goat-anti-rabbit-IgG HRP-conjugated antibodies and ECL were used for visualization. Actin levels or the respective non-phosphorylated proteins were used as loading control. Densitometry was conducted by volume analysis using ImageJ (version 1.46r, ImageJ software, National Institutes of Health, Bethesda, MD, USA).

2.2.3.3. Immunoprecipitation

Washed platelets in suspension (3×10^8) were prepared as described in Section 2.2.3.1. and subsequently treated with 2 U/ml apyrase, 5 mM EDTA and 10 μM indomethacin to prevent aggregation. Platelets were stimulated for 20 s with 0.5 μg/ml convulxin or left unstimulated at 37ºC under stirring. Reactions were terminated by the addition of ice-cold 2x lysis buffer. Samples were lysed for 1 h at 4ºC. Detergent-insoluble debris was removed by centrifugation at 16,000 *g* for 10 min and the supernatant was pre-cleared twice with protein A-Sepharose for 30 min at 4ºC. Samples were rotated with an anti-Lyn antibody (1 μg/sample) pre-coated to protein A-Sepharose for 1 h at 4ºC. Sepharose beads were pelleted, washed 4 times for 5 min with 1x lysis buffer and 2x non-reducing Laemmli SDS-sample buffer was added to the beads. Samples were boiled for 5 min and subsequently centrifuged for 10 min at 18,000 *g*. Supernatants were collected and samples were run on 12% SDS-PAGE gels, transferred onto a PVDF membrane and incubated with antibodies.

2.2.3.4. sGPVI ELISA

Nunc-Immuno™ MediSorp™ plates were coated o/n with 50 μl JAQ2 antibody (20 μg/ml), blocked with 5% milk/TBS-T for 2 h at 37 °C and washed twice with washing buffer. Mice were injected *intravenously* (i.v.) with JAQ1-IgG[biotin] (2 μg/g body weight (BW)) and blood samples were collected in heparin in Tris-buffered saline (TBS) (20 U/ml, pH 7.3) at the indicated time points. Plasma was isolated as described in Section 2.2.2., applied to the plates, incubated for 90 min at RT and washed extensively. Plates were incubated with HRP-labeled streptavidin for 45 min at RT, washed extensively and developed using 3,3,5,5-*tetramethylbenzidine* (TMB) substrate. The reaction was stopped by the addition of 0.5 M H_2SO_4. Optical densities were measured on a Multiskan Ex device (Thermo Electron Corporation, Braunschweig, Germany). Absorbance was read at 450 nm and the 620 nm filter served as reference wavelength. Samples from *$Gp6^{-/-}$* mice were measured in parallel as negative control.

2.2.3.5. Determination of platelet VWF and PF4 secretion by ELISA

Washed platelets were prepared as described in Section 2.2.4.3., diluted in Tyrode's buffer + 2 mM Ca^{2+} (5 x 10^5/μl) and were stimulated with 0.1 U/ml thrombin for 15 min at 37 °C under stirring. Samples were centrifuged for 5 min at 700 *g* and platelet aggregate-free supernatants were spun down for 5 min at 18,000 *g*.

For determination of VWF secretion, MTF ELISA plates were coated with 10 μg/ml rabbit anti-human antibody o/n at 4 °C and blocked with 5% BSA for 90 min at 37 °C. Sample dilutions were incubated for 2 h at 37 °C. After extensive washing with TBS-T, samples were incubated with an HRP-coupled rabbit anti-human VWF antibody. This anti-VWF antibody has been shown to cross-react with mouse VWF. After washing, ELISA plates were developed using TMB substrate and the reaction was stopped by the addition of 0.5 M H_2SO_4.

Platelet PF4 secretion levels were determined using a RayBio Mouse PF-4 (CXCL4) ELISA Kit according to the manufacturer's instructions. PF4 microplates pre-coated with anti-mouse PF4 were supplied together with the ELISA kit. Standards and samples (1:100 dilution) in duplicate were pipetted onto the microplates (100 μl/well) and incubated for 150 min at RT. After extensive washing with the provided washing buffer, wells were incubated with a biotinylated anti-mouse PF4 antibody for 1 h at RT with gentle shaking. Wells were extensively washed again, incubated with HRP-labeled streptavidin for 45 min at RT with gentle shaking and developed with TMB substrate for 30 min at RT in the dark with gentle shaking. Reactions were stopped by the addition of stop solution (0.2 M H_2SO_4).

Optical densities were measured on a Multiskan Ex device (Thermo Electron Corporation, Braunschweig, Germany). Absorbance was read at 450 nm and the 620 nm filter served as reference wavelength.

2.2.4. *In vitro* analyses of platelet function

2.2.4.1. Determination of platelet count, size and surface protein expression

To measure platelet count, size and surface protein expression, 50 μl blood were drawn from the retro-orbital plexus of anesthetized mice using heparinized capillaries and collected in a tube containing 300 μl heparin in *Tris-buffered saline* (TBS) (20 U/ml, pH 7.3). Blood was diluted 1:20 with Ca^{2+}-free Tyrode's buffer or 1x PBS and stained for 12 min with saturating amounts of fluorophore-conjugated antibodies described in Section 2.1.2.2. If unconjugated antibodies were used, samples were incubated with 10 μg/ml of the respective primary antibody for 12 min at RT. Reactions were stopped by the addition of 2 ml 1x PBS, samples spun down for 5 min at 700 *g*, supernatant discarded and blood pellet was subsequently incubated for 12 min at RT with saturating amounts of *fluorescein isothiocyanate* (FITC)-labeled secondary antibodies. In both cases, staining was stopped by the addition of 500 μl 1x PBS. Data were collected on a FACSCalibur (BD Biosciences, Heidelberg, Germany) and analyzed using FlowJo v7 software (FlowJo, LLC, Ashland OR, USA). Alternatively, platelet count and volume were determined on a Sysmex KX-21N™ Hematology Analyzer (Sysmex Europe, Norderstedt, Germany).

For determination of platelet counts prior to platelet transfer experiments (Section 2.2.5.3.), magnetic beads were used and platelet counts were calculated according to the following formula:[138]

$$\frac{A}{B} \times \frac{C}{D} = number\ of\ cells\ per\ \mu l$$

A = number of events for the test sample; B = number of events for the fluorescent particles; C = number of fluorescent particles per 50 μl (according to current batch of magnetic beads); D = volume of test sample initially used in μl.

2.2.4.2. Flow cytometric analysis of platelet activation responses

Whole blood was collected as described in Section 2.2.4.1. Ca^{2+}-free Tyrode's buffer (650 μl) was added to each sample and blood was centrifuged twice at 700 g for 5 min at RT and resuspended in Ca^{2+}-free Tyrode's buffer. Finally, samples were resuspended in 750 μl Tyrode's buffer + 2 mM Ca^{2+}. Washed blood (50 μl) or washed platelets (50 μl with 0.2 x 10^5 platelets/μl, preparation as described in Section 2.2.4.3.), were incubated with the respective agonist (10-fold concentrated) and saturating amounts of a 1:1 mixture of *phycoerythrin* (PE)-coupled 4H5 (anti-activated αIIbβ3) and FITC-coupled 5C8 (anti-P-selectin) antibodies. Samples were incubated for 7 min at 37 ºC and additionally for 7 min at RT. If necessary (e.g. low platelet counts), samples were additionally incubated for 3 min at RT with saturating amounts of a "gating" antibody (anti-GPIX-DyLight 649-conjugate). Reactions were stopped by the addition of 500 μl 1x PBS. Data were collected on a FACSCalibur (BD Biosciences, Heidelberg, Germany) and analyzed using FlowJo v7 software (FlowJo, LLC, Ashland OR, USA).

2.2.4.3. Preparation of washed platelets

Mice were bled under isoflurane anesthesia from the retro-orbital plexus with heparin-coated capillaries and blood was collected in 300 μl heparin/TBS (20 U/ml, pH 7.3). PRP was obtained by two centrifugation steps of 7 min at 800 rpm (Eppendorf Centrifuge 5415 C; 80 g without brake). PRP was spun down at 700 g for 5 min in the presence of prostacyclin (PGI$_2$) (0.1 μg/ml) and apyrase (0.02 U/ml). The platelet pellet was resuspended in Ca^{2+}-free Tyrode's buffer containing PGI$_2$ (0.1 μg/ml) and apyrase (0.02 U/ml) and incubated at 37 ºC for 10 min. This washing step was repeated and the platelet count of the suspension was determined using a Sysmex hematology analyzer. After centrifugation, the pellet was resuspended in Ca^{2+}-free Tyrode's buffer containing apyrase (0.02 U/ml) to adjust the platelet concentration. Platelet suspensions were incubated at 37 ºC for 30 min prior to analysis.

2.2.4.4. Aggregometry

Washed platelets (50 μl with 5 x 10^5 platelets/μl) were diluted into 110 μl Tyrode-HEPES buffer containing 2 mM Ca^{2+} and 100 μg/ml human fibrinogen (F3879). Fibrinogen-free Tyrode-HEPES buffer was used for aggregation studies with thrombin. Alternatively, heparinized PRP was used for investigation of ADP-induced aggregation. Agonists were added at indicated concentrations to the continuously stirring (1000 rpm) platelet suspension.

Light transmission was recorded on a Fibrintimer 4-channel aggregometer (APACT Laborgeräte und Analysensysteme, DiaSys Deutschland, Flacht, Germany) for 10 min and was expressed in arbitrary units with buffer representing 100% transmission and washed platelet suspension or PRP representing 0% transmission, respectively.

2.2.4.5. Luminometric measurement of ATP release

Washed platelets (80 μl with 5 x 10^5 platelets/μl) were diluted into 160 μl Tyrode-HEPES buffer containing 2 mM Ca^{2+} and incubated with Luciferase-Luciferin reagent under stirring conditions (1200 rpm), followed by addition of an agonist. ATP release and aggregation were measured simultaneously in a Lumi-aggregometer (Chrono-Log, Havertown, PA, USA).

2.2.4.6. Platelet adhesion on fibrinogen under static conditions

Rectangular glass coverslips (24 x 60 mm) were coated with 100 μg/ml human fibrinogen (F4883) diluted in sterile 1x PBS o/n at 4 °C under humidified conditions. Coverslips were blocked with 1% BSA/PBS for 2 h at RT and extensively washed with Tyrode-HEPES buffer containing 2 mM Ca^{2+}. Washed platelets (70 μl with 3 x 10^5 platelets/μl for early time points and 30 μl with 3 x 10^5 platelets/μl for late time points) were stimulated with thrombin (0.01 U/ml final concentration) and allowed to spread for the indicated time points at RT. Platelets were fixed with 4% *paraformaldehyde* (PFA) in 1x PBS and visualized with a Zeiss Axiovert 200 inverted microscope (100x/ *numerical aperture* (NA) = 1.4 oil objective, Zeiss, Oberkochen, Germany) using *differential interference contrast* (DIC) microscopy. Alternatively, platelets were fixed with PHEM buffer supplemented with 4% PFA and 1% IGEPAL CA-630, stained with anti-human-VWF-FITC, anti-α-tubulin Alexa F488 (B-5-1-2) and phalloidin-Atto647N, mounted with Fluoroshield and visualized using a Leica TCS SP5 confocal microscope (Leica Microsystems, Wetzlar, Germany).

2.2.4.7. Platelet adhesion on collagen under flow conditions

Rectangular cover slips (24 x 60 mm) were coated with 200 μg/ml fibrillar type I collagen (Horm) o/n at 37 °C and blocked for 1 h at RT with 1% BSA/PBS, rinsed with Tyrode-HEPES buffer containing 2 mM Ca^{2+} and gently fixed in a transparent flow chamber with a slit depth of 50 μm. Heparinized whole blood (700 μl blood in 300 μl heparin/TBS) was diluted with Tyrode-HEPES buffer containing 2 mM Ca^{2+} (two parts heparinized blood, one part buffer). Platelets were labeled with a DyLight 488 conjugated anti-GPIX Ig derivative (0.2 μg/ml) for 5 min at 37 °C and blood was filled into a 1 ml syringe which was connected to the flow

chamber. Perfusion was accomplished using a pulse-free pump under high shear stress equivalent to a wall shear rate of 1000 s^{-1} for 4 min. Microscopic phase-contrast images were recorded in real-time during perfusion. Thereafter, coverslips were washed by a 2 min perfusion with Tyrode-HEPES buffer containing 2 mM Ca^{2+} at the same shear rate. Phase-contrast and fluorescence images were obtained from at least seven different collagen-containing microscopic fields for each sample using a Zeiss Axiovert 200 inverted microscope (40x objective, NA = 0.75; Zeiss Oberkochen, Germany) and analyzed offline using Metavue software (Visitron, Puchheim, Germany). Thrombus formation under flow was characterized by the mean percentage of total area covered by thrombi (= surface coverage), and as the mean integrated fluorescence intensity per mm^2 (= thrombus size).

2.2.4.8. Analysis of *phosphatidylserine* (PS)-exposing platelets

Under flow conditions:

Rectangular cover slips (24 x 60 mm) were coated with 200 μg/ml fibrillar type I collagen (Horm) and blocked with 1% BSA. Heparinized whole blood was supplemented with additional 5 U/ml heparin and perfused over collagen coated coverslips through transparent flow chamber at a shear rate of 1000 s^{-1} as described above (Section 2.2.4.7.). The flow chamber was rinsed for 4 min with Tyrode-HEPES buffer containing 2 mM CaCl$_2$, 5 U/ml heparin, and 0.25 μg/ml annexin A5-DyLight 488. The flow chamber was rinsed for additional 2 min with Tyrode-HEPES buffer supplemented with 2 mM CaCl$_2$ and 5 U/ml heparin, before phase-contrast and fluorescence images were obtained using a Zeiss Axiovert 200 inverted microscope (40x objective, NA = 0.75; Zeiss Oberkochen, Germany) and analyzed offline using Metavue software (Visitron, Puchheim, Germany). Procoagulant activity was defined as the ratio of surface coverage of PS-exposing platelets (annexin A5-DyLight 488 staining of platelets) to the total surface covered by platelets.

Under static conditions:

Washed platelets were diluted into Tyrode-HEPES buffer containing 2 mM Ca^{2+} (50 μl with 0.5 x 10^5 platelets/μl) and incubated with agonists for 15 min at 37 ºC in the presence of saturating amounts of Alexa F488-coupled annexin A5. Reactions were stopped by the addition of 500 μl Tyrode-HEPES buffer containing 2 mM Ca^{2+}, data were immediately collected on a FACSCalibur (BD Biosciences, Heidelberg, Germany) and analyzed using FlowJo v7 software (FlowJo, LLC, Ashland OR, USA).

2.2.4.9. Thrombin generation assay

Thrombin generation was quantified in citrate-anticoagulated PRP (1×10^5 platelets/μl). PRP preparations were pooled from 2-4 mice with the same genotype. Platelets were activated with the indicated agonists for 10 min at 37°C. After stimulation, samples (4 vol) were transferred to a polystyrene 96-well plate containing 1 vol of thrombin calibrator or PRP reagent. Coagulation was started by adding 1 vol fluorescent thrombin substrate. Thrombin generation was measured according to the calibrated automated thrombogram method as previously described.[139] Samples were run in duplicate. Thrombin generation assays were performed by Sarah Schießl in our laboratory.

2.2.5. *In vivo* analyses of platelet function

2.2.5.1. Determination of platelet life span

Mice were injected i.v. with a DyLight 488-conjugated anti-GPIX-derivative (0.2 μg/g BW) for mice with normal peripheral platelet counts and 0.1 μg/g BW for KO mouse strains with endogenous platelet counts of < 50% of WT control). The anti-GPIX antibody labels circulating platelets without interfering with platelet activation *in vitro* or *in vivo*.[130] The antibody concentration applied was sufficient to label only circulating, but not newly generated platelets. Platelet clearance from the circulation was determined by daily blood withdrawal and subsequent flow cytometric analysis of the percentage of fluorescently labeled platelets.

2.2.5.2. Platelet depletion

Platelet depletion prior to platelet transfer:

Thrombocytopenia was induced in BALB/c WT mice by i.v. injection of anti-GPIbα antibodies (platelet depletion antibody, 0.15 μg/g BW). This low dosis of the platelet depletion antibody had no effect on the distribution of immune cell populations, hemoglobin or hematocrit levels over a period of 5 d after platelet depletion (data not shown). Peripheral platelet counts were determined by flow cytometry 12 h after platelet depletion as described above (Section 2.2.4.1.) using fluorescent particles. Mice with < 2.5% endogenous platelet counts were selected for platelet transfer experiments.

Immune thrombocytopenia:

Thrombocytopenia was induced by *intraperitoneal* (i.p.) injection of a platelet depletion antibody (2 μg/g BW; 1 μg/g BW for KO mouse strains with endogenous platelet counts of < 50% of WT control) and blood samples were collected at indicated time points until peripheral platelet counts recovered to values prior to platelet depletion.

2.2.5.3. Adoptive platelet transfer

Washed platelets from several donor mice were pooled and 10^9 platelets in 200 μl Tyrode's buffer were transferred i.v. to WT mice. Purity and resting state of the platelet suspension was ascertained by flow cytometry and microscopic inspection. Contamination by other blood cell types was further excluded using a fully automated hematology analyzer (Sysmex KX-21N™, Sysmex Europe, Norderstedt, Germany). Peripheral platelet counts were determined 30 min after platelet transfer and mice were subsequently subjected to $FeCl_3$-injury of the carotid artery, or 30 min of *transient middle cerebral artery occlusion* (tMCAO) (see below).

2.2.5.4. White blood cell transfer

WT and *Slap$^{-/-}$/Slap2$^{-/-}$* donor mice were treated with 0.5 μg/g body weight of platelet depleting anti-GPIbα antibodies 90 min prior to blood collection. White blood cells were isolated using a Histopaque® gradient (Sigma-Aldrich), washed in PBS/0.2% BSA and 10^6 cells in 100 μl PBS/0.2% BSA were transferred i.v. into WT mice which were subsequently subjected to 30 min of tMCAO.

2.2.5.5. Macrophage depletion

Mice were treated i.v. with clodronate-encapsulated or PBS-encapsulated liposomes (2 μl/g BW). Platelet counts and size were determined by flow cytometry prior to and 24, 48, 72 and 96 h after treatment.

2.2.5.6. Tail bleeding time

Saline method:

Mice were anesthetized, 1 mm of the tail tip was cut off with a scalpel and the tails were immersed in 0.9% isotonic saline (37 °C). The time until cessation of bleeding (no blood flow for 1 min) was determined.

Filter paper method:

Mice were anesthetized and 1 mm of the tail tip was cut off with a scalpel. Tail bleeding was monitored by gently absorbing blood on filter paper at 20 s intervals without making contact with the wound site. Bleeding was determined to have ceased when no blood was observed on the paper. Experiments were stopped manually after 20 min by cauterization to prevent excessive blood loss.

2.2.5.7. Splenectomy

Platelet counts were determined by flow cytometry and/or using a Sysmex hematology analyzer before surgical splenectomy. Mice were anesthetized by i.p. injection of triple anesthesia (medetomidine, midazolam, fentanyl) and placed in supine position on a heating pad to avoid hypothermia during surgery. Depth of anesthesia was ascertained by the application of a painful stimulus and forelimbs and hindlimbs were immoblized by adhesive bandages. The left upper abdominal cavity was exposed via a 1-cm-paramedian incision. After the spleen was identified, splenic arterial and venous supply was closed by ligation with knots placed with 5-0 prolene suture and the spleen was removed. The abdominal and skin incisions were closed with 5-0 prolene suture. Mice were monitored for 48 h for signs of internal bleeding and infection. After a recovery period of 7 d, platelet counts and size were followed over time and analyses of platelet and MK ultrastructure, platelet surface receptor levels, activation state and hemostatic function were performed at the indicated time points.

2.2.5.8. Intravital microscopy of thrombus formation in FeCl$_3$-injured mesenteric arterioles

Mice (4-to-5-week-old, 15–18 g) were anesthetized by i.p. injection of triple anesthesia (medetomidine, midazolam, fentanyl) and i.v. injected with 1.5 μg of a DyLight 488-conjugated anti-GPIX-derivative to label platelets *in vivo.* The mesentery was then gently exteriorized through a midline abdominal incision. Mesenterial arterioles with a diameter

between 35-60 μm were visualized with an inverted Axiovert 200 microscope (Zeiss, Oberkochen, Germany) (10x objective, NA = 0.30). The microscope was equipped with a 100 W mercury arc lamp to measure fluorescence and a CoolSNAP-EZ camera. Injury was induced by topical application of a 3 mm^2 filter paper saturated with 20% $FeCl_3$. Adhesion and aggregation of fluorescently labeled platelets was monitored until complete vessel occlusion occurred for at least 1 min or for a maximum of 40 min. MetaMorph software (Visitron, Puchheim, Germany) was used to record and analyze the digital images. Experiments were conducted by Dr. Martina Morowski in our laboratory.

2.2.5.9. Thrombus formation in $FeCl_3$-injured carotid arteries

An ultrasonic flow probe (0.5PSB699; Transonic Systems) was placed around the exposed carotid artery of anesthetized mice and thrombosis was induced by topical application of $FeCl_3$ for 90 s. $FeCl_3$ concentrations used were as follows: 2.5% for experiments with $Slap^{-/-}/Slap2^{-/-}$ mice and 15% for $RhoA^{fl/fl}/Cdc42^{fl/fl\ Pf4-Cre+}$. For $Slap^{-/-}/Slap2^{-/-}$ mice subjected to $FeCl_3$–induced injury of the carotid artery after adoptive platelet transfer, 7.5% $FeCl_3$ for 1 min was used. Blood flow was monitored until complete blood vessel occlusion occurred for at least 2 min, or for a maximum of 30 min. Surgery was performed by Dr. Martina Morowski and Sarah Schießl.

2.2.5.10. Mechanical injury of the abdominal aorta

An ultrasonic flow probe (0.5PSB699; Transonic Systems) was placed around the abdominal aorta of anesthetized mice and thrombus formation was induced by a single firm compression with forceps for 10 s. Blood flow was monitored until complete blood vessel occlusion occurred for at least 5 min, or for a maximum of 30 min. Experiments were conducted by Dr. Martina Morowski.

2.2.5.11. Transient middle cerebral artery occlusion (tMCAO)

Surgery was carried out by Dr. Peter Kraft and Dr. Michael Schuhmann from the Department of Neurology (University of Würzburg) according to the recommendations in mechanism-driven basic stroke research.[140] Focal cerebral ischemia was induced in 8-to-12-week-old mice by a *transient middle cerebral artery occlusion* (tMCAO) as previously described.[141] Briefly, anesthesia was induced by 2% isoflurane in a 70% N_2/30% O_2 mixture and a servo-controlled heating device was used to record and maintain body temperature during the surgical procedure. Operation time per animal was kept below 15 min. A silicon rubber–

coated 6.0 nylon monofilament (6021PK10, Doccol, Redlands, CA, USA) was advanced through the carotid artery up to the origin of the *middle cerebral artery* (MCA) causing an MCA infarction. After an occlusion time of 30 min, the filament was removed allowing reperfusion of the MCA territory. The extent of infarction was quantitatively assessed 24 h after reperfusion on *2,3,5-triphenyltetrazolium chloride* (TTC) (2% (w/v) solution) stained brain sections. Global neurological outcome and motor function were evaluated by the Bederson score[142] and the grip test,[143] respectively. Planimetric measurements of infarcted areas (ImageJ software, National Institutes of Health, Bethesda, MD, USA) corrected for brain edema[144] and assessment of functional outcome were performed in a blinded fashion by members of the laboratories of Prof. Dr. Guido Stoll and Prof. Dr. Christoph Kleinschnitz (Department of Neurology, University of Würzburg).

2.2.6. *Megakaryocyte* (MK) studies

2.2.6.1. *In vitro* differentiation and cultivation of fetal liver cell-derived MKs

Embryonic day 13.5 – 14.5 (E13.5 – 14.5) mouse embryos were dissected in sterile 1x PBS. Fetal livers were transferred into 1 ml pre-warmed *Iscove's Modified Dulbecco's Medium* (IMDM) and homogenized by being twisted through an 18-gauge (18G) and a 22G needle with a 1 ml syringe. Cell suspensions were centrifuged at 900 rpm (Heraeus Multifuge 3S-R Thermo Scientific, Braunschweig, Germany) for 5 min at RT. The supernatant was discarded and cells were resuspended in 3 ml MK differentiation medium. Single-cell suspensions were divided into 3 wells per liver of a 12-well plate and cultured for 2 days at 37 °C and 5% CO_2 in a humidified incubator.

On day 3 of culture, MKs were enriched by a 2-step density gradient filtration with 3% BSA (lower phase) and 1.5% BSA (upper phase). Cell suspensions were centrifuged at 200 g for 5 min at RT. Cell pellets were resuspended in 1 ml pre-warmed IMDM, gently overlaid on the upper phase of the BSA gradient and incubated for 30-45 min at RT. Approximately 3.2 ml of the density gradient and cell suspension were removed and the lowest 800 µl containing sedimented MKs were diluted in 10 ml IMDM and centrifuged at 200 g for 5 min at RT. Cell pellets were resuspended in 1 ml MK differentiation medium and incubated in a 12-well plate for additional 24 h at 37° C and 5% CO_2 in a humidified incubator. On day 4 of culture, MKs were analyzed for proplatelet formation under a light microscope (20x objective). A minimum of 10 visual fields containing at least 10 differentiated MKs without contact inhibition were counted per well and the percentage of proplatelet-producing MKs per visual field was determined. Images of proplatelet-forming MKs were acquired using a Zeiss Axiovert 200 imaging microscope (Zeiss, Oberkochen, Germany).

2.2.6.2. *In vitro* differentiation and cultivation of *bone marrow* (BM)-derived MKs

Hematopoietic stem cells were isolated by flushing BM cells from femora of male mice followed by a negative selection using a magnetic bead-based negative depletion kit (Dynabeads®, with a polyclonal sheep anti-rat IgG antibody bound to the beads surface) according to the manufacturer's protocol (Life Technologies). MK precursor cells were enriched by removing other cell types using 0.5 μg/10^7 cells of the following rat anti-mouse antibodies which were coupled to the magnetic beads: CD45R/B220, TER-119, CD3, Ly-6G/C and CD11b. Cells were cultured in MK differentiation medium supplemented with 50 ng/ml recombinant Thpo and 50 μg/ml recombinant hirudin at 37°C, 5% CO_2 for 3 days, prior to MK purification using a 1.5%-3% BSA gradient as described in Section 2.2.6.1.

2.2.6.3. Fluorescent staining of MKs

Cultured MKs were spun onto glass slides (Shandon Cytospin 4, Thermo Scientific, Braunschweig, Germany), fixed and permeabilized with PHEM buffer supplemented with 4% PFA and 1% IGEPAL CA-630, stained with anti-α-tubulin Alexa F488 (B-5-1-2) and phalloidin-Atto647N, mounted with Fluoroshield containing DAPI, visualized using a Leica TCS SP5 confocal microscope (Leica Microsystems, Wetzlar, Germany) and further processed with ImageJ (version 1.46r, ImageJ software, National Institutes of Health, Bethesda, MD, USA).

2.2.6.4. Hematoxylin/eosin staining of paraffin sections

Spleen and femora of 8-to-12-week-old mice were fixed in 4% PFA/PBS o/n at 4 °C. Organs were washed in 1x PBS. Spleens were immediately dehydrated and embedded in paraffin, whereas femora were treated with decalcification buffer at RT for 5 days (daily exchange of buffer). Upon dehydration and paraffin embedding, organs were sectioned on a Microm HM 355 (Walldorf, Germany) (section thickness 5 μm). Staining was performed at RT. For deparaffinization, slides were incubated twice in xylol for 3 min. Samples were rehydrated by treatment with decreasing concentrations of ethanol (100%, 96%, 90%, 80% and 70%) and deionized H_2O (incubation for 2 min per step). Sections were stained with hematoxylin for 30 sec and washed with tap water for 10 min prior to staining with 0.05% Eosin Y for 2 min. Slides were briefly washed in deionized H_2O and dehydrated in ethanol in reverse order (70%, 80%, 90%, 96% and 100% ethanol), followed by incubation in xylol (2x 3 min). Slides

were mounted with xylol-based medium (Eukitt®, Sigma-Aldrich). Images were acquired using a Leica DMI 4000 B imaging microscope (Wetzlar, Germany).

2.2.6.5. Immunofluorescence staining of whole femora cryosections

Mouse femora were isolated, fixed in 4% PFA/PBS containing 5 mM sucrose for 2 h at RT and subsequently transferred into 10% sucrose/PBS and dehydrated using a graded sucrose series (incubation in 10% sucrose/PBS, followed by 20% sucrose/PBS and 30% sucrose/PBS, respectively, for 24 h at 4 °C). Samples were embedded in Cryo-Gel and shock-frozen in liquid nitrogen. Cryosections were produced using a CryoJane tape transfer system (Leica Biosystems, Wetzlar, Germany). MKs were visualized using anti-GPIb antibodies, whereas endothelium was stained with an anti-CD105 antibody. Nuclei were counterstained with *4',6-diamidino-2-phenylindole* (DAPI). Samples were visualized on a Leica TCS SP5 confocal microscope (Leica Microsystems, Wetzlar, Germany).

2.2.6.6. Determination of MK ploidy

Both femora of male mice were isolated and BM flushed and resuspended in 2 ml modified CATCH buffer. One tenth of the cell suspension was centrifuged for 5 min at 1200 rpm (Heraeus Multifuge 3S-R Thermo Scientific, Braunschweig, Germany) and resuspended in CATCH buffer containing 5% FSC/PBS. Unspecific binding sites were blocked by incubation with an anti-CD16/CD32 antibody (FcγRII/III, clone 2.4G2) for 15 min on ice. Subsequently, samples were stained with a FITC-conjugated anti-CD41 Ig derivative (clone MWReg30) or with an isotype-matched control rat anti-mouse antibody for 20 min on ice. Staining was stopped by the addition of CATCH buffer supplemented with 5% FSC/PBS. Cells were fixed in 1x PBS containing 1% PFA/0.1% EDTA for 10 min on ice, washed with 1x PBS, permeabilized in 0.1% Tween® 20/PBS for 10 min on ice and stained with a propidium iodide staining solution containing RNase A o/n at 4 °C in the dark. Data were collected on a FACSCalibur (BD Biosciences, Heidelberg, Germany) and analyzed using FlowJo v7 software (FlowJo, LLC, Ashland OR, USA).

2.2.6.7. Determination of plasma *thrombopoietin* (Thpo) levels

Plasma Thpo levels were determined using a Mouse Thrombopoietin DuoSet kit (R&D Systems). 96-well microplates were coated o/n at 4 °C with 100 μl/well of a rat anti-mouse Thpo antibody diluted in 1x PBS (2 μg/ml final concentration). Wells were washed three times with PBS/0.05% Tween® 20 (PBS-T), subsequently blocked for 1 h at RT with

1% BSA/PBS and washed again with PBS-T. Blood samples were collected in Na-citrate, plasma was isolated as described in Section 2.2.2. and diluted 1:4 in reagent diluent (1% BSA/PBS supplemented with 2% heat inactivated normal goat serum). Standards and samples were pipetted onto the microplates (100 μl/well) in duplicate and incubated for 2 h at RT. Upon extensive washing with PBS-T, wells were incubated with biotinylated goat anti-mouse Thpo antibodies for 2 h at RT. Microplates were extensively washed with PBS-T, incubated with HRP-labeled streptavidin for 20 min at RT, washed again with PBS-T and developed with TMB substrate. Reactions were stopped by the addition of 1 M H_2SO_4. Optical densities were measured on a Multiskan Ex device (Thermo Electron Corporation, Braunschweig, Germany). Absorbance was read at 450 nm and the 620 nm filter served as reference wavelength.

2.2.7. Electron microscopy

2.2.7.1. *Transmission electron microscopy* (TEM) analysis of resting platelets in suspension

For TEM analysis, PRP was isolated as described in Section 2.2.4.3. and let rest for 30 min at 37 °C in the presence of apyrase (0.02 U/ml). PRP was incubated with 2.5% glutar-aldehyde in 0.1 M cacodylate buffer for 10 min at 37 ºC, 1 h at RT and at 4 ºC until further processing. Samples were washed 3 times for 5 min in 1 ml cacodylate buffer and subsequently centrifuged at 1500 *g* for 5 min at 37 °C. A 2% low melting agarose solution in cacodylate buffer was kept at 45 °C. After the final washing step, platelets were carefully resuspended in 1 ml 2% agarose solution and centrifuged at 18,000 *g* for 5 min at 37 °C. Approximately 100 μl agarose solution were retained, the remaining supernatant was discarded and samples were incubated on ice for 10 min. Hardened agarose pellets were cut into approximately 1 mm^2 pieces and transferred into cacodylate buffer until fixation in 1% osmium tetroxide (in cacodylate buffer) for 1 h at RT. Samples were washed twice with ddH_2O and incubated in 2% uranyl acetate in ddH_2O for 1 h at 4 °C. Upon extensive washing (3x ddH_2O), samples were dehydrated in 70% (4x 5 min), 95% (3x 15 min) and 100% (3x 15 min) ethanol and incubated in 100% propylene oxide (2x 10 min), and subsequently in a 1:1 mixture of propylene oxide/epon for 1 h at RT under rotation. Two further incubation steps in epon at RT followed (for 2-3 h under rotation). Samples were embedded in gelatin capsules, left to harden for 48 h at 60 ºC and sectioned on an ultra microtom (Leica Ultracut UCT, Wetzlar, Germany) (section thickness 50 nm), contrasted and analyzed on a Zeiss EM900 transmission electron microscope (Zeiss, Oberkochen, Germany).

2.2.7.2. TEM analysis of BM MKs *in situ*

For TEM analysis of BM MKs, femora of mice were incubated in Karnovsky's fixative for 10 min at RT and subsequently o/n at 4 °C under rotation. Femora were treated with decalcification buffer at RT for 5 days (daily exchange of buffer) and subsequently washed with 50 mM cacodylate buffer 3x 10 min at 4 °C. Samples were then fixed with 2% osmium tetroxide in 50 mM sodium cacodylate (pH 7.2) for 2 h at 4 °C, washed with ddH$_2$O and subsequently stained o/n with 0.5% aqueous uranyl acetate. Upon dehydration with ethanol and embedding in Epon 812, ultrathin sections were stained with 2% uranyl acetate (in 100% ethanol) followed by lead citrate as described.[145] Samples were analyzed on a Zeiss EM900 transmission electron microscope (Zeiss, Oberkochen, Germany).

2.2.7.3. Transmission electron microscopy analysis of occlusive thrombi in FeCl$_3$-injured carotid arteries

The right carotid artery of *wild-type* (WT) and *Slap$^{-/-}$/Slap2$^{-/-}$* mice was injured by topical application of 5% FeCl$_3$ for 1 min, or 10% FeCl$_3$ for 1 min (only WT mice) and blood flow was monitored with a Doppler flow probe until complete vessel occlusion occurred for at least 2 min, or for a maximum of 30 min as described in Section 2.2.5.9. Carotid arteries were excised, incubated in Karnovsky's fixative, postfixed in 2% osmium tetroxide in 50 mM cacodylate buffer, dehydrated and embedded in epoxy resin. Semithin sections (0.5 µm) were stained in toluidine blue. Upon identification of the thrombus, ultrathin sections (50 nm) were prepared and stained with 2% uranyl acetate and lead citrate. Sections were analyzed on an EM900 electron microscope (Zeiss, Oberkochen, Germany).

2.2.8. Statistical analyses

Results are shown as mean ± SD from three individual experiments per group, unless indicated otherwise. Statistical analysis was conducted using the Student's t-test, apart from the Fischer's exact test which was applied to assess variance between non-occluded vessels in models of arterial thrombosis or in tail bleeding assays and the Mann-Whitney U test which was used for analysis of Bederson score and grip test after tMCAO. Differences between more than two groups were analyzed with one-way ANOVA with Dunnett's T3 as post-hoc test, with SPSS 21. *P*-values < .05 were considered statistically significant.

3. Results

3.1. SLAP/SLAP2 prevent excessive platelet (hem)ITAM signaling in arterial thrombosis and ischemic stroke in mice

SLAP proteins have been identified as negative regulators of TCR and BCR expression levels and signaling.[75] Platelet GPVI/FcRγ signaling resembles the signaling pathways downstream of the TCR and BCR complexes. Therefore, it has been hypothesized that SLAP and SLAP2 might have the capacity to regulate (hem)ITAM signaling in platelets. This hypothesis has been initially tested in the laboratory of Dr. Michael Tomlinson (University of Birmingham, UK). It has been demonstrated that overexpression of SLAP or SLAP2 in a heterologous cell line almost completely inhibited GPVI and CLEC-2 signaling without affecting expression levels of transfected GPVI or CLEC-2.[146]

3.1.1. Absence of SLAP or SLAP2 has only mild effects on platelet activation *in vitro*

To extend these previous data obtained in a heterologous system and to further investigate the role of SLAP family proteins in platelet biology, mice deficient for SLAP[86] or SLAP2[133] were analyzed. Western blot analysis confirmed the absence of SLAP in *Slap*^{-/-} and of SLAP2 in *Slap2*^{-/-} platelet lysates (Figure 7A and Figure 8A). Furthermore, upregulation of SLAP expression in *Slap2*^{-/-} platelets was observed (increase by ~35% compared to WT platelets) (Figure 8A). The two SLAP2 protein bands of 25 and 28 kDa are in line with previous reports that alternative translation leads to the expression of two SLAP2 isoforms (Figure 7A, Figure 8A, arrowheads).[72-74] *Slap*^{-/-} and *Slap2*^{-/-} mice had normal platelet counts and size (Table 3-1).

Flow cytometric measurement of prominent platelet surface receptors and Western blot analysis showed slightly increased surface expression of GPVI in *Slap*^{-/-} platelets, whereas CLEC-2 levels were slightly elevated in *Slap2*^{-/-} platelets (Table 3-1, Figure 7B, Figure 8B). The effect of SLAP or SLAP2 deficiency on platelet activation was analyzed by aggregation studies and flow cytometric measurements of agonist-induced inside-out activation of $\alpha IIb\beta 3$ integrin and degranulation-dependent P-selectin surface exposure.

	WT	*Slap*^{-/-}	WT	*Slap2*^{-/-}
Platelets (nl^{-1})	985 ± 139	1106 ± 66	1145 ± 62	1215 ± 132
MPV (fl)	5.64 ± 0.25	5.54 ± 0.15	5.56 ± 0.15	5.46 ± 0.17
GPIb	337 ± 10	357 ± 31	335 ± 9	355 ± 25
GPV	237 ± 15	254 ± 20	248 ± 5	258 ± 19
GPIX	372 ± 19	380 ± 37	381 ± 6	404 ± 24
CD9	1114 ± 19	1119 ± 63	1068 ± 20	1046 ± 20
GPVI	55 ± 2	60 ± 2*	50 ± 3	50 ± 2
CLEC-2	129 ± 5	126 ± 15	117 ± 2	127 ± 4†
α2	41 ± 1	42 ± 1	43 ± 1	43 ± 1
β1	97 ± 9	102 ± 4	109 ± 2	110 ± 6
αIIbβ3	522 ± 46	558 ± 34	565 ± 15	549 ± 23
WBC (nl^{-1})	8.00 ± 1.63	8.50 ± 1.91	9.20 ± 1.79	7.20 ± 1.10
RBC (x 10^3 nl^{-1})	715 ± 30	830 ± 173	636 ± 63	584 ± 36
HCT (%)	36.00 ± 1.63	42.00 ± 8.49	31.60 ± 2.97	32.00 ± 2.00
HGB (g dl^{-1})	10.00 ± 0	13.00 ± 3.46	10.40 ± 0.89	10.40 ± 0.89

Table 3-1. Analysis of surface expression of glycoproteins in WT, *Slap*^{-/-} and *Slap2*^{-/-} platelets. Diluted whole blood was stained with saturating amounts of fluorophore-labeled antibodies and platelets were analyzed by flow cytometry. Results express MFI ± SD (n = 4 mice per group) and are representative of 3 independent experiments. Basic blood parameters were analyzed on a Sysmex KX-21N™ Hematology Analyzer. MPV: *mean platelet volume*; WBC: *white blood cells*; RBC: *red blood cells*; HCT: *hematocrit*; HGB: *hemoglobin*. *$P < .05$, †$P < .01$. (Cherpokova *et al.*, *Blood* 2015)[146]

Stimulation of platelets with GPVI-specific agonists - *collagen-related peptide* (CRP) or the snake venom protein convulxin - or with the CLEC-2 agonist rhodocytin, resulted in slightly elevated integrin activation and α-granule release, in particular at high agonist concentrations (Figure 7C-D, Figure 8C-D). In contrast, activation responses to low concentrations of (hem)ITAM-specific agonists or to soluble agonists operating via *G protein-coupled receptors* (GPCR), such as ADP, the thromboxane A$_2$ analog U-46619 and thrombin, were normal. These results suggested a potential negative regulatory function for SLAP family proteins downstream of (hem)ITAM receptors in platelets, but functional compensation might be largely masking this in the single knockouts.
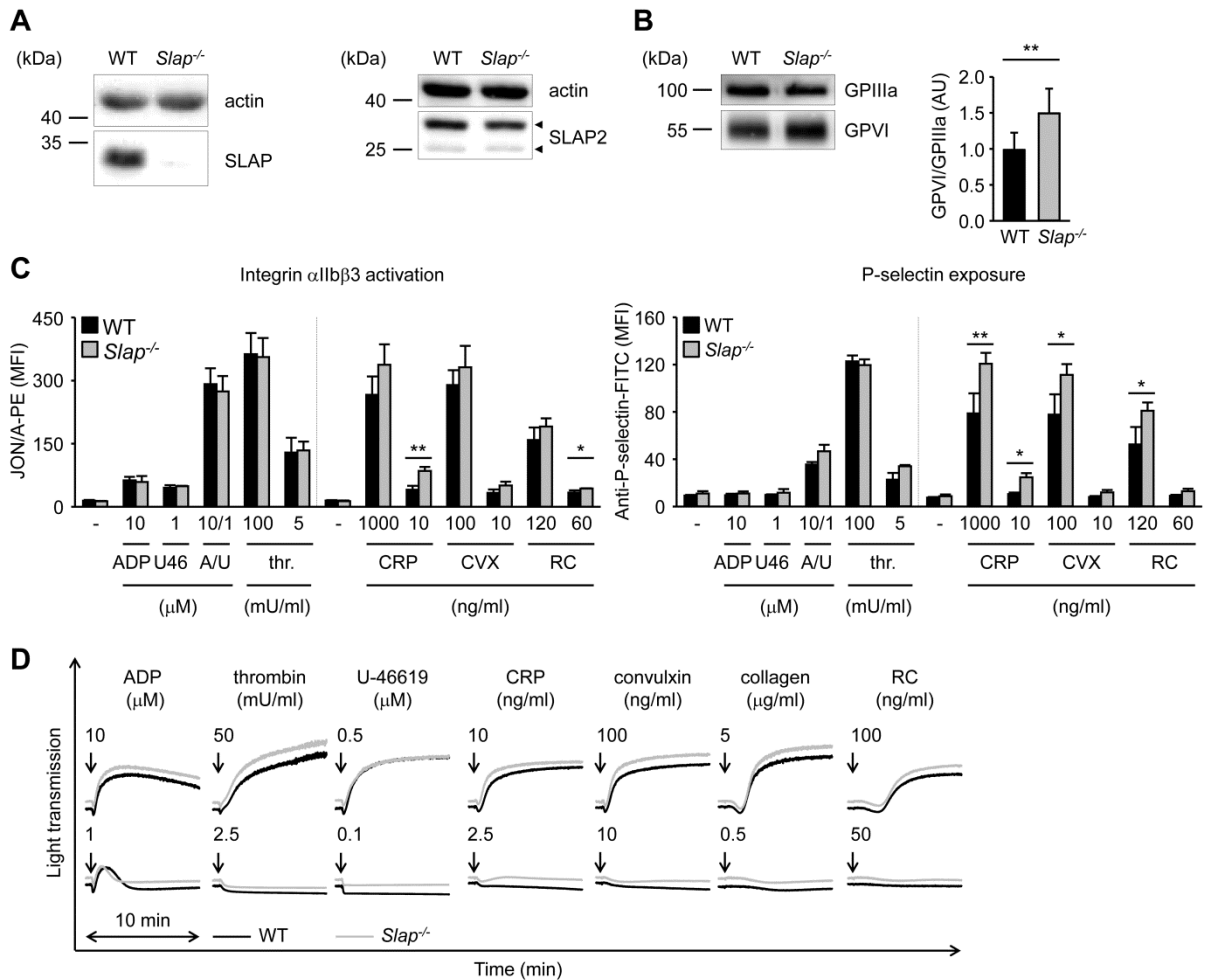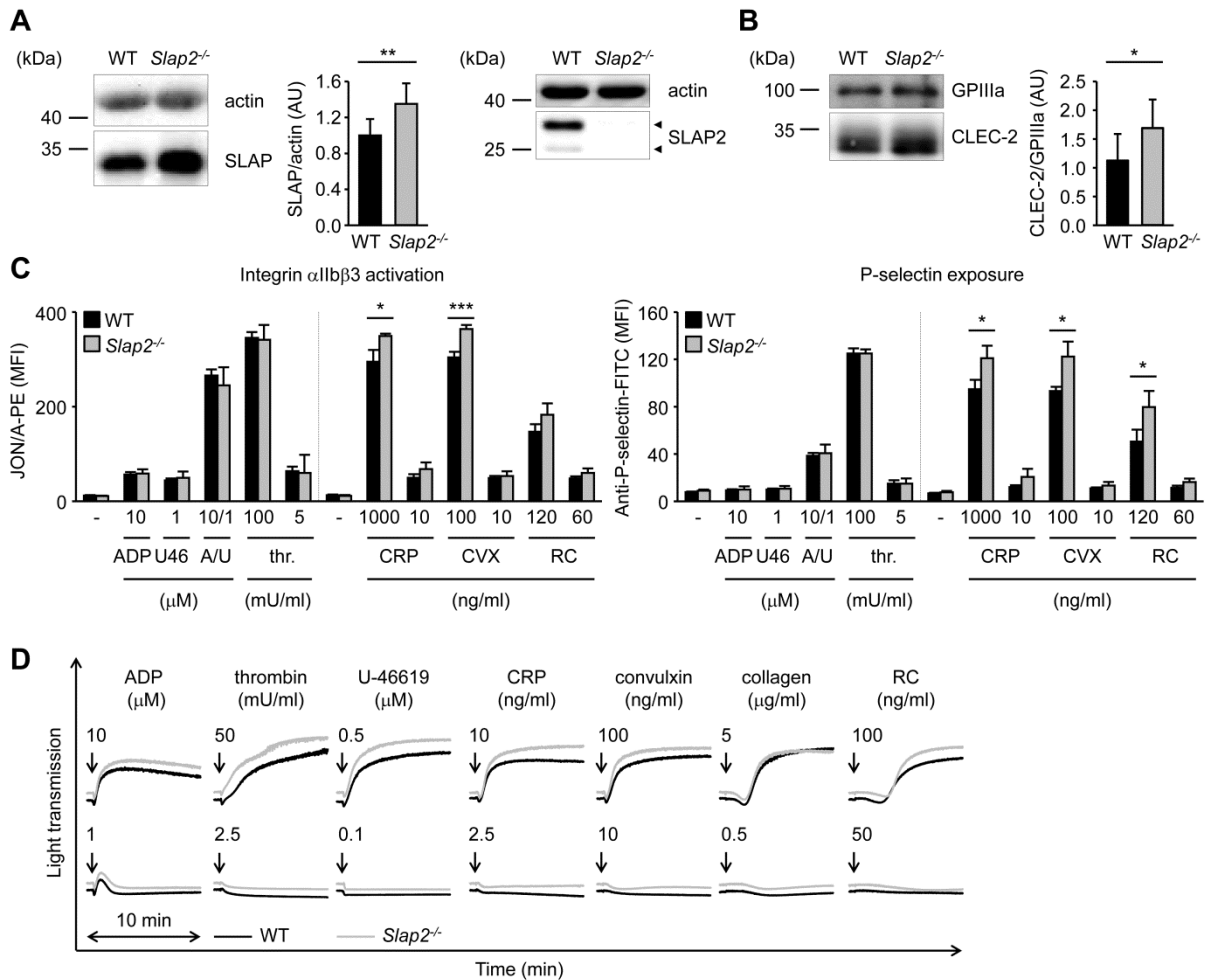
Figure 7. Unaltered integrin activation, α-granule release and aggregation response of *Slap*^{−/−} platelets. (A) Western blot analysis demonstrating absence of SLAP (left panel) and unaltered expression of SLAP2 (right panel) in *Slap*^{−/−} platelets. Arrowheads indicate both SLAP2 isoforms (25 and 28 kDa). Actin expression was used as loading control. (B) Western blot analysis of GPVI expression in *Slap*^{−/−} platelets. GPIIIa expression was used as loading control and for quantification. Equal protein amounts were loaded and expression levels were quantified by densitometry with ImageJ software (NIH, USA) on 8 samples per genotype. Results represent mean ± SD. Expression levels were adjusted such that the GPVI-to-GPIIIa ratio in WT platelets was set to 1. (C) Flow cytometric analysis of activated integrin αIIbβ3 (binding of JON/A-PE) (left panel) and degranulation-dependent P-selectin exposure (right panel) upon stimulation with the indicated agonists in WT and *Slap*^{−/−} platelets. Results are expressed as MFI ± SD (n = 4 mice per group) and are representative of 4 independent experiments. Dividing lines indicate separate measurements. (D) Washed platelets were activated with the indicated agonists and light transmission was recorded on a Fibrintimer 4-channel aggregometer. ADP measurements were performed in PRP. Aggregation traces representative of 2 independent experiments with n = 3 are depicted. Arrows indicate addition of the respective agonist. U46, U-46619; A/U, ADP + U-46619; thr., *thrombin*; CVX, *convulxin*; CRP, *collagen-related peptide*; RC, *rhodocytin*. *P < .05; **P < .01. (Cherpokova *et al.*, *Blood* 2015)[146]

Figure 8. Unaltered integrin activation, α-granule release and aggregation response of Slap2^{-/-} platelets. (A) Western blot analysis demonstrating increased expression of SLAP (left panel) and absence of SLAP2 (right panel) in *Slap2^{-/-}* platelets. Arrowheads indicate both SLAP2 isoforms (25 and 28 kDa) in WT platelets. Actin expression was used as loading control and for quantification. (B) Western blot analysis of CLEC-2 expression in *Slap2^{-/-}* platelets. GPIIIa expression was used as loading control and for quantification. (A, B) Equal protein amounts were loaded and expression levels were quantified by densitometry with ImageJ software (NIH, USA) on 10 (A) or 8 (B) samples per genotype. Results represent mean ± SD. Expression levels were adjusted such that SLAP-to-actin (A) or CLEC-2-to-GPIIIa (B) ratio in WT platelets was set to 1. (C) Flow cytometric analysis of activated integrin αIIbβ3 (binding of JON/A-PE) (left panel) and degranulation-dependent P-selectin exposure (right panel) upon stimulation with the indicated agonists in WT and *Slap2^{-/-}* platelets. Results are expressed as MFI ± SD (n = 4 mice per group) and are representative of 4 independent experiments. Dividing lines indicate separate measurements. (D) Washed platelets were activated with the indicated agonists and light transmission was recorded on a Fibrintimer 4-channel aggregometer. ADP measurements were performed in PRP. Aggregation traces representative of 2 independent experiments with n = 3 are depicted. Arrows indicate addition of the respective agonist. U46, U-46619; A/U, ADP + U-46619; thr., *thrombin*; CVX, *convulxin*; CRP, *collagen-related peptide*; RC, *rhodocytin*. *$P < .05$; **$P < .01$; ***$P < .001$. (Cherpokova *et al.*, *Blood* 2015)[146]

3.1.2. *Slap^{-/-}/Slap2^{-/-}* platelets are hyperreactive to (hem)ITAM-specific agonists

To assess a potential functional redundancy of the two adapter proteins, SLAP/SLAP2 double-deficient mice were generated and absence of both proteins confirmed by Western

blot analysis of platelet lysates (Figure 9A). *Slap$^{-/-}$/Slap2$^{-/-}$* platelets exhibited a significant ($P < .001$) ~23% increase in surface expression of GPVI and ~15% increase in CLEC-2 compared to WT controls, as determined by flow cytometry (Table 3-2) and confirmed by Western blot analyses (Figure 9B). Expression of all other major platelet surface receptors was unaltered (Table 3-2).

	WT	*Slap$^{-/-}$/Slap2$^{-/-}$*
Platelets (nl^{-1})	1129 ± 201	1191 ± 199
MPV (fl)	5.6 ± 0.26	5.53 ± 0.13
GPIb	335 ± 12	306 ± 25
GPV	357 ± 19	344 ± 34
GPIX	536 ± 40	509 ± 37
CD9	1437 ± 60	1464 ± 101
GPVI	57 ± 2	70 ± 3*
CLEC-2	109 ± 4	125 ± 4*
α2	52 ± 2	53 ± 5
β1	146 ± 7	154 ± 14
αIIbβ3	528 ± 41	599 ± 55
WBC (nl^{-1})	5.88 ± 1.45	5.6 ± 1.64
RBC (x 10^3 nl^{-1})	638 ± 34	718 ± 145
HCT (%)	32.48 ± 1.61	37.38 ± 7.06
HGB (g dl^{-1})	9.94 ± 0.91	11.62 ± 2.02

Table 3-2. Analysis of surface expression of glycoproteins in WT and *Slap$^{-/-}$/Slap2$^{-/-}$* platelets. Diluted whole blood was stained with saturating amounts of fluorophore-labeled antibodies and platelets were analyzed by flow cytometry. Results express MFI ± SD (n = 4 mice per group) and are representative of 5 independent experiments. Basic blood parameters were analyzed on a Sysmex KX-21N™ Hematology Analyzer. MPV: *mean platelet volume*; WBC: *white blood cells*; RBC: *red blood cells*; HCT: *hematocrit*; HGB: *hemoglobin*. *P < .001. (Cherpokova *et al.*, *Blood* 2015)[146]

Slap$^{-/-}$/Slap2$^{-/-}$ platelets displayed a marked hyperreactivity in response to GPVI or CLEC-2 stimulation (Figure 9C, Figure 10A-B). This effect was most evident at sub-threshold concentrations of GPVI agonists - CRP, convulxin and collagen - and the CLEC-2 agonist rhodocytin, which did not induce activation of WT platelets, but resulted in integrin activation, α- and dense-granule secretion (assessed by ATP release upon activation) and robust aggregation of the mutant platelets. Importantly, activation responses to GPCR-specific agonists were unaltered in *Slap$^{-/-}$/Slap2$^{-/-}$* platelets (Figure 9C, Figure 10A-B). Together, these results indicated that SLAP and SLAP2 have redundant functions in the regulation of (hem)ITAM signaling in platelets.
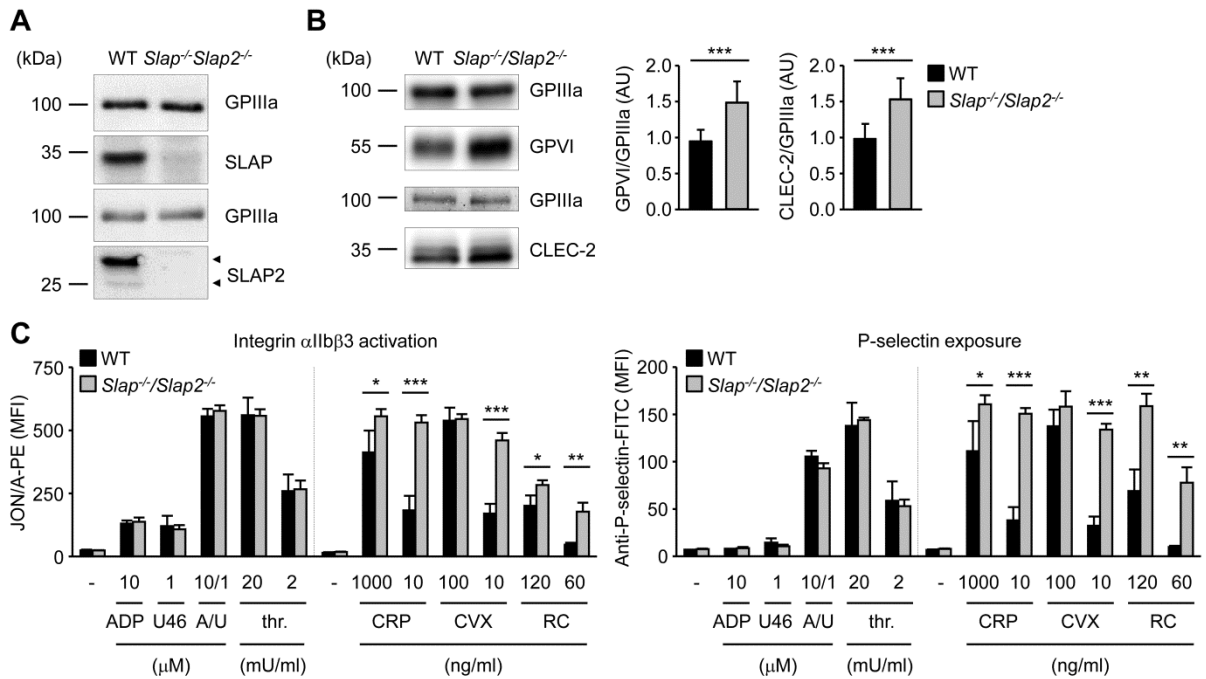
Figure 9. Increased integrin activation and α–granule release in *Slap⁻ᐟ⁻/Slap2⁻ᐟ⁻* platelets upon GPVI or CLEC-2 stimulation. (A) Western blot analysis demonstrating absence of SLAP and SLAP2 in *Slap⁻ᐟ⁻/Slap2⁻ᐟ⁻* platelets. GPIIIa expression was used as loading control. Arrowheads indicate both SLAP2 isoforms (25 and 28 kDa) in WT platelets. (B) Western blot analysis of GPVI and CLEC-2 expression in *Slap⁻ᐟ⁻/Slap2⁻ᐟ⁻* platelets. GPIIIa expression was used as loading control and for quantification. Equal protein amounts were loaded and expression levels were quantified by densitometry with ImageJ software (NIH, USA) on 12 samples per genotype. Results represent mean ± SD. Expression levels were adjusted such that GPVI-to-GPIIIa or CLEC-2-to-GPIIIa ratio in WT platelets was set to 1. (C) Flow cytometric analysis of activated integrin αIIbβ3 (binding of JON/A-PE) (left panel) and degranulation-dependent P-selectin exposure (right panel) upon stimulation with the indicated agonists in WT and *Slap⁻ᐟ⁻/Slap2⁻ᐟ⁻* platelets. Results are expressed as MFI ± SD (n = 4 mice per group) and are representative of 6 independent experiments. Dividing lines indicate separate measurements. U46, U-46619; A/U, ADP + U-46619; thr., *thrombin*; CVX, *convulxin*; CRP, *collagen-related peptide*; RC, *rhodocytin*. *P < .05; **P < .01; ***P < .001. (Cherpokova *et al.*, *Blood* 2015)[146]
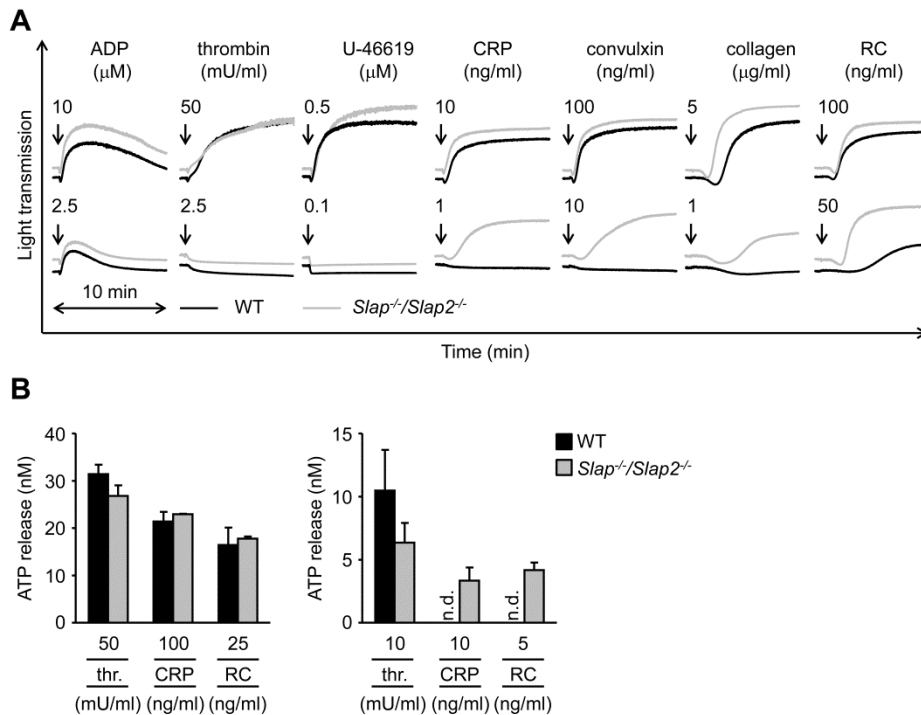
Figure 10. Enhanced aggregation and dense granule release in *Slap$^{-/-}$/Slap2$^{-/-}$* platelets upon GPVI or CLEC-2 stimulation. (A) Washed platelets were activated with the indicated agonists and light transmission was recorded on a Fibrintimer 4-channel aggregometer. ADP measurements were performed in PRP. Aggregation traces representative of 3 independent experiments with n = 4 are depicted. Arrows indicate addition of the respective agonist. (B) Washed platelets were incubated with Luciferase-Luciferin reagent and ATP release was measured in a Lumi-aggregometer upon stimulation with thrombin, CRP or rhodocytin. Results are representative of 2 individual experiments with n = 4. Results represent mean ± SD. thr., *thrombin*; CRP, *collagen-related peptide*; RC, *rhodocytin*. (Cherpokova *et al.*, *Blood* 2015)[146]

To examine whether increased GPVI signaling in *Slap$^{-/-}$/Slap2$^{-/-}$* platelets can be explained by the elevated GPVI surface expression levels in SLAP/SLAP2-deficient mice, *Slap$^{-/-}$/Slap2$^{-/-}$Gp6$^{+/-}$* mice were generated by crossing *Slap$^{-/-}$/Slap2$^{-/-}$* mice with *Gp6$^{-/-}$* mice.[44] Flow cytometric and Western blot analyses confirmed that both surface and total GPVI expression levels in *Slap$^{-/-}$/Slap2$^{-/-}$/Gp6$^{+/-}$* platelets were reduced by approximately 50% compared to platelets of *Slap$^{-/-}$/Slap2$^{-/-}$/Gp6$^{+/+}$* litter-matched mice and were also significantly lower than in WT platelets (Figure 11A-B). Despite reduced GPVI surface expression levels, *Slap$^{-/-}$/Slap2$^{-/-}$/Gp6$^{+/-}$* platelets were markedly hyperreactive to GPVI agonists, as shown by analysis of integrin αIIbβ3 activation, P-selectin exposure and aggregation in response to GPVI-specific agonists, most notably at low and intermediate concentrations (Figure 11C-D). These results clearly demonstrated that the enhanced GPVI activation in SLAP/SLAP2 deficient platelets occurs independently of the increased GPVI expression levels in these cells and indicate a specific defect in the negative regulation of GPVI signaling.
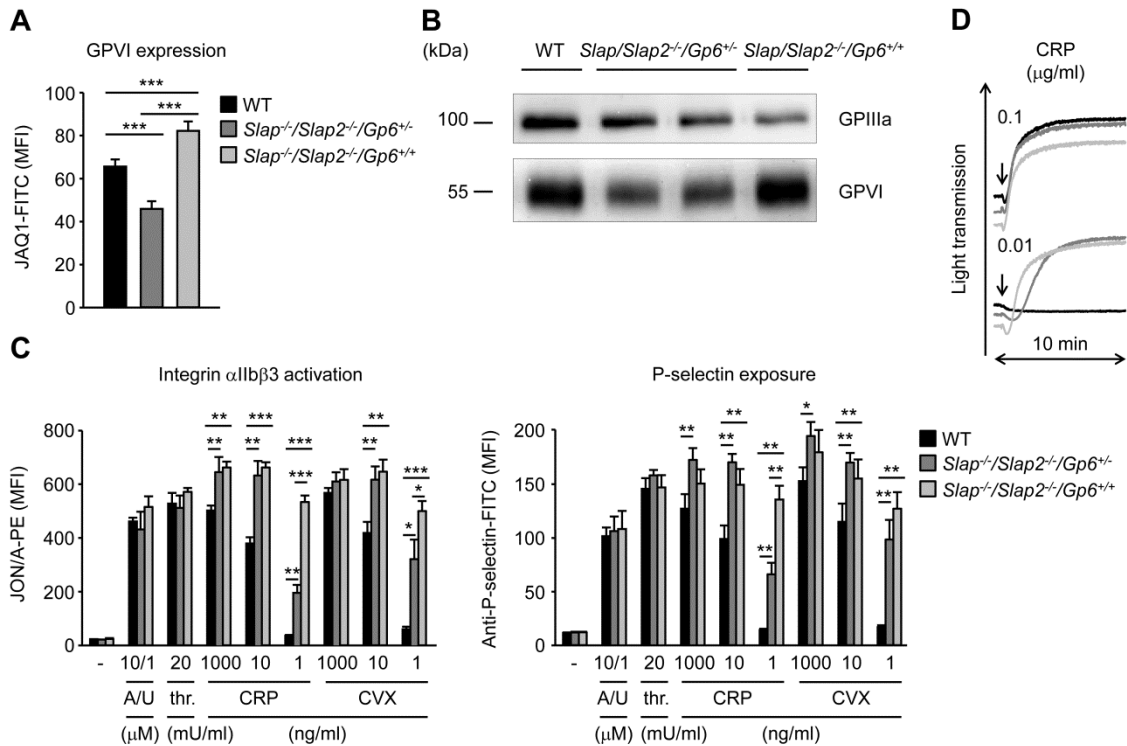
Figure 11. Increased GPVI signaling in *Slap$^{-/-}$/Slap2$^{-/-}$* platelets occurs independently of elevated GPVI expression levels. (A) Analysis of GPVI expression levels in WT, *Slap$^{-/-}$/Slap2$^{-/-}$/Gp6$^{+/-}$* and *Slap$^{-/-}$/Slap2$^{-/-}$/Gp6$^{+/+}$* platelets. Diluted whole blood was stained with FITC-labeled JAQ1 antibody and platelets were analyzed by flow cytometry (n = 4 mice per group). (B) Western blot analysis of GPVI expression in WT, *Slap$^{-/-}$/Slap2$^{-/-}$/Gp6$^{+/-}$* and *Slap$^{-/-}$/Slap2$^{-/-}$/Gp6$^{+/+}$* platelets. GPIIIa expression was used as loading control. (C) Detection of integrin αIIbβ3 activation (binding of JON/A-PE) (left panel) and α-granule release (right panel) in response to the indicated agonists in WT, *Slap$^{-/-}$/Slap2$^{-/-}$/Gp6$^{+/-}$* and *Slap$^{-/-}$/Slap2$^{-/-}$/Gp6$^{+/+}$* platelets. Results are expressed as MFI ± SD (n = 4 mice per group). (C) Washed platelets were activated with CRP and light transmission was monitored on a Fibrintimer 4-channel aggregometer. Results in all panels are representative of 3 independent experiments. A/U, ADP + U-46619; thr., *thrombin*; CVX, *convulxin*; CRP, *collagen-related peptide*; RC, *rhodocytin*. *P < .05; **P < .01; ***P < .001. (Cherpokova *et al.*, *Blood* 2015)[146]

To study the function of SLAP/SLAP2 in ITAM signaling in more detail, changes in protein tyrosine phosphorylation in WT, *Slap$^{-/-}$/Slap2$^{-/-}$/Gp6$^{+/-}$* and *Slap$^{-/-}$/Slap2$^{-/-}$/Gp6$^{+/+}$* platelets were assessed upon stimulation with convulxin (Figure 12). SLAP/SLAP2 double deficiency was associated with enhanced and sustained tyrosine phosphorylation of key signaling molecules in the GPVI/ITAM activation pathway, including the FcRγ-chain, Syk (Y519/520) and PLCγ2 (Y759). Increased phosphorylation of these proteins was observed also in *Slap$^{-/-}$/Slap2$^{-/-}$/Gp6$^{+/-}$* platelets and thus largely independent of GPVI expression levels (Figure 12).

To address the mechanism by which SLAP proteins inhibit GPVI signaling, the hypothesis that SLAP proteins might compete with *Src family kinases* (SFKs) for binding to the GPVI/FcRγ signaling complex was tested. This assumption was based on the fact that Lyn and other SFKs are known to interact with GPVI,[25,27] and because of the sequence similarity between Lyn and SLAP/SLAP2 (33-34% identity for SH3 and 51% identity for SH2

domains). Indeed, strongly increased binding of Lyn to activated GPVI was detected in the absence of SLAP/SLAP2 compared to control (Figure 13), consistent with the increased tyrosine phosphorylation of downstream signaling proteins (Figure 12).
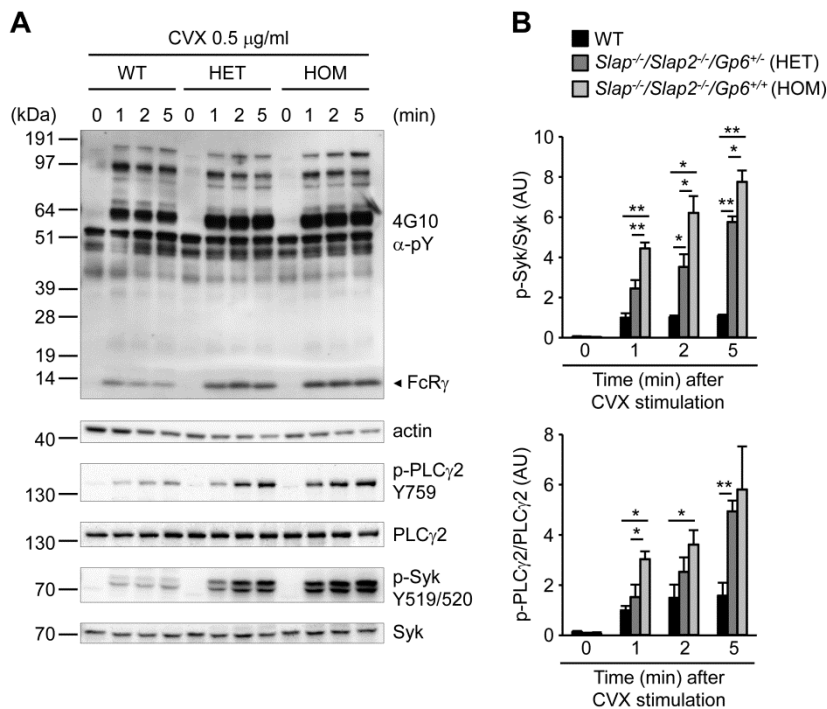

Figure 12. Increased tyrosine phosphorylation of Syk and PLCγ2 upon stimulation of SLAP/SLAP2 deficient platelets with a GPVI-specific agonist. (A) WT, *Slap⁻/⁻/Slap2⁻/⁻/Gp6⁺/⁻* (HET) and *Slap⁻/⁻/Slap2⁻/⁻/Gp6⁺/⁺* (HOM) platelets were stimulated with 0.5 μg/ml convulxin for the indicated time points. Whole-cell lysates were Western blotted and probed with the anti-phosphotyrosine antibody 4G10 or with phospho-specific antibodies. Staining of the respective non-phosphorylated proteins and actin served as loading control. (B) Expression levels of phosphorylated proteins were quantified by densitometry with ImageJ software (NIH, USA), normalized to the expression of the respective non-phosphorylated proteins and adjusted such that the values in WT samples after 1 min of stimulation were set to 1. Results are expressed as mean ± SD and are representative of 3 independent experiments. CVX, *convulxin*. *$P < .05$; **$P < .01$. (Cherpokova *et al.*, *Blood* 2015)[146]
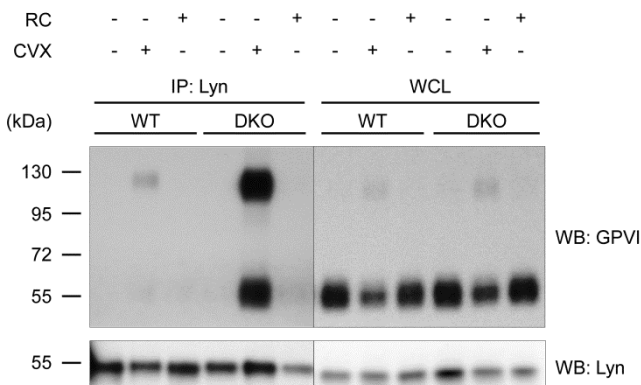
Figure 13. SLAP/SLAP2 attenuate Lyn binding to activated GPVI. Washed WT and *Slap⁻/⁻/Slap2⁻/⁻* (DKO) platelets were left unstimulated or, as indicated, stimulated with 0.5 μg/ml *convulxin* (CVX) or 1 μg/ml *rhodocytin* (RC) for 20 s, lysed and proteins *immunoprecipitated* (IP) with Lyn were resolved by SDS-PAGE under non-reducing conditions and immunoblotted (*Western blot*, WB) for GPVI or Lyn. An immunoblot of *whole cell lysate* (WCL) loaded at 0.4% of Lyn immunoprecipitation input is also shown. Note that GPVI is detected as an ~65 kDa monomer and an ~120 kDa dimer, respectively. Dividing lines denote gaps between different sections and different exposure times of the same membrane. Results are representative of 3 independent experiments. (unpublished and Cherpokova *et al.*, *Blood* 2015)[146]

Notably, markedly enhanced tyrosine phosphorylation of downstream signaling molecules was observed also upon stimulation of SLAP/SLAP2 deficient platelets with the CLEC-2 specific-agonist rhodocytin (Figure 14).
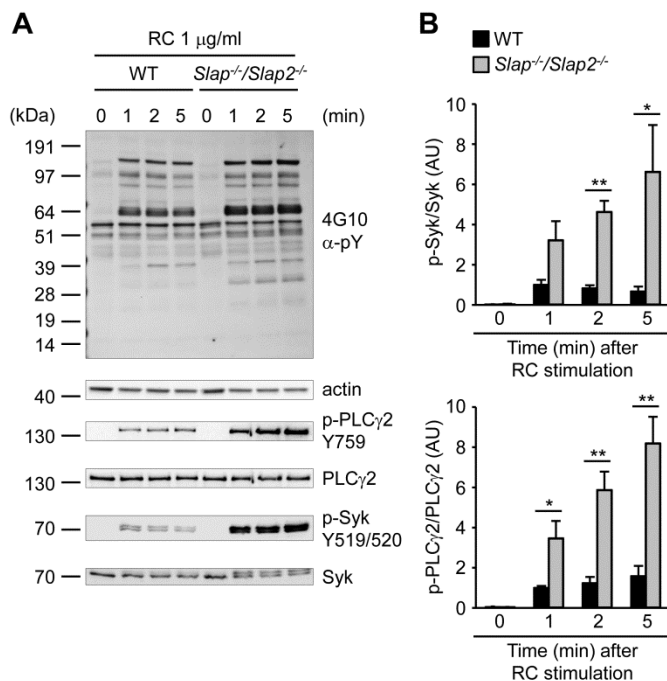

Figure 14. Increased tyrosine phosphorylation of Syk and PLCγ2 upon stimulation of SLAP/SLAP2 deficient platelets with a CLEC-2-specific agonist. (A) WT and Slap$^{-/-}$/Slap2$^{-/-}$ platelets were stimulated with 1 μg/ml *rhodocytin* (RC) for the indicated time points. Whole-cell lysates were Western blotted and probed with the anti-phosphotyrosine antibody 4G10 or with phospho-specific antibodies. Staining of the respective non-phosphorylated proteins and actin served as loading control. (B) Expression levels of phosphorylated proteins were quantified by densitometry with ImageJ software (NIH, USA), normalized to the expression of the respective non-phosphorylated proteins and adjusted such that the values in WT samples after 1 min of stimulation were set to 1. Results are expressed as mean ± SD and are representative of 3 independent experiments. RC, *rhodocytin*. *P < .05; **P < .01. (Cherpokova *et al.*, *Blood* 2015)[146]

The (hem)ITAM-bearing receptors GPVI and CLEC-2 share several similarities in proximal signaling events. It has been demonstrated that the key signaling molecule in the LAT signalosome, the adapter protein LAT, is critically involved in (hem)ITAM-dependent platelet aggregation, especially at low agonist concentrations.[47,147] Due to the marked hyperreactivity in the (hem)ITAM signaling pathway and in particular because of the profound activation of the kinase Syk in the absence of SLAP/SLAP2, it was hypothesized that both adapter proteins might participate in the negative regulation of LAT-dependent PLCγ2 phosphorylation and α-granule release. Platelets isolated from Slap$^{-/-}$/Slap2$^{-/-}$Lat$^{-/-}$ mice (Figure 15A), which were generated within another project (see Section 3.2.3.), displayed unaltered P-selectin exposure and aggregation compared to the respective WT control, in particular upon stimulation with intermediate concentrations of rhodocytin, at which responses of Lat$^{-/-}$ were completely abolished (Figure 15B-C). In line with the functional responses upon stimulation with rhodocytin, Slap$^{-/-}$/Slap2$^{-/-}$Lat$^{-/-}$ platelets exhibited enhanced phosphorylation of PLCγ2 (Figure 15D). By contrast, reductions in α-granule release and aggregation after stimulation with low concentrations of the potent GPVI-specific agonist convulxin could not be overcome in Slap$^{-/-}$/Slap2$^{-/-}$Lat$^{-/-}$ platelets (Figure 15B and data not shown), despite largely preserved phosphorylation of downstream signaling molecules (Figure 15D). These results revealed the presence of a LAT-independent pathway of platelet

activation downstream of CLEC-2 which appears to be controlled by interactions between SLAP/SLAP2 and Syk.
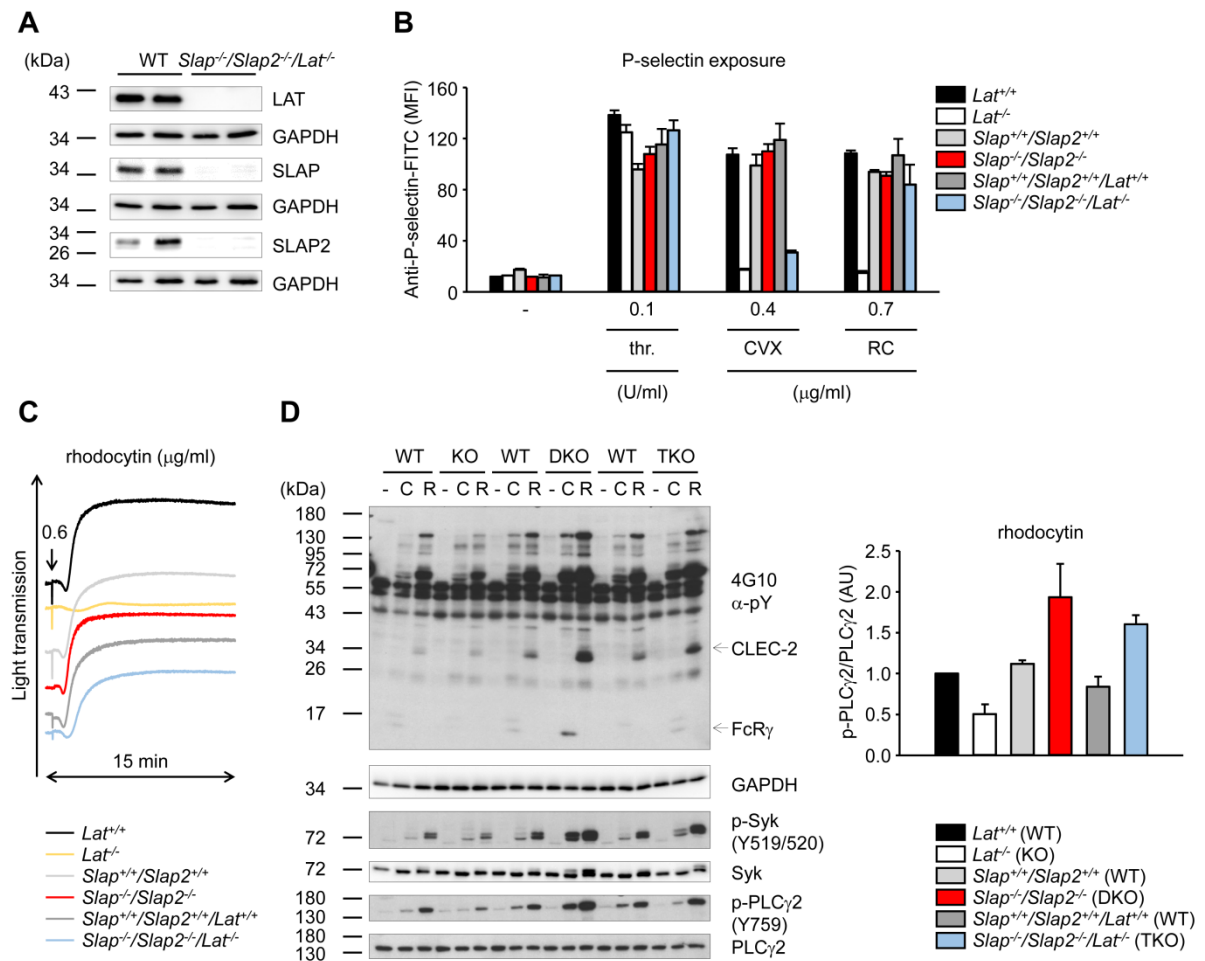

Figure 15. SLAP/SLAP2 deficiency results in LAT-independent enhanced PLCγ2 phosphorylation upon CLEC-2 stimulation. (A) Western blot analysis demonstrating absence of SLAP, SLAP2 and LAT in *Slap⁻/⁻/Slap2⁻/⁻/Lat⁻/⁻* platelets. GAPDH expression was used as loading control. (B) Flow cytometric analysis of degranulation-dependent P-selectin exposure upon stimulation with the indicated agonists. Results are expressed as MFI ± SD (n = 2 mice per group) and are representative of 3 independent experiments. (C) Washed platelets were activated with rhodocytin and light transmission was monitored on a Fibrintimer 4-channel aggregometer. (D) (Left panel) Platelets were stimulated with 0.5 µg/ml convulxin (C) or 1 µg/ml rhodocytin (R) for 2 min. Whole-cell lysates were Western blotted and probed with the anti-phosphotyrosine antibody 4G10 or with phospho-specific antibodies. Staining of the respective non-phosphorylated proteins and GAPDH served as loading control. (Right panel) Expression levels of phosphorylated PLCγ2 upon CLEC-2 stimulation were quantified by densitometry with ImageJ software (NIH, USA), normalized to the expression of total PLCγ2 and adjusted such that the values in *Lat⁺/⁺* samples were set to 1. Note that the 3 KO mouse strains were on a different WT background and therefore, the respective WT were used as control. Results in all panels are representative of 3 independent experiments. thr., *thrombin*; CVX, *convulxin*; RC, *rhodocytin*.

3.1.3. Markedly enhanced GPVI-dependent procoagulant activity in *Slap$^{-/-}$/Slap2$^{-/-}$* platelets

Next, consequences of SLAP/SLAP2 deficiency on platelet adhesion to collagen and aggregate formation under flow were investigated using a whole blood perfusion system. Unexpectedly, WT and *Slap$^{-/-}$/Slap2$^{-/-}$* platelets formed aggregates to the same extent and with the same kinetics at intermediate shear rates of 1000 s^{-1} (Figure 16A-B).

GPVI signaling leads to a marked increase in cytosolic Ca^{2+} concentrations, subsequent surface exposure of procoagulant *phosphatidylserine* (PS) and resultant thrombin generation.[13,14] To test whether SLAP/SLAP2 regulate the procoagulant activity of platelets, blood from WT and *Slap$^{-/-}$/Slap2$^{-/-}$* mice was anticoagulated, perfused over immobilized collagen at a shear rate of 1000 s^{-1} and PS exposure was determined by annexin-A5-staining. The surface covered by collagen-adherent platelets was similar in WT and mutant samples, whereas PS exposure was markedly increased in *Slap$^{-/-}$/Slap2$^{-/-}$* blood (Figure 16C-D).
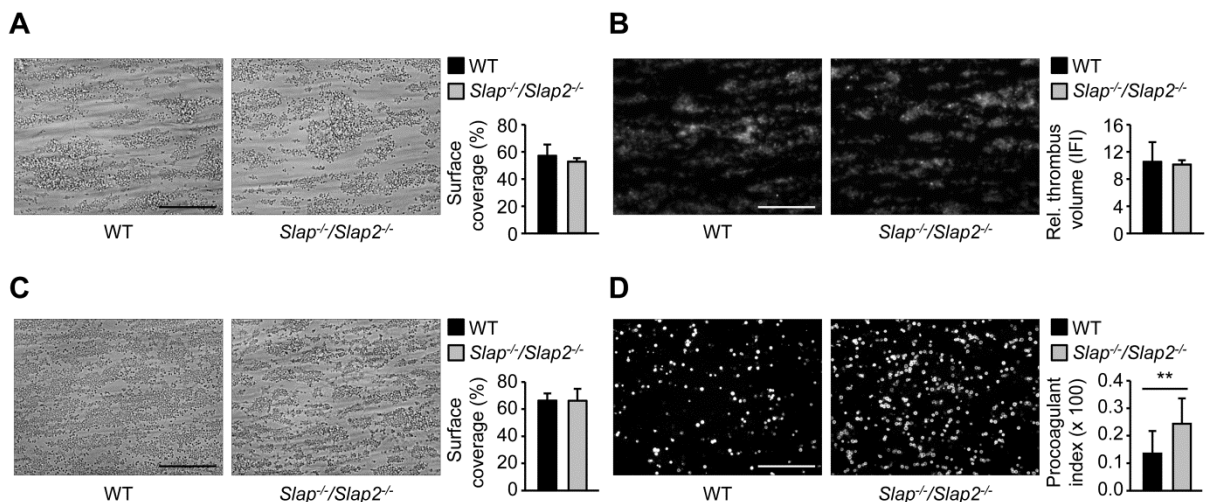
Figure 16. SLAP/SLAP2 deficiency enhances procoagulant activity under flow. Unaltered adhesion and aggregate formation of *Slap$^{-/-}$/Slap2$^{-/-}$* platelets on collagen under flow *ex vivo*. Heparinized whole blood was perfused over immobilized fibrillar collagen at a shear rate of 1000 s^{-1} and surface coverage (A) and relative aggregate volume (B) (estimated by the integrated fluorescence intensity (IFI) of fluorescently labeled platelets per visual field) were determined. Representative phase-contrast (A) and fluorescence (B) images after 2 min washing with Tyrode-HEPES buffer are depicted. (C) Unaltered surface coverage by collagen-adherent platelets in WT and *Slap$^{-/-}$/Slap2$^{-/-}$* blood. Representative phase-contrast images are depicted. (D) Increased *phosphatidylserine* (PS) exposure of *Slap$^{-/-}$/Slap2$^{-/-}$* platelets, as demonstrated by annexin-A5-DyLight 488 staining of platelets. Procoagulant index indicates the ratio of surface coverage of PS-exposing platelets (annexin-A5-DyLight 488 staining of platelets) to the total surface covered by platelets. Results in all panels are representative of 2 independent experiments with n ≥ 6. Bars: 50 μm **$P < .01$. (Cherpokova *et al.*, *Blood* 2015)[146]

Enhanced (hem)ITAM-dependent procoagulant activity of *Slap$^{-/-}$/Slap2$^{-/-}$* platelets was confirmed by flow cytometric analysis of annexin-A5-positive cells upon stimulation with

different agonists (Figure 17). Notably, combined stimulation of GPVI and GPCR was required to induce high PS exposure in WT platelets (Figure 17). In stark contrast, stimulation with GPVI-specific agonists alone (CRP or convulxin) was sufficient to induce significant procoagulant activity in *Slap⁻ᐟ⁻/Slap2⁻ᐟ⁻* platelets (Figure 17).

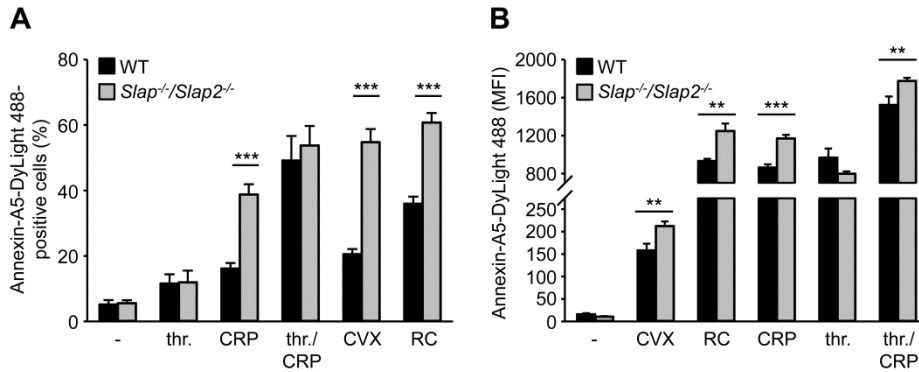**Figure 17. SLAP/SLAP2 deficiency is associated with increased PS exposure.** (A) Washed platelets were stimulated with 0.1 U/ml thrombin, 20 μg/ml CRP, a combination of both thrombin and CRP, 1 μg/ml convulxin, or 0.12 μg/ml rhodocytin, stained with saturating amounts of annexin-A5-DyLight 488 and directly analyzed by flow cytometry. Results are representative of 2 independent experiments with n = 5. (B) Washed platelets were stimulated with 1 μg/ml convulxin, 1.2 μg/ml rhodocytin, 20 μg/ml CRP, 0.1 U/ml thrombin or a combination of both thrombin and CRP, stained with saturating amounts of annexin-A5-DyLight 488 and anti-GPIX-DyLight 649 derivatives and directly analyzed by flow cytometry. Results are expressed as MFI ± SD (n = 4 mice per group) and are representative of 2 independent experiments. thr., *thrombin*; CVX, *convulxin*; CRP, *collagen-related peptide*; RC, *rhodocytin*. $**P < .01$; $***P < .001$. (Cherpokova *et al.*, *Blood* 2015)[146]

PS exposure triggers powerful platelet procoagulant activity and provides high affinity binding sites for key coagulations factors.[14] This in turn enhances the assembly of the tenase and prothrombinase complexes and leads to rapid thrombin generation.[148] In agreement with enhanced PS-exposure, lack of SLAP/SLAP2 resulted in an altered maximal amount of newly generated thrombin (Figure 18B) and significantly accelerated response upon stimulation with (hem)ITAM-specific agonists (Figure 18C). The overall amount of produced thrombin was comparable to the values in WT control samples (Figure 18A). Importantly, SLAP/SLAP2 deficiency did not affect plasma coagulation, as confirmed by unaltered activated plasma thromboplastin time and prothrombin time in *Slap⁻ᐟ⁻/Slap2⁻ᐟ⁻* mice compared to the WT control (data not shown).
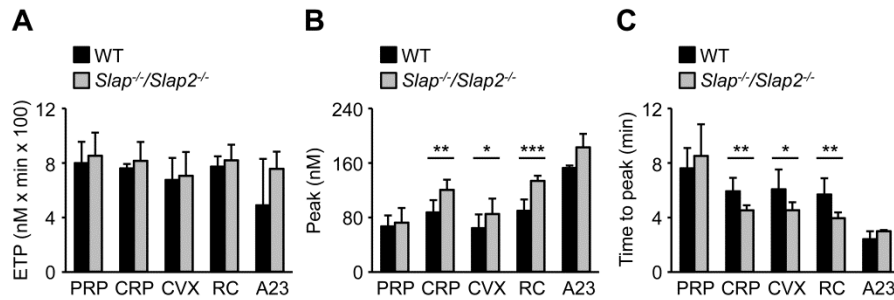
Figure 18. SLAP/SLAP2 deficiency enhances (hem)ITAM-dependent thrombin generation in platelets. Citrate-anticoagulated *platelet-rich plasma* was left unstimulated (PRP), or platelets were activated by incubation with *convulxin* (CVX) (1 μg/ml), *collagen-related peptide* (CRP) (20 μg/ml), *rhodocytin* (RC) (1 μg/ml) or the Ca^{2+} ionophore A23187 (A23) (10 μM) for 10 min at 37°C. Thrombin generation was triggered with tissue factor/$CaCl_2$. (A) *Endogenous thrombin potential* (ETP). (B) Quantification of thrombin peak height. (C) Quantification of time to peak. n = 3 for A23187; n = 7 for CRP and RC; n = 10 for PRP and CVX. *$P < .05$; **$P < .01$; ***$P < .001$. (Cherpokova *et al.*, *Blood* 2015)[146]

3.1.4. SLAP/SLAP2 limit thrombus formation

In a next set of experiments, the role of SLAP and SLAP2 in hemostasis and thrombosis was studied. Combined deficiency of SLAP and SLAP2 did not affect platelet hemostatic functions (mean tail bleeding time: 188 ± 62 s in WT mice vs. 213 ± 90 s in *Slap⁻/⁻/Slap2⁻/⁻* mice, *P* = 0.5; Figure 19A).

PS exposure and thrombin generation have been demonstrated to play a key role in the progression of thrombus growth in mouse models of arterial thrombosis.[149,150] To assess the extent to which the above described hyperreactive platelet phenotype affects thrombotic events *in vivo*, *Slap⁻/⁻/Slap2⁻/⁻* and WT mice were subjected to two models of occlusive arterial thrombosis. These experiments were performed by Dr. Martina Morowski. In the first model, the abdominal aorta is mechanically injured and thrombus formation occurs mainly through collagen-dependent mechanisms.[151] The severity of injury was reduced and correspondingly, stable vessel occlusion was achieved in only 20% of the WT mice. In marked contrast, the majority (89%) of *Slap⁻/⁻/Slap2⁻/⁻* mice formed stable vessel occlusion which also occurred significantly faster (*Slap⁻/⁻/Slap2⁻/⁻* mice: 282 ± 151 s vs. 713 ± 131 s in the WT; Figure 19B). In a second model, the carotid artery was injured by topical application of $FeCl_3$. Thrombus formation is driven by both collagen- and thrombin-dependent mechanisms in this model.[151] Stable vessel occlusion occurred in 93% of all tested *Slap⁻/⁻/Slap2⁻/⁻* mice, whereas 60% of the WT mice (9 out of 15) were not able to form occlusive thrombi within the observation period of 30 min (*P* < .01; mean time to occlusion: WT: 607 ± 146 s; *Slap⁻/⁻/Slap2⁻/⁻* mice: 483 ± 149 s; Figure 19C). Importantly, similar results were obtained upon adoptive platelet transfer of *Slap⁻/⁻/Slap2⁻/⁻* platelets into platelet-depleted WT mice, thus excluding a contribution of other cell types than platelets to the observed phenotype (stable vessel

occlusion in 30% of mice transfused with WT platelets, vessel occlusion in 92% of mice transfused with $Slap^{-/-}/Slap2^{-/-}$ platelets, $P < .01$, Figure 19D).

In the model of FeCl$_3$-induced injury of the carotid artery, the applied concentration of FeCl$_3$ was reduced to a critical threshold at which stable occlusion was not observed in the majority of the WT animals (Figure 19C). Notably, application of a low concentration of FeCl$_3$ resulted in the formation of occlusive platelet-rich thrombi in $Slap^{-/-}/Slap2^{-/-}$ mice which did not differ morphologically from those observed in WT control mice treated with a higher concentration of FeCl$_3$ (Figure 20). These data indicated that thrombus formation in $Slap^{-/-}/Slap2^{-/-}$ mice is initiated at a significantly lower threshold of vessel damage. Together, these findings demonstrated that SLAP/SLAP2 deficiency in platelets results in a prothrombotic phenotype, confirming the notion that these adapter proteins negatively regulate platelet activation *in vivo* and thereby efficiently prevent occlusive thrombus formation and infarction.
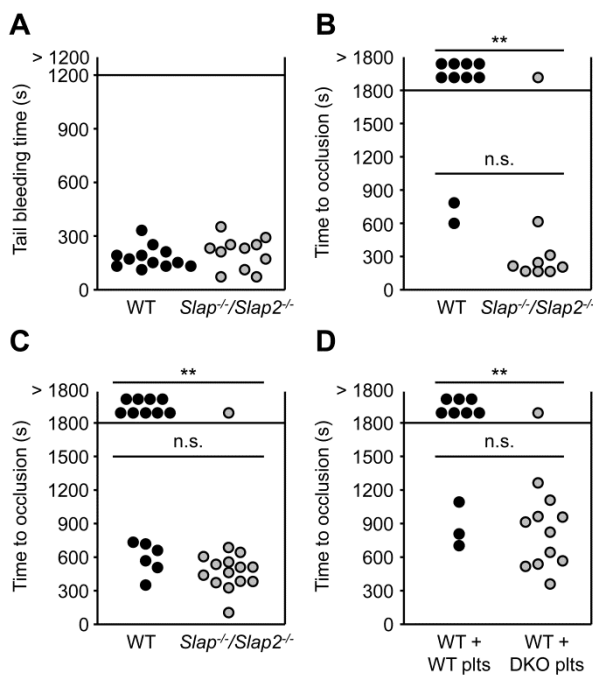
Figure 19. SLAP/SLAP2 limit thrombus formation. (A) SLAP/SLAP2 deficiency does not influence hemostatic function in $Slap^{-/-}/Slap2^{-/-}$ mice as demonstrated by unaltered tail bleeding times of $Slap^{-/-}/Slap2^{-/-}$ mice. Each symbol represents 1 animal. (B) The abdominal aorta was mechanically injured using forceps (compression for 10 s) and blood flow was monitored by an ultrasonic flow probe until complete vessel occlusion for at least 5 min, or for a maximum of 30 min. Each symbol represents 1 animal. (C) The right carotid artery of WT and $Slap^{-/-}/Slap2^{-/-}$ mice was injured by topical application of 2.5% FeCl$_3$ for 90 s and blood flow was monitored with a Doppler flow probe until complete vessel occlusion for at least 2 min, or for a maximum of 30 min. Each symbol represents 1 animal. (D) WT mice were treated with platelet-depleting anti-GPIbα antibodies. Platelet-depleted WT mice were transfused with WT or $Slap^{-/-}/Slap2^{-/-}$ (DKO) platelets and 7.5% FeCl$_3$ were topically applied to the right carotid arteries of these mice for 1 min. Time to complete vessel occlusion was determined as described for panel (C). Each symbol represents 1 animal. **P < .01; n.s., not significant. (Cherpokova *et al.*, *Blood* 2015)[146]
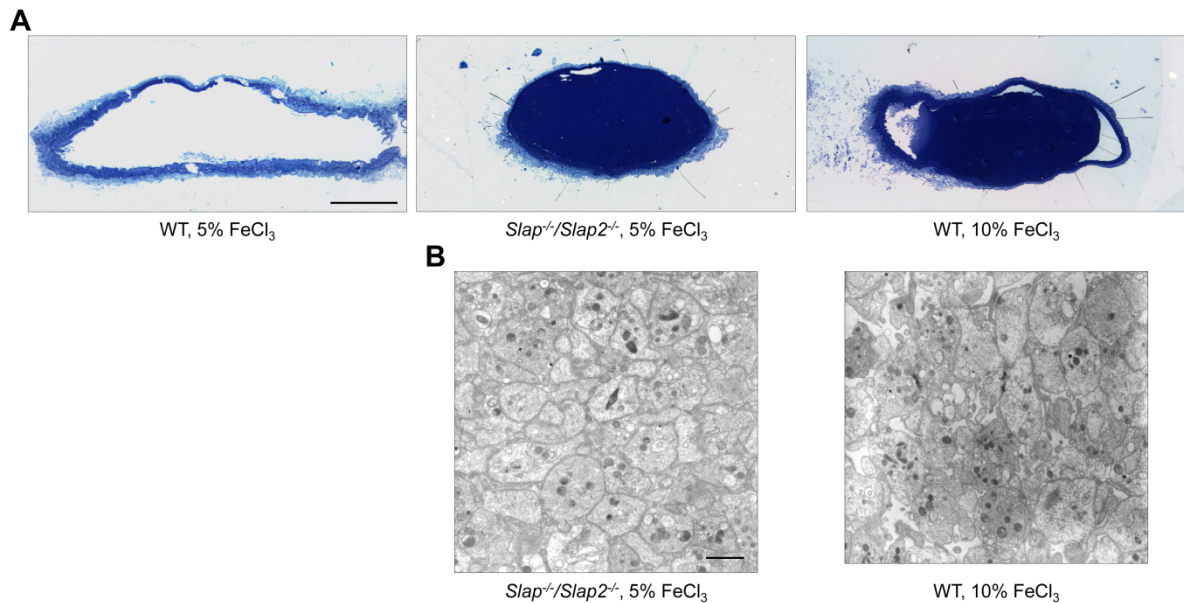
Figure 20. Occlusive thrombi in *Slap^-/-^/Slap2^-/-* mice consist of platelets and are indistinguishable from WT thrombi. (A) The right carotid artery of WT and *Slap^-/-^/Slap2^-/-* mice was injured by topical application of 5% $FeCl_3$ for 1 min, or 10% $FeCl_3$ for 1 min (only WT mice) and blood flow was monitored with a Doppler flow probe until complete vessel occlusion for at least 2 min, or for a maximum of 30 min. Note that carotid arteries of WT mice were injured with a higher concentration of $FeCl_3$ to induce formation of occlusive thrombi with the same kinetics as in *Slap^-/-^/Slap2^-/-* mice. Injured vessels were excised, fixed and stained with toluidine blue. Bar: 200 μm. (B) Ultrastructural analysis of occlusive thrombi by TEM. Note that thrombi formed in the absence of SLAP and SLAP2 consisted of platelets and did not differ from occlusive thrombi in WT mice. Bar: 1.1 μm. Images are representative of 4-6 mice per group. (Cherpokova *et al.*, *Blood* 2015)[146]

3.1.5. SLAP/SLAP2 deficiency in platelets dramatically aggravates neurological damage after focal cerebral ischemia

Ischemic stroke is a complex disease with multiple cellular interactions involved in the progression of thromboembolic vessel occlusion to infarct development.[12] Although the exact mechanisms by which platelets contribute to the development of ischemic brain infarction are still poorly understood, there is increasing evidence that GPVI (and GPIb) plays a major role in this process.[12,30,32] To determine the effect of SLAP/SLAP2 deficiency on cerebral infarct development, *Slap^-/-^/Slap2^-/-* and WT mice were subjected to the *transient middle cerebral artery occlusion* (tMCAO) model of acute stroke where the origin of the middle cerebral artery is occluded by a filament for 30 min, thereby reducing cerebral flow by >90%.[32,141] Surgery was carried out by Dr. Peter Kraft and Dr. Michael Schuhmann from the Department of Neurology (University of Würzburg).

In agreement with previous reports,[141] WT mice developed small infarctions after only 30 min of ischemia. In sharp contrast, infarct volumes in *Slap^-/-^/Slap2^-/-* mice were increased by ~92% compared to WT mice (58.8 ± 33.5 mm^3 in WT vs. 113.1 ± 14.3 mm^3 in *Slap^-/-^/Slap2^-/-* mice; $P < .001$; Figure 21A). The increase in infarct size was functionally

relevant, as it was associated with an overall impairment of neurological and motor function, demonstrated by the significantly worsened outcome in the Bederson score and grip test, respectively (Figure 21B-C). The dramatic increase in infarct volume was accompanied by increased intracerebral thrombosis, as demonstrated by the markedly elevated number of occluded vessels (Figure 21D). Consistent with the higher proportion of occluded vessels, immunohistochemical and Western blot analyses revealed increased accumulation of fibrin(ogen) in the infarcted basal ganglia and cortices of $Slap^{-/-}/Slap2^{-/-}$ mice (data not shown).
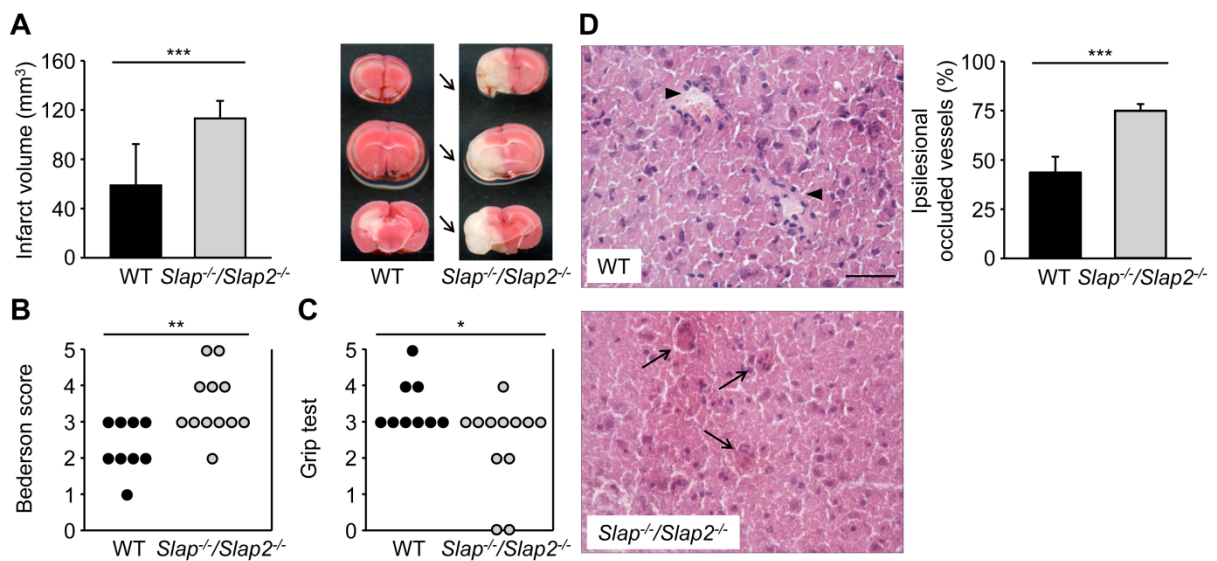
Figure 21. SLAP/SLAP2 deficiency dramatically aggravates neurological damage after focal cerebral ischemia. Infarct volumes (A) and functional outcome (B, C) 24 h after focal cerebral ischemia in WT and $Slap^{-/-}/Slap2^{-/-}$ mice were investigated in a murine model of ischemic stroke. Mice were subjected to 30 min of tMCAO. (A) Brain infarct volumes in WT (n = 9) and $Slap^{-/-}/Slap2^{-/-}$ (n = 12) mice were measured by planimetry (left panels). Results represent mean ± SD. Representative images of 3 coronal brain sections stained with TTC 24 h after 30 min tMCAO (right panel). Arrows indicate infarcted areas in $Slap^{-/-}/Slap2^{-/-}$ mice. (B) Bederson score and (C) grip test were determined 24 h after tMCAO. Each symbol represents 1 animal. (D) SLAP/SLAP2 deficiency dramatically increases microvascular thrombosis after 30 min of tMCAO. Representative hematoxylin and eosin stains from the ipsilesional hemispheres of WT (n = 6) and $Slap^{-/-}/Slap2^{-/-}$ (n = 8) mice (left panel) and determination of the percentage of occluded vessels (right panel). Number of thrombotic vessels was significantly increased in $Slap^{-/-}/Slap2^{-/-}$ mice (arrows), whereas the microvascular patency was largely preserved in WT mice (arrowheads). Bar: 50 μm. *$P < .05$; **$P < .01$; ***$P < .001$. (Cherpokova *et al.*, *Blood* 2015)[146]

To specifically investigate the role of platelet SLAP and SLAP2 in the progression of ischemic stroke, adoptive platelet transfer into platelet-depleted WT mice was performed. Importantly, the transfused platelet populations did not show any signs of activation and were free of leukocytes, as tested by flow cytometry, microscopical inspection and automated blood cell analysis. Furthermore, flow cytometric and transmission EM analyses confirmed that the platelet suspensions were also free of (leukocyte- or platelet-derived) microparticles (data not shown). Strikingly, infarct volumes in WT mice transfused with $Slap^{-/-}/Slap2^{-/-}$ platelets were dramatically increased by ~97% compared to WT mice

transfused with WT platelets (123.0 ± 23.4 mm^3 vs. 62.6 ± 31.8 mm^3; $P <$ .001; Figure 22A), and this was accompanied by severe neurological deficits (Figure 22B-C). These findings demonstrated that SLAP/SLAP2 activity in platelets is critically involved in limiting infarct growth following focal cerebral ischemia.
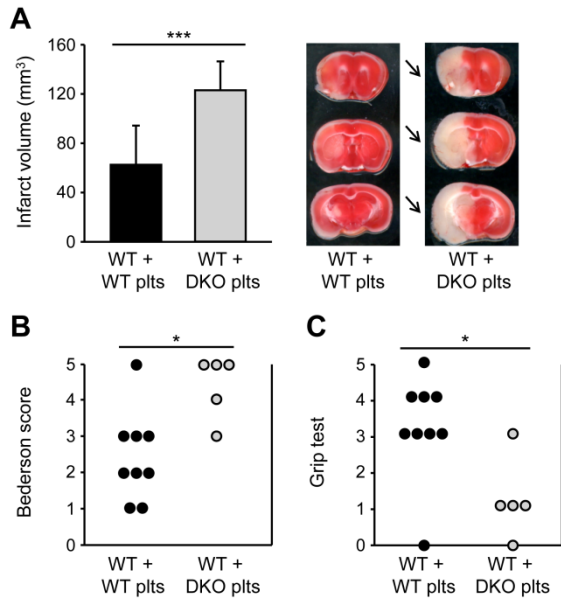

Figure 22. SLAP/SLAP2 deficiency in platelets induces a dramatic increase in infarct volume in a model of ischemic stroke. Infarct volumes (A) and functional outcome (B, C) 24 h after focal cerebral ischemia in WT mice reconstituted with WT or $Slap^{-/-}/Slap2^{-/-}$ (DKO) platelets after depletion of endogenous platelets were investigated in a murine model of ischemic stroke. Mice were subjected to 30 min of tMCAO. (A) Brain infarct volumes in platelet-depleted WT mice transfused with WT (n = 12) or $Slap^{-/-}/Slap2^{-/-}$ (n = 8) platelets were measured by planimetry (left panels). Results represent mean ± SD. Representative images of 3 coronal brain sections stained with TTC 24 h after 30 min tMCAO (right panel). Arrows indicate infarcted areas in WT mice recipients of $Slap^{-/-}/Slap2^{-/-}$ platelets. (B) Bederson score and (C) grip test were determined 24 h after tMCAO. Each symbol represents 1 animal. *$P <$ .05; ***$P <$ .001. (Cherpokova et al., Blood 2015)[146]

In a control experiment, WT mice received leukocytes isolated from the blood of $Slap^{-/-}/Slap2^{-/-}$ or WT mice and were then subjected to a 30 min tMCAO. Both groups of mice developed only small infarcts, clearly demonstrating that leukocytes are not responsible for the increased susceptibility of $Slap^{-/-}/Slap2^{-/-}$ mice towards ischemic stroke (Figure 23).
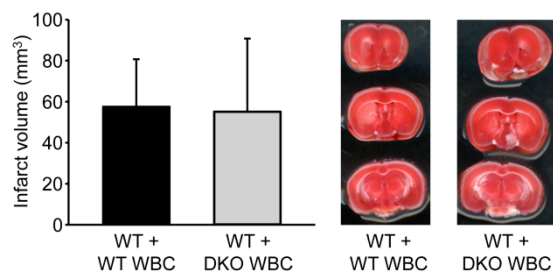

Figure 23. Adoptive transfer of $Slap^{-/-}/Slap2^{-/-}$ leukocytes into WT mice does not alter infarct size. Infarct volumes in WT mice transfused with WT or $Slap^{-/-}/Slap2^{-/-}$ (DKO) white blood cells (WBC) were investigated in a murine model of ischemic stroke. Mice were subjected to 30 min of tMCAO. Brain infarct volumes were measured by planimetry (left panels). Results represent mean ± SD. Representative images of 3 coronal brain sections stained with TTC 24 h after 30 min of tMCAO (right panel). n = 5 animals per group. (Cherpokova et al., Blood 2015)[146]

Furthermore, induction of local cytokine production, infiltration by T cells (which have been shown to contribute to infarct growth in this model)[152-154] complement activation and the stability of the blood-brain barrier were comparable between WT and $Slap^{-/-}/Slap2^{-/-}$ mice 24 h after 30 min of tMCAO (data not shown). Together, these results further corroborated the notion that enhanced thrombotic, rather than proinflammatory, activity is a major determinant of the increased susceptibility of SLAP/SLAP2-deficient mice towards ischemic brain infarction.

3.2. *In vivo* depletion of GPVI in SLAP/SLAP2-deficient mice is associated with prolonged severe thrombocytopenia

The central platelet collagen receptor GPVI can be specifically and irreversibly removed from the surface of circulating mouse platelets *in vivo* by treatment with monoclonal antibodies (JAQ1-3).[39,40] GPVI immunodepletion in mice leads to a prolonged GPVI-knockout-like phenotype with absence of the receptor for more than two weeks upon treatment with a single bolus injection of the antibody.[39,40] Loss of the receptor is associated with a transient thrombocytopenia, but a long-term antithrombotic protection in different models of experimental arterial thrombosis and is accompanied by only moderately increased bleeding *in vivo*.[39,155,156] GPVI is therefore regarded as an attractive potential target for antithrombotic therapy.[13,38]

Antibody-induced GPVI down-regulation *in vivo* is currently considered to occur through two principal mechanisms: ectodomain shedding and internalization followed by intracellular degradation.[41,43] Both mechanisms require signaling through the ITAMs in the FcRγ-chain.[41] Moreover, key downstream signaling molecules, such as LAT and PLCγ2, are indispensable for shedding, whereas receptor down-regulation by internalization and degranulation still occurs in the absence of both proteins.[41] SLAP proteins contribute essentially to the down-regulation of TCR and BCR expression levels by targeting components of the TCR and BCR complexes for degradation after stimulation and internalization.[80-82] This raises the possibility that SLAP/SLAP2 may be involved in similar mechanisms underlying the degradation of the GPVI/FcRγ complex after internalization. SLAP/SLAP2-deficient mice were used to investigate this hypothesis in the following section of this thesis.

3.2.1. SLAP and SLAP2 are dispensable for antibody-induced GPVI down-regulation

To study the role of SLAP and SLAP2 in antibody-induced GPVI down-regulation, *Slap*$^{-/-}$, *Slap2*$^{-/-}$ and WT mice were treated with the monoclonal anti-GPVI antibody JAQ1 (4 μg/g *body weight* (BW) *intravenously* (i.v.)) and platelet counts, JAQ1 binding to the platelet surface and GPVI surface protein expression were monitored by flow cytometry. Consistent with previous reports,[39-41] antibody treatment was in all 3 groups accompanied by a transient thrombocytopenia with a maximal drop in peripheral platelet counts 30 min after JAQ1 injection (Figure 24A). Surface-bound JAQ1 was detected only at very early time points after antibody administration, suggesting rapid removal of the JAQ1-GPVI complex from the platelet surface (Figure 24B-C) associated also with clearance of the FcRγ chain (Figure 24D). Of note, *Slap*$^{-/-}$ mice recovered from the antibody-induced severe thrombocytopenia,

but peripheral platelet counts remained at ~50-60% of control values in the following 3 weeks after treatment (Figure 24A). Collectively, these data demonstrated that SLAP and SLAP2 each are dispensable for antibody-induced GPVI down-regulation.
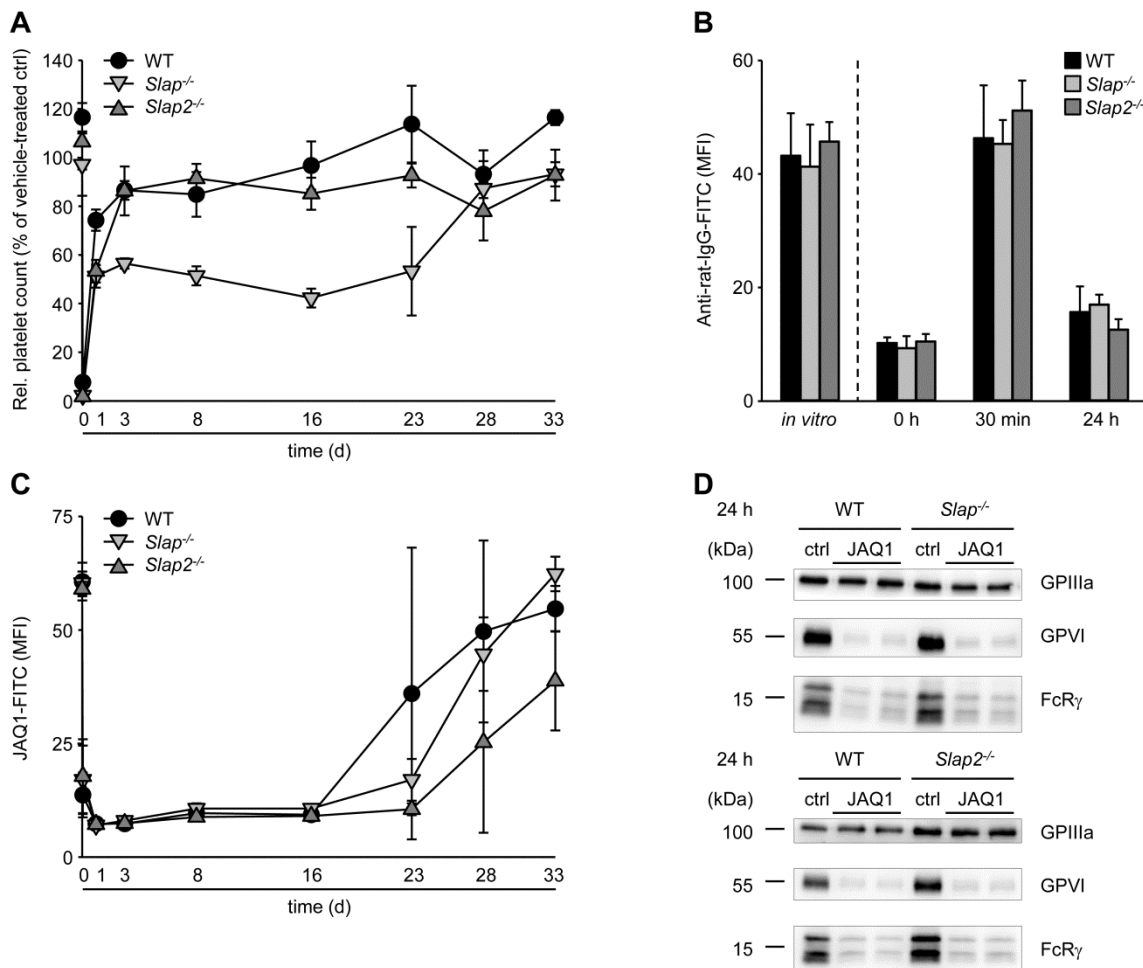

Figure 24. SLAP and SLAP2 are dispensable for antibody-induced GPVI down-regulation. (A) Relative platelet counts in WT (●), $Slap^{-/-}$ (▼) and $Slap2^{-/-}$ (▲) mice at the indicated time points after treatment with 4 μg/g BW JAQ1-IgG. Platelet counts are expressed as percentage of vehicle-treated control mice. (B) Detection of surface-bound JAQ1 by an anti-rat IgG antibody *in vitro*, prior to (0 h), 30 min and 24 h after JAQ1-IgG treatment. (C) Determination of GPVI surface expression by flow cytometry. (A-C) Results are expressed as MFI ± SD (n ≥ 4 mice per group) and are representative of 3 independent experiments. (D) Western blot analysis of total GPVI and FcRγ expression levels 24 h after JAQ1-IgG treatment. GPIIIa levels served as loading control. Blots are representative of 2 independent experiments.

3.2.2. Antibody-induced GPVI down-regulation results in prolonged severe thrombocytopenia in $Slap^{-/-}/Slap2^{-/-}$ mice

The results presented in the first part of this thesis clearly demonstrated a functional redundancy of SLAP and SLAP2 in the modulation of platelet (hem)ITAM signaling. It was thus hypothesized that both adapter proteins may play redundant roles in antibody-induced GPVI down-regulation as well. Unexpectedly, JAQ1-IgG injection resulted in severe

prolonged thrombocytopenia in *Slap⁻/⁻/Slap2⁻/⁻* mice which lasted over 4 weeks before peripheral platelet counts recovered to initial values (Figure 25A). Importantly, antibody treatment led to rapid loss of GPVI/FcRγ and JAQ1-GPVI complex (Figure 25B-D), revealing that JAQ1-induced GPVI down-regulation occurs independently of both SLAP and SLAP2.
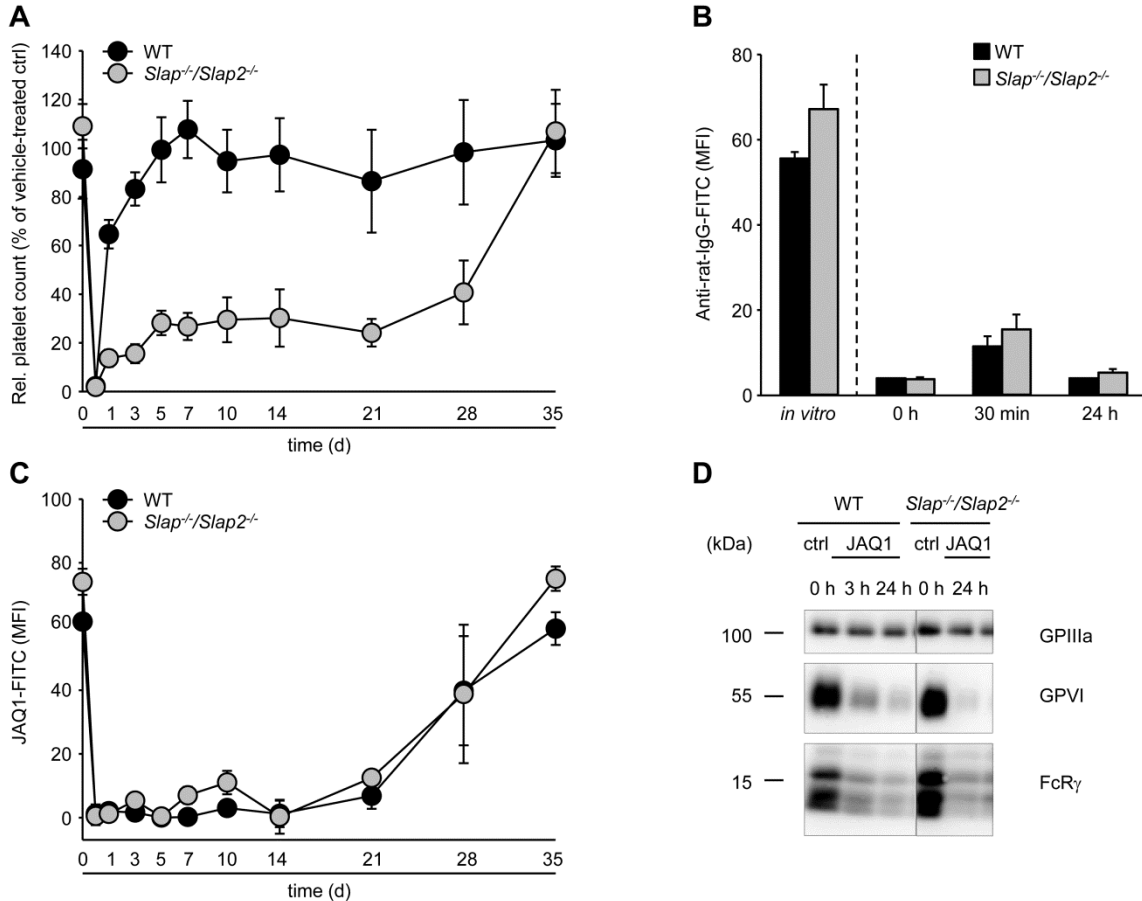

Figure 25. SLAP/SLAP2 deficiency is associated with prolonged severe thrombocytopenia following antibody-induced GPVI down-regulation. (A) Relative platelet counts in WT (black circles) and *Slap⁻/⁻/Slap2⁻/⁻* (gray circles) mice at the indicated time points after treatment with 4 μg/g BW JAQ1-IgG. Platelet counts are expressed as percentage of vehicle-treated control mice. (B) Detection of surface-bound JAQ1 by an anti-rat IgG antibody *in vitro*, prior to (0 h), 30 min and 24 h after JAQ1-IgG treatment. (C) Determination of GPVI surface expression by flow cytometry. (A-C) Results are expressed as MFI ± SD (n ≥ 4 mice per group) and are representative of 6 independent experiments. (D) Western blot analysis of total GPVI and FcRγ expression levels at the indicated time points after JAQ1-IgG treatment. GPIIIa levels served as loading control. Dividing lines denote gaps between different sections of the same membrane. Blots are representative of 2 independent experiments.

Although combined deficiency of SLAP and SLAP2 proved dispensable for GPVI down-regulation, the striking phenotype of acquired thrombocytopenia in *Slap⁻/⁻/Slap2⁻/⁻* mice after a single bolus injection of JAQ1 was investigated in more detail. In the next set of experiments, the influence of elevated GPVI expression levels in *Slap⁻/⁻/Slap2⁻/⁻* mice on the observed phenotype was examined by studying effects of JAQ1 treatment in *Slap⁻/⁻/Slap2⁻/⁻/Gp6⁺/⁻* mice which exhibited GPVI expression levels reduced by 50% compared to litter-matched *Slap⁻/⁻/Slap2⁻/⁻/Gp6⁺/⁺* mice (Figure 11). JAQ1 administration resulted in acute sustained

thrombocytopenia in *Slap^{-/-}/Slap2^{-/-}/Gp6^{+/-}* mice (Figure 26), demonstrating that thrombocytopenia severity occurs largely independently of GPVI surface expression levels.
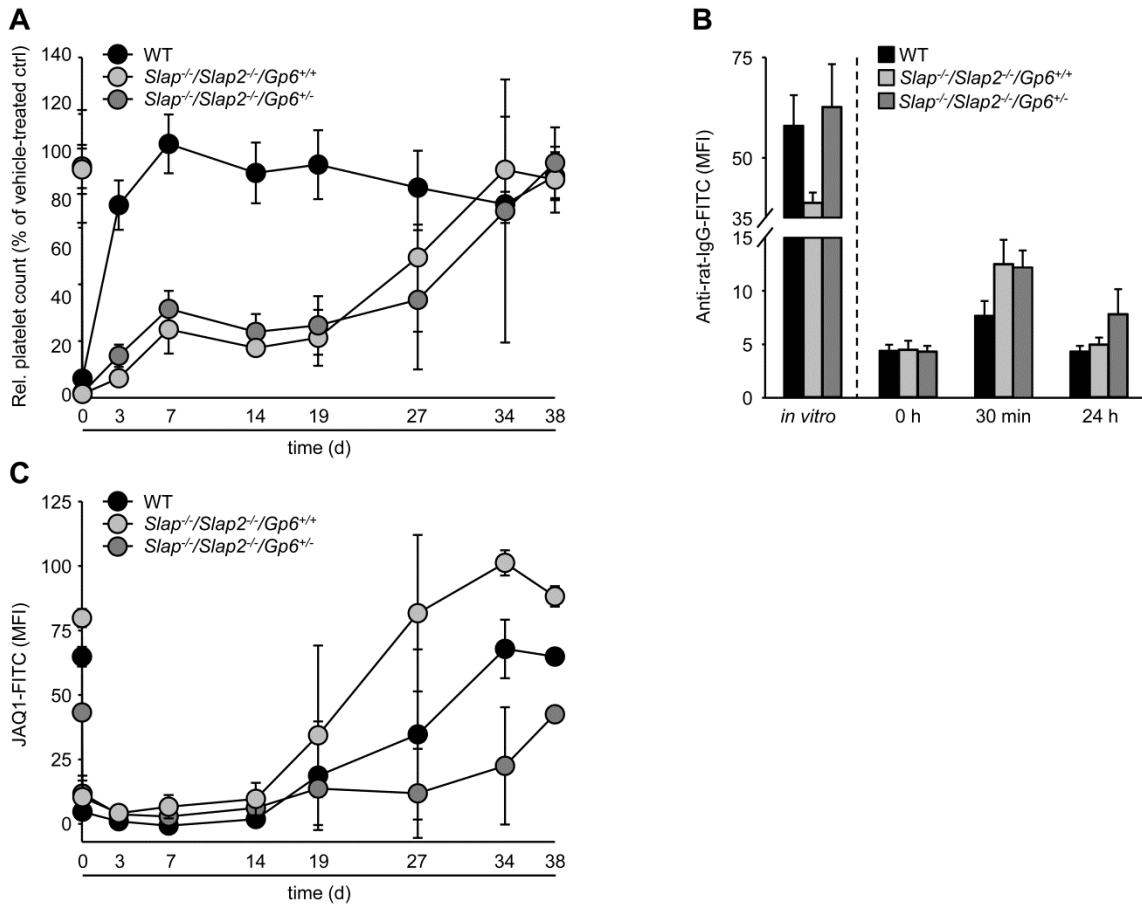

Figure 26. Prolonged severe thrombocytopenia following antibody-induced GPVI down-regulation occurs largely independently of GPVI surface expression levels. (A) Relative platelet counts in WT (black circles), *Slap^{-/-}/Slap2^{-/-}/Gp6^{+/+}* (light gray circles) and *Slap^{-/-}/Slap2^{-/-}/Gp6^{+/-}* (dark gray circles) mice at the indicated time points after treatment with 4 μg/g BW JAQ1-IgG. Platelet counts are expressed as percentage of vehicle-treated control mice. (B) Detection of surface-bound JAQ1 by an anti-rat IgG antibody *in vitro*, prior to (0 h), 30 min and 24 h after JAQ1-IgG treatment. (C) Determination of GPVI surface expression by flow cytometry. (A-C) Results are expressed as MFI ± SD (n ≥ 5 mice per group) and are representative of 3 independent experiments.

To investigate whether the Fc-part of the JAQ1 antibody is required for GPVI down-regulation and the concomitant transient thrombocytopenia to occur, WT and SLAP/SLAP2-deficient mice were treated with JAQ1-F(ab')$_2$ (4 μg/g BW, i.v.) and effects on peripheral platelet counts and GPVI expression were monitored by flow cytometry. F(ab')$_2$-fragments induced GPVI-immunodepletion, but, importantly, had no significant effects on peripheral platelet counts in WT animals (Figure 27), thus demonstrating that the transient thrombocytopenia associated with JAQ1-induced GPVI down-regulation occurs through Fc-dependent mechanisms. By contrast, GPVI immunodepletion by JAQ1-F(ab')$_2$-fragments caused a rapid platelet count drop in SLAP/SLAP2-deficient mice and, similarly to the IgG-treatment, eventually resulted in severe thrombocytopenia (Figure 27). Notably, treatment with the FcγRIII/FcγRIIB-blocking antibody 2.4G2 prior to JAQ1 administration, which

prevents JAQ1-induced thrombocytopenia and the generation of soluble GPVI (sGPVI), but does not affect GPVI down-regulation through internalization/intracellular degradation (data not shown and David Stegner, unpublished), could not ameliorate acute thrombocytopenia in *Slap⁻/⁻/Slap2⁻/⁻* mice (data not shown). Taken together, these findings strongly suggested that interactions of the JAQ1-GPVI complex with FcγR-bearing cells may not be the major determinant of JAQ1-induced prolonged thrombocytopenia in *Slap⁻/⁻/Slap2⁻/⁻* mice.
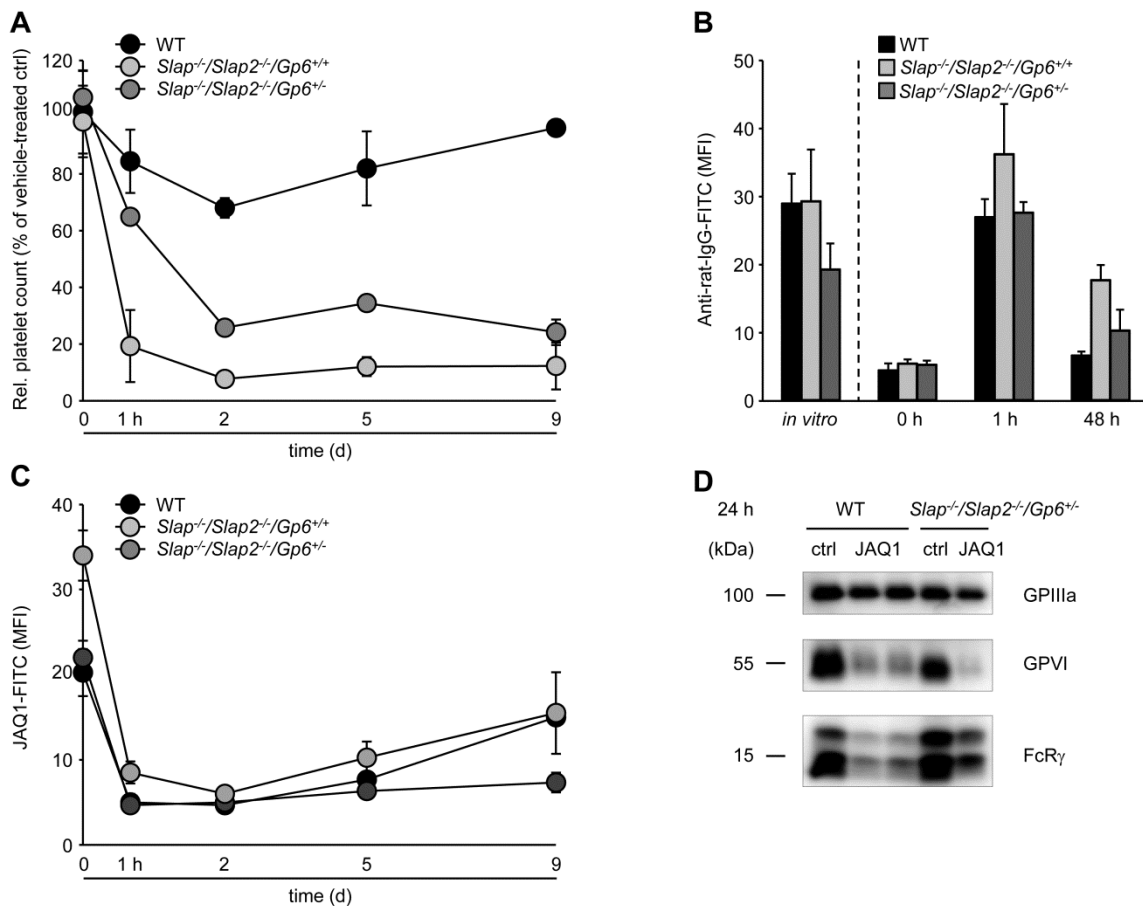

Figure 27. Prolonged severe thrombocytopenia following antibody-induced GPVI down-regulation occurs through an Fc-independent mechanism in SLAP/SLAP2-deficient mice. (A) Relative platelet counts in WT (black circles), *Slap⁻/⁻/Slap2⁻/⁻/Gp6⁺/⁺* (light gray circles) and *Slap⁻/⁻/Slap2⁻/⁻/Gp6⁺/⁻* (dark gray circles) mice at the indicated time points after treatment with 4 μg/g BW JAQ1-F(ab')₂. Platelet counts are expressed as percentage of vehicle-treated control mice. (B) Detection of surface-bound JAQ1 by an anti-rat IgG antibody *in vitro*, prior to (0 h), 1 h and 48 h after JAQ1-F(ab')₂ treatment. (C) Determination of GPVI surface expression by flow cytometry. (A-C) Results are expressed as MFI ± SD (n = 4 mice per group) and are representative of 2 independent experiments. (D) Western blot analysis of total GPVI and FcRγ expression levels 24 h after JAQ1-F(ab')₂ treatment. GPIIIa levels served as loading control.

Importantly, JAQ1 could not induce aggregation of WT platelets by itself, but only upon cross-linking of surface-bound JAQ1 by an anti-rat IgG secondary antibody (Figure 28A and Nieswandt *et al.*, 2000[22], 2001[157]). In marked contrast, the antibody mediated irreversible aggregation of *Slap⁻/⁻/Slap2⁻/⁻* platelets *in vitro* (Figure 28A). Of note, unbound JAQ1 was detectable in the plasma of both WT and *Slap⁻/⁻/Slap2⁻/⁻* mice for up to 2 weeks post treatment (Figure 28B and David Stegner, unpublished). Furthermore, treatment with a low dose of

JAQ1 (0.2 μg/g BW, ~5 μg JAQ1/mouse) induced severe thrombocytopenia in *Slap$^{-/-}$/Slap2$^{-/-}$* mice and even doses as low as 1 μg JAQ1/mouse led to a platelet count drop by 50% (data not shown). Importantly, JAQ1 treatment did not interfere with (pro-)platelet production *in vitro* and ultrastructure, development and localization of MKs following JAQ1 treatment were unaltered in WT and *Slap$^{-/-}$/Slap2$^{-/-}$* mice (data not shown and Daniela Semeniak, Harald Schulze, unpublished). In addition, peripheral platelet count recovery upon induction of immune thrombocytopenia by anti-GPIbα- or anti-GPIIb/IIIa-antibodies took place at a comparable rate in WT and *Slap$^{-/-}$/Slap2$^{-/-}$* mice (data not shown). Collectively, these data indicated that rapid activation of platelets followed by their clearing from the circulation likely contributes to the observed JAQ1-induced prolonged severe thrombocytopenia in *Slap$^{-/-}$/Slap2$^{-/-}$* mice.
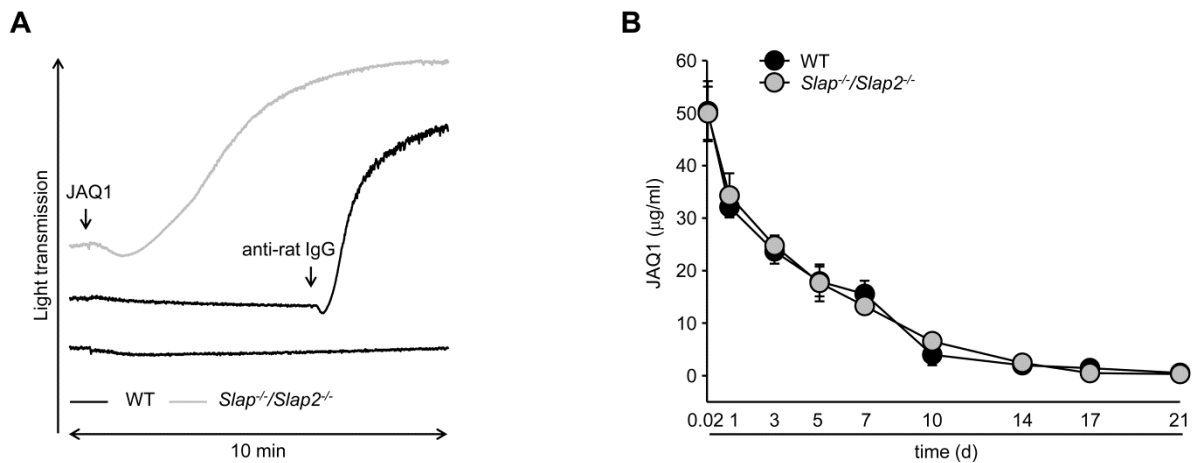

Figure 28. JAQ1 induces aggregation of *Slap$^{-/-}$/Slap2$^{-/-}$* platelets *in vitro*. (A) Washed platelets were activated with JAQ1-IgG and light transmission was recorded on a Fibrintimer 4-channel aggregometer. Addition of an anti-rat IgG secondary antibody induced clustering of GPVI in WT platelets and subsequent platelet aggregation. Aggregation traces representative of experiments with n = 10 different JAQ1 batches yielding similar results are depicted. Arrows indicate addition of the respective antibody. (B) Detection of unbound JAQ1 IgG in the plasma of WT (black circles) or *Slap$^{-/-}$/Slap2$^{-/-}$* (light gray circles) mice treated with 4 μg/g BW JAQ1-IgG^{biotin}. Results are expressed as MFI ± SD (n = 3 mice per group) and are representative of 2 independent experiments, as previously described in the Master thesis "Studies on the ITAM signaling machinery in megakaryocytes and platelets in SLAP/SLAP2-deficient mice" (Deya Cherpokova, 2011).

In a next set of experiments, it was investigated whether prolonged thrombocytopenia occurs also upon immunodepletion of the second (hem)ITAM-bearing receptor on mouse platelets CLEC-2. In contrast to JAQ1, the monoclonal anti-CLEC-2 antibody INU1 induces aggregation of WT mouse platelets *in vitro* and leads to a more severe thrombocytopenia in WT mice *in vivo* with platelet count recovery within 4 days and CLEC-2 loss for > 5 days post treatment.[44,49,59] Importantly, peripheral platelet counts and surface CLEC-2 expression recovered to initial values in *Slap$^{-/-}$*, *Slap2$^{-/-}$* and *Slap$^{-/-}$/Slap2 $^{-/-}$* mice with similar kinetics like in WT control mice (Figure 29). These data demonstrated, firstly, that SLAP and SLAP2, as well as combined loss of both adapter proteins, are dispensable for antibody-induced

CLEC-2 down-regulation. Secondly, the findings confirmed that the prolonged severe thrombocytopenia in *Slap⁻/⁻/Slap2⁻/⁻* mice occurs specifically upon immunodepletion of GPVI.
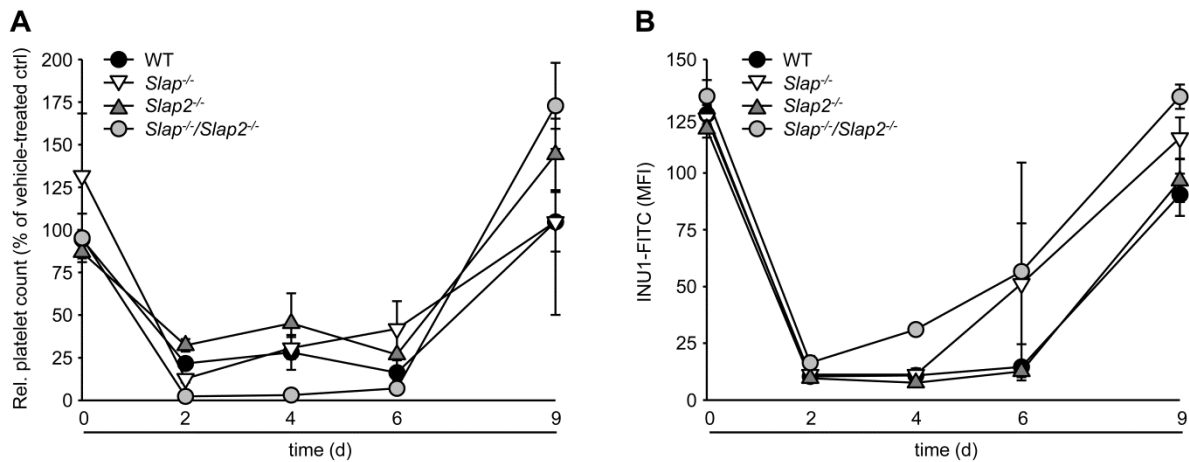

Figure 29. SLAP and SLAP2 are dispensable for antibody-induced CLEC-2 down-regulation. Relative platelet counts in WT (black circles), *Slap⁻/⁻* (▼) and *Slap2⁻/⁻* (▲) and *Slap⁻/⁻/Slap2⁻/⁻* (light gray circles) mice at the indicated time points after treatment with 4 μg/g BW INU1-IgG. Platelet counts are expressed as percentage of vehicle-treated control mice. (B) Determination of CLEC-2 surface expression by flow cytometry. Results are expressed as MFI ± SD (n ≥ 4 mice per group) and are representative of 2 independent experiments in *Slap⁻/⁻* and *Slap2⁻/⁻* mice and 4 independent experiments in *Slap⁻/⁻/Slap2⁻/⁻* mice.

3.2.3. SLAP/SLAP2 are dispensable for LAT- and Syk-independent GPVI immunodepletion

Cellular activation by JAQ1 and subsequent rapid platelet removal might mask effects of SLAP/SLAP2 deficiency on antibody-induced GPVI down-regulation. To specifically investigate the role of SLAP/SLAP2 in receptor internalization and subsequent proteolytic degradation, *Slap⁻/⁻/Slap2⁻/⁻* mice were intercrossed with *Lat⁻/⁻* mice (Figure 15) in which ectodomain shedding is abolished and antibody-induced GPVI down-regulation occurs exclusively through internalization.[41] Consistent with previous studies,[41] JAQ1-treatment had no effects on platelet counts in *Lat⁻/⁻* mice, whereas a transient platelet count drop down to < 50% was observed in *Slap⁻/⁻/Slap2⁻/⁻/Lat⁻/⁻* mice (Figure 30A). Although the generation of sGPVI was abolished in *Slap⁻/⁻/Slap2⁻/⁻/Lat⁻/⁻* mice (Figure 30D), loss of the JAQ1-GPVI complex from the platelet surface (Figure 30B-C) and intracellular degradation of GPVI occurred within a few hours after antibody treatment (Figure 30E), suggesting that internalization of the JAQ1-GPVI complex is functional in the mutant mice despite SLAP/SLAP2/LAT deficiency.
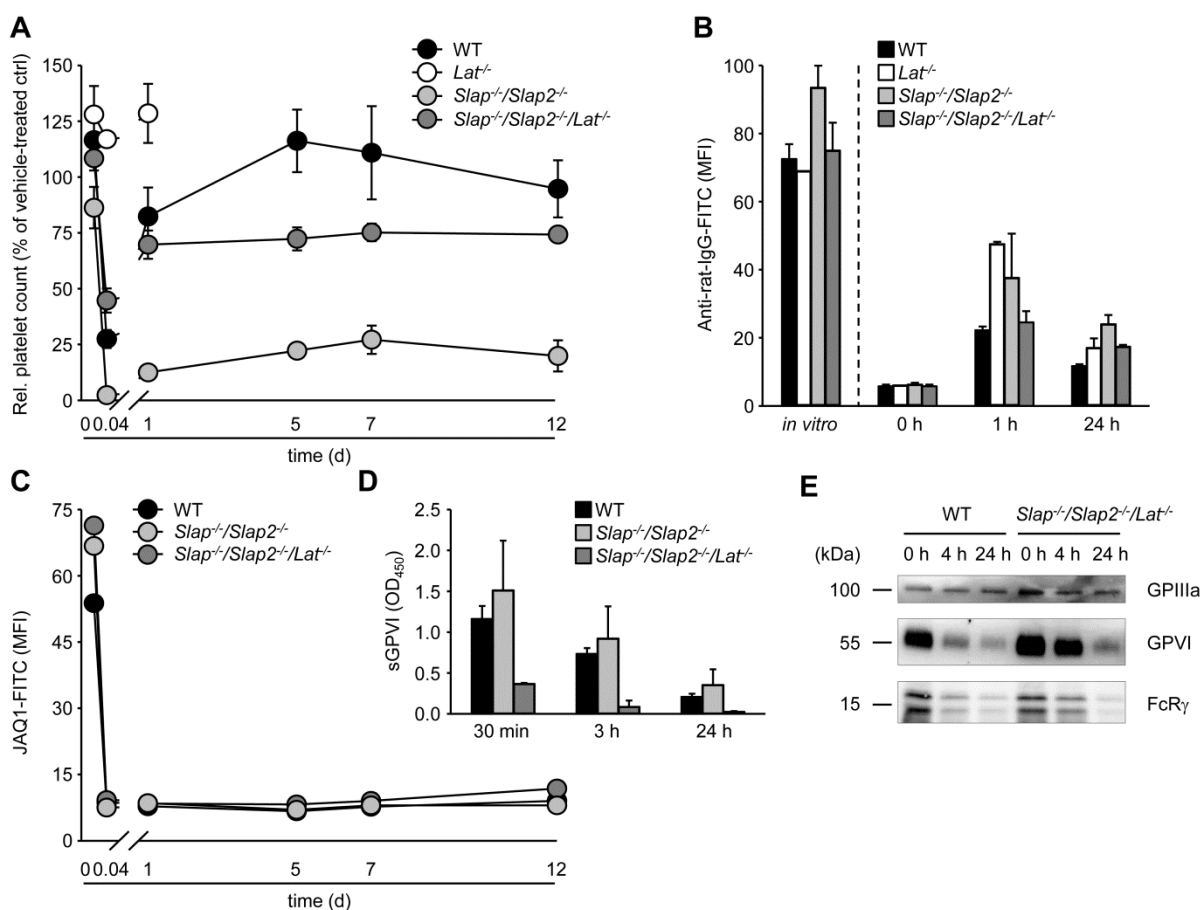
Figure 30. SLAP/SLAP2 are dispensable for LAT-independent antibody-induced GPVI down-regulation. (A) Relative platelet counts in WT (black circles), $Lat^{-/-}$ (white circles), $Slap^{-/-}/Slap2^{-/-}$ (light gray circles) and $Slap^{-/-}/Slap2^{-/-}/Lat^{-/-}$ (dark gray circles) mice at the indicated time points after treatment with 4 µg/g BW JAQ1-IgG. Platelet counts are expressed as percentage of vehicle-treated control mice. (B) Detection of surface-bound JAQ1 by an anti-rat IgG antibody *in vitro*, prior to (0 h), 1 h and 24 h after JAQ1-IgG treatment. (C) Determination of GPVI surface expression by flow cytometry. (A-C) Results are expressed as MFI ± SD (n = 4 mice per group) and are representative of 3 independent experiments. (D) Plasma levels of sGPVI at the indicated time points after treatment with JAQ1-IgG were determined using an ELISA system. Background levels detected on $Gp6^{-/-}$ platelets were subtracted. Results are representative of 2 independent experiments which were performed by Dr. Markus Bender. (E) Western blot analysis of total GPVI and FcRγ expression levels at the indicated time points after treatment with JAQ1-IgG. GPIIIa levels served as loading control. Blots are representative of 2 independent experiments.

To assess the contribution of GPVI signaling to receptor down-regulation in more detail and to further characterize the conditions under which JAQ1-induced thrombocytopenia occurs in a SLAP/SLAP2-deficient background, $Slap^{-/-}/Slap2^{-/-}$ mice were intercrossed with MK-/platelet-specific Syk KO mice ($Syk^{fl/fl\ Pf4-Cre+}$)[59] to generate $Slap^{-/-}/Slap2^{-/-}/Syk^{fl/fl\ Pf4-Cre+}$ animals (Figure 31A). Notably, JAQ1 administration did not induce thrombocytopenia in Syk-deficient mice, irrespective of concomitant deficiency of SLAP/SLAP2 (Figure 31B), demonstrating that Syk is essential for JAQ1-induced thrombocytopenia to occur in $Slap^{-/-}/Slap2^{-/-}$ mice. Syk was required for the generation of sGPVI (Figure 32A and David Stegner, unpublished).
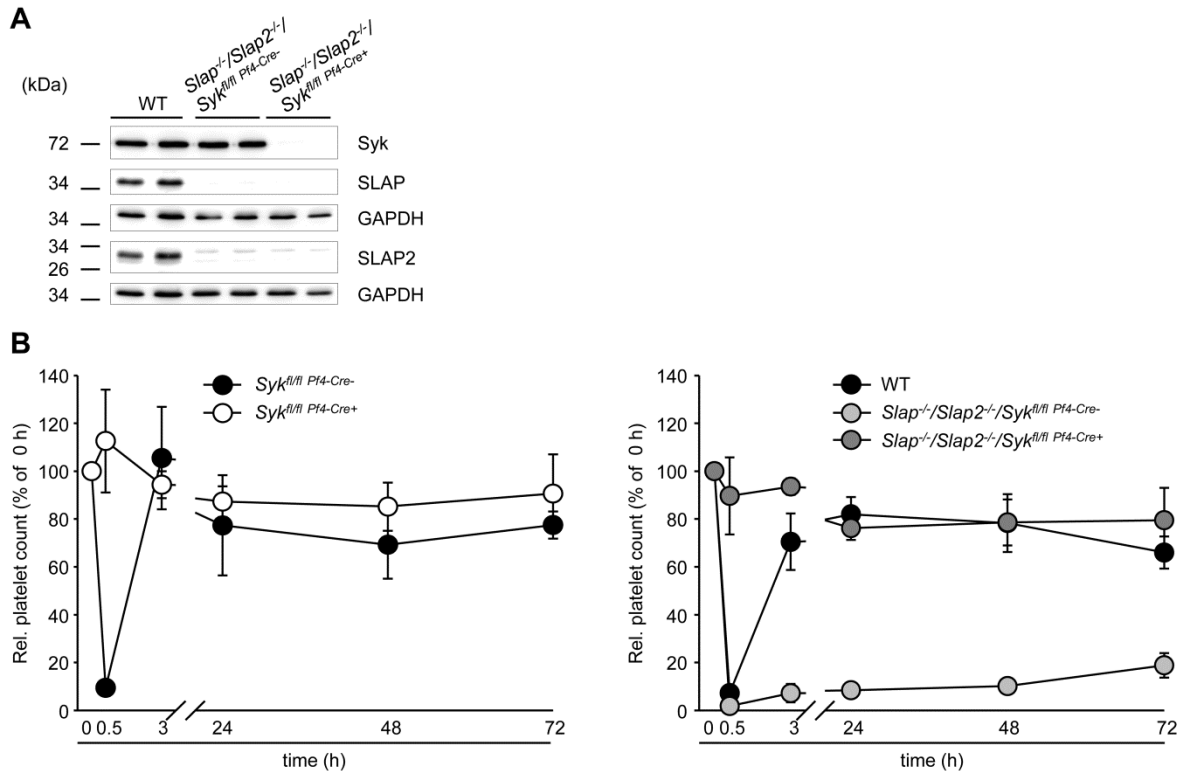
Figure 31. Platelet-specific Syk deficiency prevents JAQ1-induced thrombocytopenia in
Slap$^{-/-}$/Slap2$^{-/-}$ **mice.** (A) Western blot analysis demonstrating absence of SLAP, SLAP2 and Syk in
Slap$^{-/-}$/Slap2$^{-/-}$/Syk$^{fl/fl\ Pf4-Cre+}$ platelets. GAPDH expression was used as loading control. (B) Relative
platelet counts in WT (black circles), *Syk$^{fl/fl\ Pf4-Cre+}$* (white circles), *Slap$^{-/-}$/Slap2$^{-/-}$/Syk$^{fl/fl\ Pf4-Cre-}$* (light gray
circles) and *Slap$^{-/-}$/Slap2$^{-/-}$/Syk$^{fl/fl\ Pf4-Cre+}$* (dark gray circles) mice at the indicated time points after
treatment with 2 µg/g BW JAQ1-IgG^{biotin}. Experiments were simultaneously performed, but results are
depicted on different graphs for clarity. Results are expressed as MFI ± SD (n = 4 mice per group) and
are representative of 2 independent experiments.

Despite abolished ectodomain shedding in Syk-deficient mice, GPVI was consistently
removed from the platelet surface, albeit with slower kinetics as compared to WT mice
(Figure 32B). This was further confirmed by Western blot analyses of the total amount of
GPVI and JAQ1 which steadily decreased in both *Syk$^{fl/fl\ Pf4-Cre+}$* and *Slap$^{-/-}$/Slap2$^{-/-}$/Syk$^{fl/fl\ Pf4-Cre+}$*
platelets (Figure 33). The discrepancy in the rates of intracellular clearing of the JAQ1-GPVI
complex were likely due to considerable differences in (total) GPVI expression levels
between both mutant mouse strains. These findings indicated that SLAP/SLAP2 are
dispensable for Syk-independent internalization of GPVI upon receptor immunodepletion.

Collectively, the data presented in the first and second part of this thesis demonstrated
that SLAP and SLAP2 have essential overlapping functions in the control of the (hem)ITAM
signaling cascade in mouse platelets which may have important implications in thrombotic
and thrombo-inflammatory disease states. Although both adapter proteins were dispensable
for the targeted down-regulation of (hem)ITAM receptors to occur, SLAP and SLAP2 seem to
play redundant roles in the prevention of therapeutically undesired thrombocytopenia
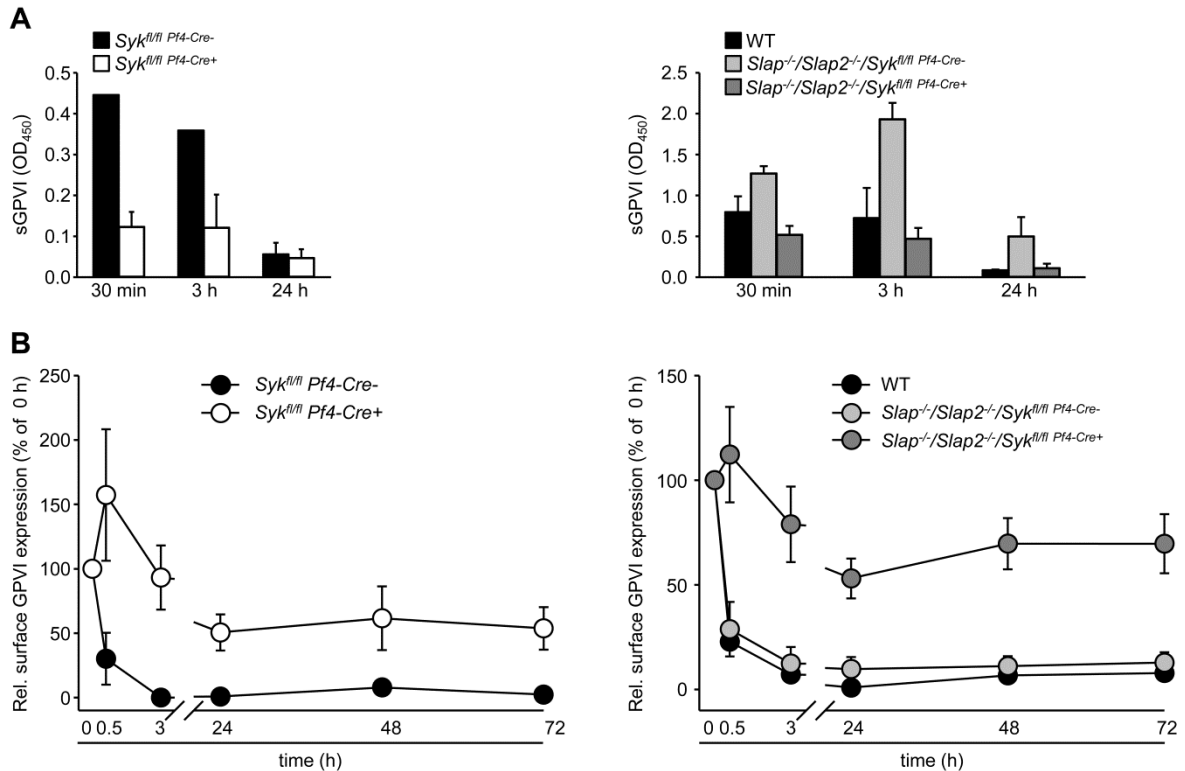following GPVI immunodepletion.

Figure 32. SLAP/SLAP2 are dispensable for Syk-independent antibody-induced GPVI down-regulation. (A) Plasma levels of sGPVI upon treatment with 2 μg/g BW JAQ1-IgG^{biotin} were determined using an ELISA system. Background levels detected on $Gp6^{-/-}$ platelets were subtracted. Note the differences in the Y-axis scale between the left and the right panel. (B) Surface expression of GPVI on the platelet surface in WT (black circles), $Syk^{fl/fl\ Pf4-Cre+}$ (white circles), $Slap^{-/-}/Slap2^{-/-}/Syk^{fl/fl\ Pf4-Cre-}$ (light gray circles) and $Slap^{-/-}/Slap2^{-/-}/Syk^{fl/fl\ Pf4-Cre+}$ (dark gray circles) mice was determined by flow cytometry using an anti-rat IgG-FITC antibody. Start values were determined by *in vitro* incubation of platelets with JAQ-IgG followed by detection with an anti-rat IgG antibody and were set to 100%. Experiments were simultaneously performed, but results are depicted on different graphs for clarity. Results are expressed as MFI ± SD (n = 4 mice per group) and are representative of 2 independent experiments.
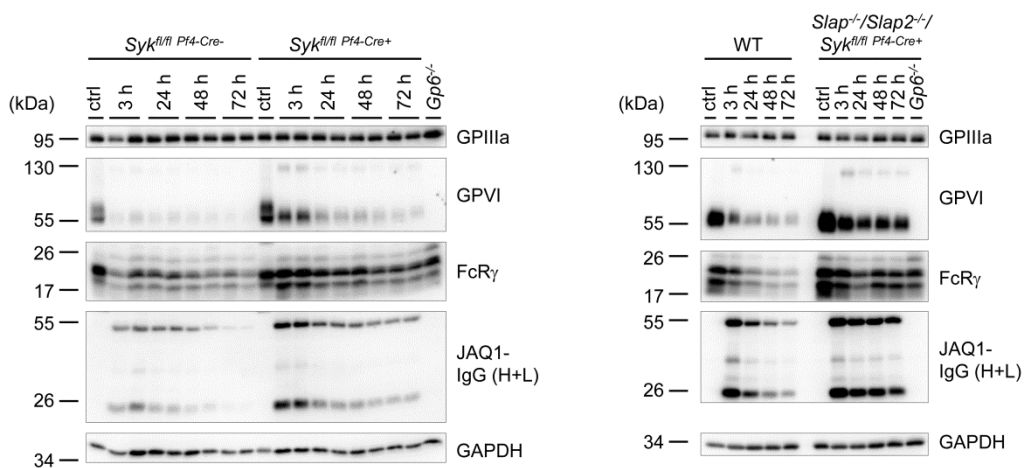

Figure 33. SLAP/SLAP2 are dispensable for Syk-independent intracellular clearing of JAQ1-GPVI upon antibody-induced receptor down-regulation. Western blot analysis of JAQ1 levels and total GPVI and FcRγ expression levels at the indicated time points after treatment with 2 μg/g BW JAQ1-IgG^{biotin}. GPIIIa levels served as loading control. Experiments were simultaneously performed, but samples were loaded onto different gels for clarity. Blots are representative of 2 independent experiments.

3.3. Combined deficiency of RhoA and Cdc42 causes abnormal megakaryocyte development, severe macrothrombocytopenia and defective tubulin organization

Rho GTPases, such as RhoA, Cdc42 and Rac1, have been established as key regulators of cytoskeletal rearrangements in platelets, but their specific roles and possible functional redundancies during platelet biogenesis and preceding reorganization of the MK actin and tubulin cytoskeleton are only beginning to be understood. For instance, a redundant function of Rac1 and Cdc42 has recently been demonstrated in the regulation of microtubule dynamics and (pro-)platelet formation,[127] emphasizing the existence of overlapping roles of Rho GTPases in these processes. In this part of the thesis, putative functional redundancies between RhoA and Cdc42 in platelet production and function were investigated.

3.3.1. Combined deficiency of RhoA and Cdc42 leads to severe macrothrombocytopenia

To study the consequences of combined loss of RhoA and Cdc42 specifically in the MK-/platelet-lineage, mice carrying both the RhoA[135] and the Cdc42[136] genes flanked by loxP sites - $RhoA^{fl/fl}/Cdc42^{fl/fl}$ - were intercrossed with transgenic mice carrying the Cre-recombinase under the control of the MK-/platelet-specific PF4 promoter.[137] Resulting double-deficient $RhoA^{fl/fl}/Cdc42^{fl/fl\ Pf4-Cre+}$ (further referred to as $RhoA^{-/-}/Cdc42^{-/-}$) and littermate control mice $RhoA^{fl/fl}/Cdc42^{fl/fl\ Pf4-Cre-}$ (further referred to as WT) were used in all studies. In some experiments, conditional single deficient mice - $RhoA^{fl/fl\ Pf4-Cre+}$ ($RhoA^{-/-}$) and $Cdc42^{fl/fl\ Pf4-Cre+}$ ($Cdc42^{-/-}$) - were used in parallel in order to better discriminate between redundant and non-redundant functions of both GTPases.

In agreement with previous studies,[112,113] $RhoA^{-/-}$ and $Cdc42^{-/-}$ mice displayed only moderately decreased platelet counts, whereas double deficiency of RhoA and Cdc42 (Figure 34A) resulted in severe thrombocytopenia with peripheral platelet counts lower than 25% of WT mice (1026 ± 113/nl in WT vs. 234 ± 44/nl in $RhoA^{-/-}/Cdc42^{-/-}$ mice, Figure 34B and Table 3-3). Consistent with previous reports,[112,113] flow cytometric and *transmission electron microscopy* (TEM) analyses revealed only slightly increased size of $Cdc42^{-/-}$ platelets and a moderate increase in size and a roundish shape of $RhoA^{-/-}$ platelets, whereas, importantly, subcellular morphology and granule distribution were largely unaltered in the mutant cells (Figure 34C-D). In stark contrast, RhoA/Cdc42 deficiency resulted in a significant increase in platelet volume accompanied by a severely altered ultrastructure (Figure 34C-D).
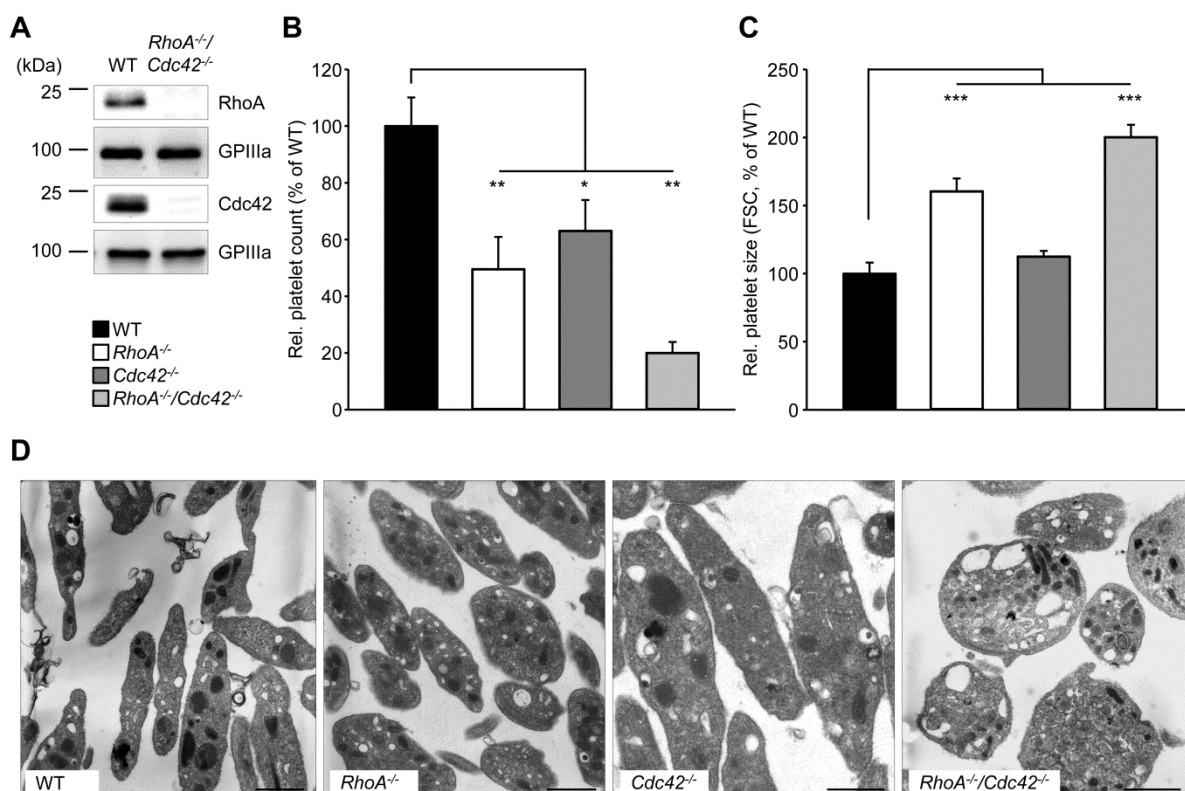
Figure 34. RhoA/Cdc42 deficiency results in severe macrothrombocytopenia. (A) Western blot analysis demonstrating absence of RhoA and Cdc42 in MK-/platelet-specific RhoA/Cdc42 KO mice. GPIIIa expression was used as loading control. Peripheral platelet counts (B) and relative platelet size (C) of WT (black bars), *RhoA*$^{-/-}$ (white bars), *Cdc42*$^{-/-}$ (dark gray bars) and *RhoA*$^{-/-}$*/Cdc42*$^{-/-}$ (light gray bars) mice were determined by flow cytometry. Values were normalized to WT levels which were set to 100%. Resuts are expressed as MFI ± SD (n = 4 mice per group) representative of 3 independent experiments. (D) TEM analysis of resting WT, *RhoA*$^{-/-}$,[112] *Cdc42*$^{-/-}$ [127] and *RhoA*$^{-/-}$*/Cdc42*$^{-/-}$ platelets. Bars: 2.5 μm for WT and *RhoA*$^{-/-}$*/Cdc42*$^{-/-}$ platelets, 1 μm for *RhoA*$^{-/-}$ platelets and 0.5 μm for *Cdc42*$^{-/-}$ platelets. *P < .05; **P < .01; ***P < .001.

	WT	*RhoA*$^{-/-}$*/Cdc42*$^{-/-}$
Platelets (nl^{-1})	1026 ± 113	234 ± 44‡
MPV (fl)	5.04 ± 0.10	7.24 ± 0.48‡
WBC (nl^{-1})	4.40 ± 0.97	4.67 ± 1.75
RBC (x 10^{3} nl^{-1})	710 ± 125	695 ± 56
HCT (%)	34.80 ± 6.09	33.83 ± 2.33
HGB (g dl^{-1})	10.70 ± 1.84	9.92 ± 0.69

Table 3-3. Analysis of basic blood parameters in WT and *RhoA*$^{-/-}$*/Cdc42*$^{-/-}$ mice. Heparinized whole blood was analyzed on a Sysmex KX-21N™ Hematology Analyzer. Results express mean ± SD (n ≥ 6 mice per group) and are representative of 5 independent experiments. MPV: *mean platelet volume*; WBC: *white blood cells*; RBC: *red blood cells*; HCT: *hematocrit*; HGB: *hemoglobin*. ‡ P < .001.

Detailed analysis of resting *RhoA*$^{-/-}$*/Cdc42*$^{-/-}$ platelets by TEM revealed severe defects in the tubulin structure and the microtubule coils in the marginal band were not or only barely visible (Figure 35A). These findings were confirmed by immunohistochemical analysis of the microtubule organization in spread platelets (Figure 35B, upper panel) and in the swellings

and tips of proplatelets (Figure 35B, lower panel). TEM analysis further revealed heterogeneous size and shape of resting $RhoA^{-/-}/Cdc42^{-/-}$ platelets which were virtually devoid of granules or contained structures reminiscent of empty granules or vacuoles instead (Figure 35C). Collectively, these results revealed critical overlapping functions of RhoA and Cdc42 in platelet production, granule biogenesis and microtubule organization.
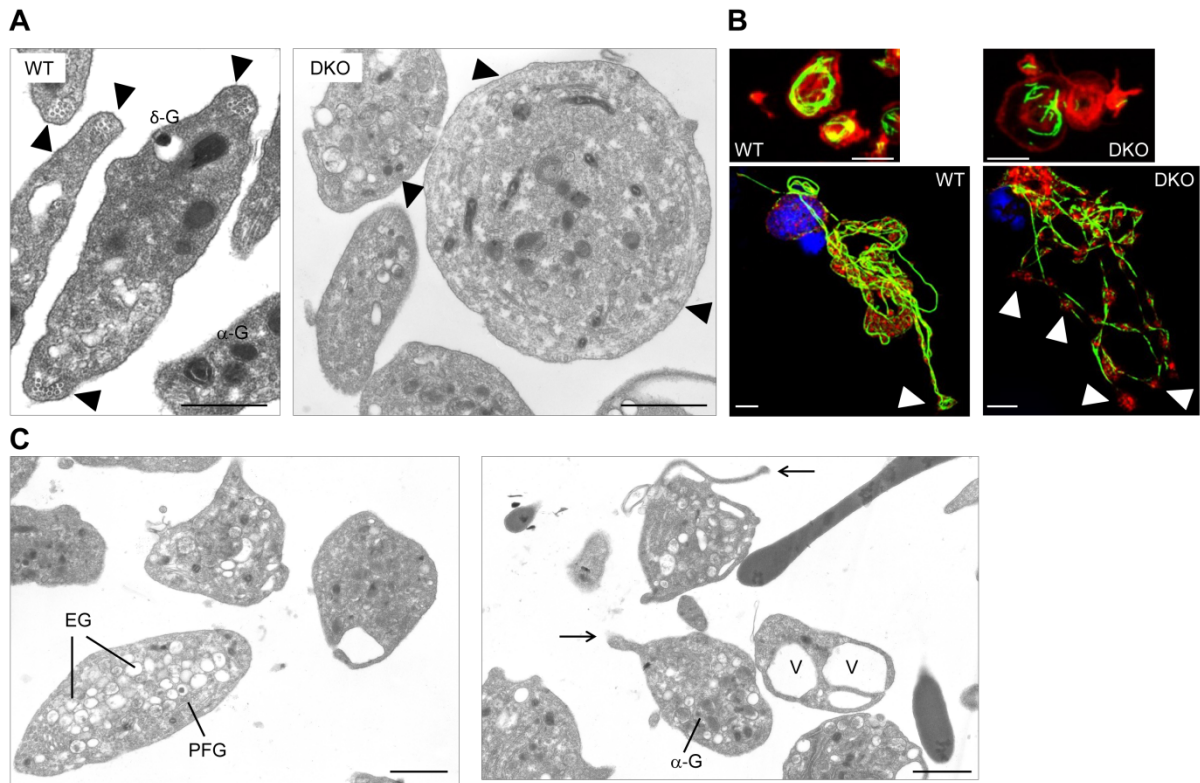

Figure 35. $RhoA^{-/-}/Cdc42^{-/-}$ platelets display abnormal ultrastructure and severely altered microtubule organization. (A) TEM analysis of microtubule distribution in resting platelets. Arrowheads indicate marginal microtubule coils which are clearly visible in WT platelets, in contrast to $RhoA^{-/-}/Cdc42^{-/-}$ platelets. Bars: 1 μm. (B) Analysis of the actin cytoskeleton (F-actin: red – Phalloidin-Atto647N) and tubulin structure (green – anti-α-Tubulin-Alexa488) in platelets spread on fibrinogen for 30 min (upper panel) or in proplatelet forming fetal liver cell-derived MKs (lower panel). Bars: 5 μm (upper panel); 10 μm (lower panel). (C) Representative TEM images of resting $RhoA^{-/-}/Cdc42^{-/-}$ platelets demonstrating the heterogeneous nature of different mutant platelets with respect to size, shape, granule and vacuole content. Arrows point at protrusions. Bars: 1 μm. DKO: $RhoA^{-/-}/Cdc42^{-/-}$; δ-G: *dense granule*; α-G: *α-granule*; EG: *empty granules*; PFG: *partially filled granules*; V: *vacuoles*.

3.3.2. Combined deficiency of RhoA and Cdc42 results in defective hemostasis, but largely preserved thrombus formation *in vivo*

Next, the effect of RhoA/Cdc42 deficiency on platelet function was assessed. Flow cytometric analysis of the surface expression of major platelet receptors revealed reduced expression of subunits of the GPIb-V-IX complex and of GPVI in $RhoA^{-/-}/Cdc42^{-/-}$ platelets which strongly resembled the phenotype of $Cdc42^{-/-}$ platelets (Table 3-4).

$RhoA^{-/-}/Cdc42^{-/-}$ platelets displayed severe defects in integrin $\alpha IIb\beta 3$ activation which were stronger than the reductions observed in RhoA and Cdc42 single KO platelets (Figure 36A, left panel). In particular, $RhoA^{-/-}/Cdc42^{-/-}$ platelets (and $Cdc42^{-/-}$ platelets) were refractory especially to stimulation with the ITAM-specific agonists CRP and convulxin, which could, at least in part, be explained by the reduced expression of GPVI (Table 3-4 and Figure 36B) that has been demonstrated to be affect particularly platelet activation with CRP.[158]

Remarkably, however, α-granule secretion was largely preserved in $RhoA^{-/-}/Cdc42^{-/-}$ platelets, especially after stimulation of GPCRs, as demonstrated by flow cytometric analysis of degranulation-dependent P-selectin exposure (Figure 36A, right panel) and analysis of secreted platelet VWF and PF4 by ELISA systems (Figure 36C). These findings were particularly surprising because of the striking morphology of the $RhoA^{-/-}/Cdc42^{-/-}$ platelets and the large number of mutant platelets virtually devoid of (α-) granules (Figure 34, Figure 35). Notably, the secretion defect downstream of G_{13} and G_q in $RhoA^{-/-}$ platelets[112] was overcome by a concomitant loss of Cdc42 which has previously been demonstrated to negatively regulate platelet degranulation.[113] Of note, $RhoA^{-/-}/Cdc42^{-/-}$ platelets did not show any signs of preactivation under resting conditions or upon *in vitro* stimulation with the weak agonist epinephrine which can potentiate existing platelet activation[157] (Figure 36). Taken together, these findings indicated the existence of both overlapping and distinct functions of RhoA and Cdc42 in platelet activation.

	WT	$RhoA^{-/-}$	$Cdc42^{-/-}$	$RhoA^{-/-}/Cdc42^{-/-}$
GPIb	308 ± 17	271 ± 33	235 ± 13[†]	205 ± 6[†]
GPV	202 ± 10	218 ± 2	168 ± 6*	170 ± 9*
GPIX	344 ± 15	346 ± 28	279 ± 10[†]	252 ± 22[†]
CD9	983 ± 28	910 ± 121	935 ± 18	925 ± 36
GPVI	47 ± 3	54 ± 6	37 ± 3*	36 ± 6*
CLEC-2	97 ± 9	104 ± 5	103 ± 3	107 ± 9
$\alpha 2$	39 ± 1	40 ± 3	37 ± 1	38 ± 2
$\beta 1$	108 ± 5	116 ± 14	91 ± 1*	111 ± 7
$\alpha IIb\beta 3$	388 ± 28	441 ± 58	362 ± 32	344 ± 32

Table 3-4. Analysis of surface expression of glycoproteins in WT, *RhoA$^{-/-}$*, *Cdc42$^{-/-}$* and *RhoA$^{-/-}$/Cdc42$^{-/-}$* platelets. Diluted whole blood was stained with saturating amounts of fluorophore-labeled antibodies and platelets were analyzed by flow cytometry. Results express MFI ± SD (n = 4 mice per group) and are representative of 3 independent experiments. Statistical analyses represent comparison to WT platelets. * $P < .05$; [†] $P < .01$.
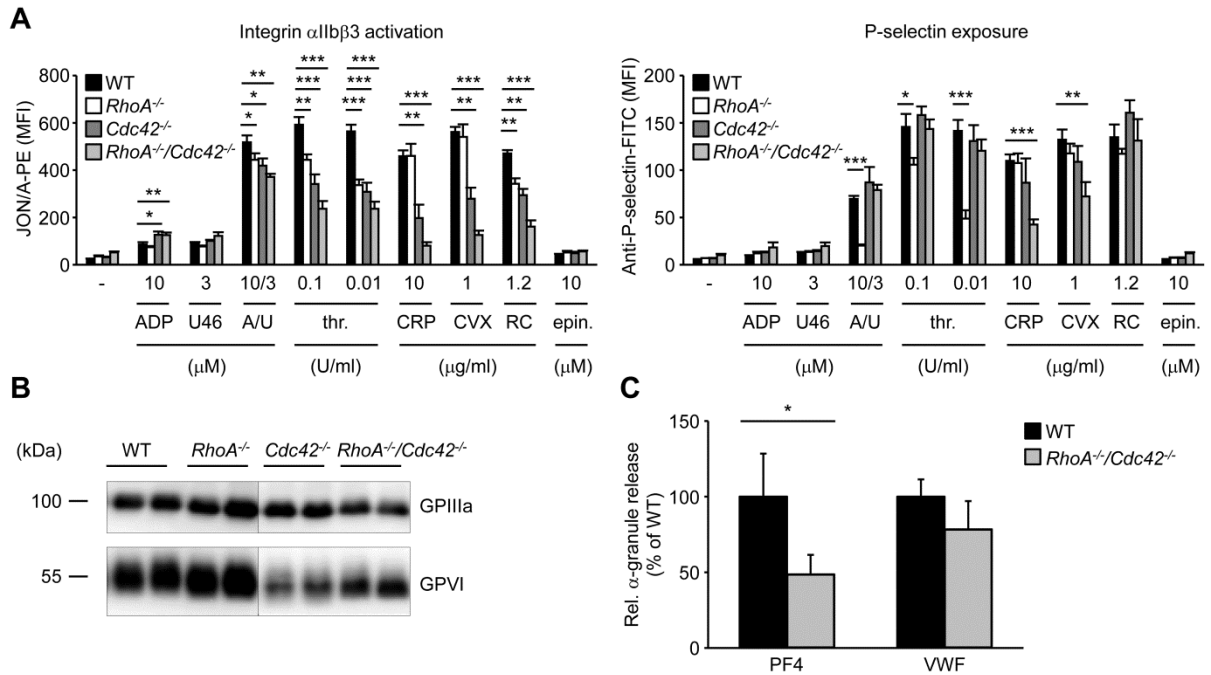
Figure 36. Markedly impaired integrin activation, but largely preserved α-granule release in **RhoA$^{-/-}$/Cdc42$^{-/-}$** **platelets.** (A) Flow cytometric analysis of activated integrin αIIbβ3 (binding of JON/A-PE) (left panel) and degranulation-dependent P-selectin exposure (right panel) upon stimulation with the indicated agonists in WT (black bars), RhoA$^{-/-}$ (white bars), Cdc42$^{-/-}$ (dark gray bars) and RhoA$^{-/-}$/Cdc42$^{-/-}$ (light gray bars) platelets. Results are expressed as MFI ± SD (n = 4 mice per group) and are representative of 3 independent experiments. (B) Western blot analysis of total GPVI expression levels in WT, RhoA$^{-/-}$, Cdc42$^{-/-}$ and RhoA$^{-/-}$/Cdc42$^{-/-}$ platelets. GPIIIa levels served as loading control. Dividing lines denote gaps between different sections of the same membrane. Blots are representative of 2 independent experiments with n = 2-4 samples per genotype. (C) ELISA-measurement of secreted PF4 and VWF in the supernatant of WT and RhoA$^{-/-}$/Cdc42$^{-/-}$ platelets activated with 0.1 U/ml thrombin for 15 min. Results are expressed as MFI ± SD and are representative of 2 independent experiments with n = 4. U46, U-46619; A/U, ADP + U-46619; thr., *thrombin*; CVX, *convulxin*; CRP, *collagen-related peptide*; epin., *epinephrine*; PF4, *platelet factor 4*; RC, *rhodocytin*; VWF, *von Willebrand factor*. Statistical analyses represent comparison to WT platelets.*$P < .05$; **$P < .01$; ***$P < .001$.

To investigate the effects of RhoA/Cdc42 deficiency on platelet spreading, thrombin-activated WT and RhoA$^{-/-}$/Cdc42$^{-/-}$ platelets were allowed to spread on fibrinogen - a process dependent on integrin αIIbβ3 induced outside-in signaling for adhesion and cytoskeletal remodeling.[16] Thrombin-activated RhoA$^{-/-}$/Cdc42$^{-/-}$ platelets spread on fibrinogen to a similar extent and with similar kinetics to WT platelets (Figure 37) and were also able to centralize α-granules (data not shown). However, spread RhoA$^{-/-}$/Cdc42$^{-/-}$ platelets were either devoid of or only exhibited disrupted marginal microtubule coils and a more diffuse F-actin pattern (Figure 35B, upper panel). Together, these results indicated that RhoA and Cdc42 are dispensable for spreading of platelets on fibrinogen, but both Rho GTPases are significantly involved in the regulation of cytoskeletal rearrangements upon platelet activation.
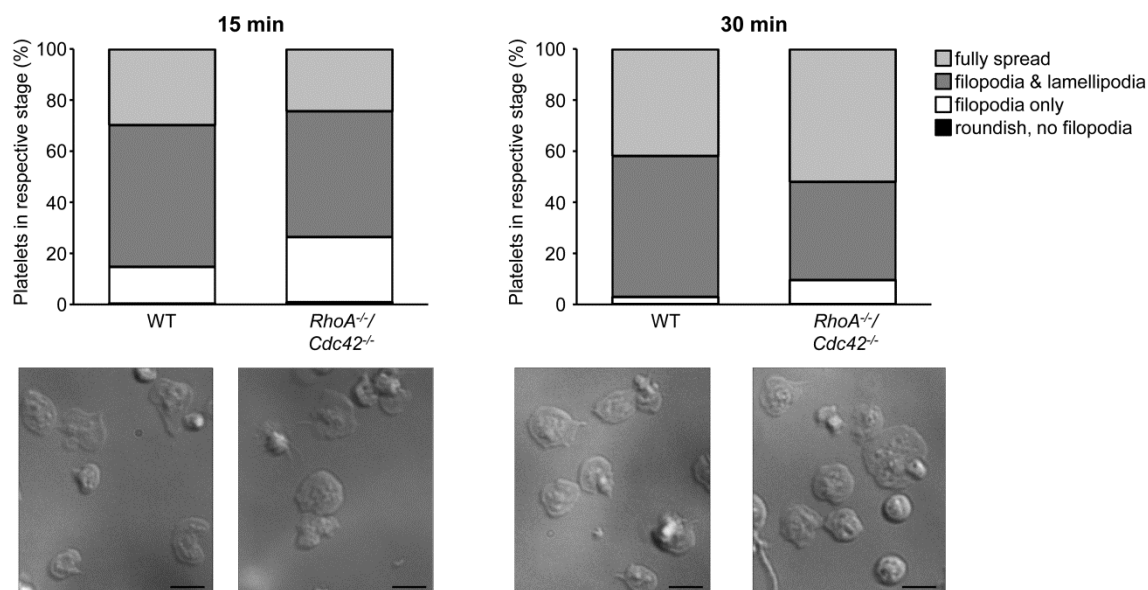
Figure 37. Unaltered spreading of *RhoA⁻/⁻/Cdc42⁻/⁻* platelets on fibrinogen upon activation. Washed platelet from WT and *RhoA⁻/⁻/Cdc42⁻/⁻* mice were allowed to spread on immobilized human fibrinogen (100 µg/ml) after activation with 0.01 U/ml thrombin for the indicated time periods. (Upper panel) Statistical analysis of the percentage of platelets in the respective stage. (Lower panel) Representative differential interference contrast images of spread platelets. Results are representative of 2 independent experiments with n = 3 samples per genotype. Bar: 5 µm.

To assess the impact of RhoA/Cdc42 deficiency on hemostasis, tail bleeding times were determined (Figure 38A). *RhoA⁻/⁻/Cdc42⁻/⁻* mice displayed a severe hemostatic defect characterized by the inability to arrest bleeding within an observation period of 20 min (mean tail bleeding time in WT mice: 438 ± 224 sec). The hemostatic function in RhoA/Cdc42-deficient mice was more severely affected than in the respective single KO mice,[112,113] demonstrating a functional redundancy of RhoA and Cdc42 in the formation and stabilization of a hemostatic plug.

Importantly, previous studies have shown that RhoA deficiency is associated with thrombus instability and resultant frequent embolization of occlusive thrombi, leading to a profound protection in models of arterial thrombosis,[112] whereas loss of Cdc42 induces accelerated formation of occlusive thrombi.[113] To examine the extent to which the above described defects influence thrombotic events *in vivo*, *RhoA⁻/⁻/Cdc42⁻/⁻* and WT mice were subjected to two models of occlusive arterial thrombus formation. In the first model, thrombus formation after injury of small mesenteric arterioles by $FeCl_3$ was monitored by intravital fluorescence microscopy. Surprisingly, both the beginning of thrombus formation (data not shown) and the subsequent formation of stable occlusive thrombi followed similar kinetics in WT and *RhoA⁻/⁻/Cdc42⁻/⁻* mice (Figure 38B). In a second model of occlusive arterial thrombosis, the carotid artery – a medium-sized vessel in which moderate shear rates prevail - was injured by topical application of $FeCl_3$. Unexpectedly, 63% of the *RhoA⁻/⁻/Cdc42⁻/⁻* mice (5 out of 8) were still able to form occlusive thrombi, but the mean

occlusion time was significantly increased in these animals ($RhoA^{-/-}/Cdc42^{-/-}$ mice: 634 ± 144 s vs. 345 ± 106 s in WT mice; Figure 38C). These findings are in agreement with a previous report, demonstrating a significant increase in the mean occlusion times of the chemically injured carotid artery in mice in which platelet counts were reduced to 200-299 platelets/nl (~20-30% of control).[138] Importantly, platelet counts in $RhoA^{-/-}/Cdc42^{-/-}$ mice, in which no occlusive thrombus formation was observed, were reduced to less than 20% of those in littermate controls simultaneously subjected to this model and thus close to the threshold platelet count required for occlusive thrombus formation to occur in the carotid artery.[138] Therefore, a second group of $RhoA^{-/-}/Cdc42^{-/-}$ mice received platelets from 2 donor $RhoA^{-/-}/Cdc42^{-/-}$ mice each to reach platelet counts of ≥ 30% compared to WT controls. Notably, mean occlusion times in these animals did not significantly differ from those in littermate controls ($RhoA^{-/-}/Cdc42^{-/-}$ mice transfused with $RhoA^{-/-}/Cdc42^{-/-}$ platelets: 415 ± 150 s vs. 345 ± 106 s in WT mice; Figure 38C). Collectively, these results demonstrated largely unaltered susceptibility of $RhoA^{-/-}/Cdc42^{-/-}$ mice to arterial thrombosis models despite severely defective hemostasis and further emphasized divergent roles for platelet RhoA and Cdc42 in thrombosis and hemostasis.
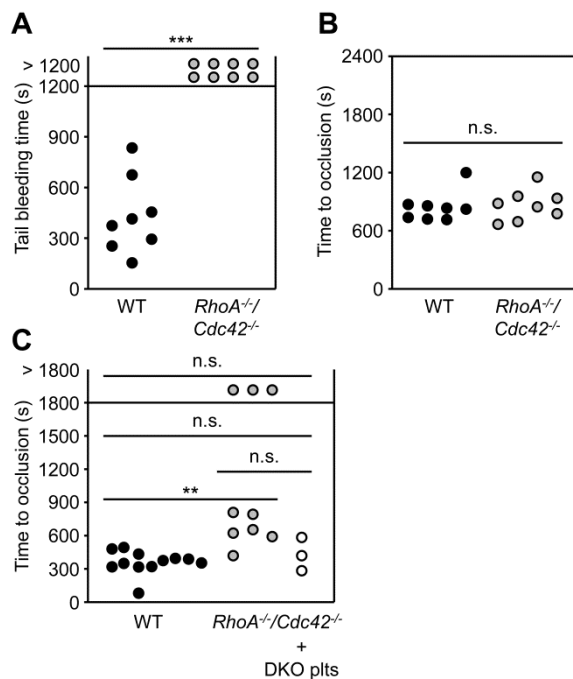

Figure 38. Defective hemostasis, but largely preserved thrombus formation *in vivo* in $RhoA^{-/-}/Cdc42^{-/-}$ mice. (A) Infinite tail bleeding times in $RhoA^{-/-}/Cdc42^{-/-}$ mice. Each symbol represents 1 animal. (B) Mesenteric arterioles were injured with 20% $FeCl_3$ and thrombus formation of fluorescently labeled platelets was monitored *in vivo* by intravital fluorescence microscopy. Time to complete vessel occlusion (stable vessel occlusion for at least 1 min) is depicted. Each symbol represents 1 animal. (C) The right carotid artery of WT and $RhoA^{-/-}/Cdc42^{-/-}$ mice was injured by topical application of 15% $FeCl_3$ for 90 s and blood flow was monitored with a Doppler flow probe until complete vessel occlusion for at least 2 min, or for a maximum of 30 min. Each symbol represents 1 animal. White circles indicate occlusion times of $RhoA^{-/-}/Cdc42^{-/-}$ mice which received platelets from 2 donor $RhoA^{-/-}/Cdc42^{-/-}$ mice each to reach peripheral platelet counts of ≥ 30% of WT controls. **$P < .01$; ***$P < .001$; n.s., not significant.

3.3.3. $RhoA^{-/-}/Cdc42^{-/-}$ mice display reduced platelet life span, but unaltered platelet production upon platelet depletion

In a next set of experiments, the effects of combined RhoA/Cdc42 deficiency on the rate of platelet clearance and platelet production were investigated. $RhoA^{-/-}/Cdc42^{-/-}$ platelets displayed a strongly decreased half-life of less than 24 h in the circulation - a life span

considerably shorter than that of both *RhoA⁻ᐟ⁻* platelets and *Cdc42⁻ᐟ⁻* platelets (Figure 39A). Interestingly, platelet count recovery rates following anti-GPIbα antibody-mediated platelet depletion were similar in *RhoA⁻ᐟ⁻/Cdc42⁻ᐟ⁻* and WT mice, thus excluding a global defect in platelet production in *RhoA⁻ᐟ⁻/Cdc42⁻ᐟ⁻* mice (Figure 39B). Consistent with these findings, an *in vitro* proplatelet formation assay revealed unaltered numbers of proplatelet-forming MKs in cultures derived from *fetal liver cells* (FLCs) (Figure 39C) and these data were confirmed with *in vitro* cultured BM-derived MKs (data not shown).
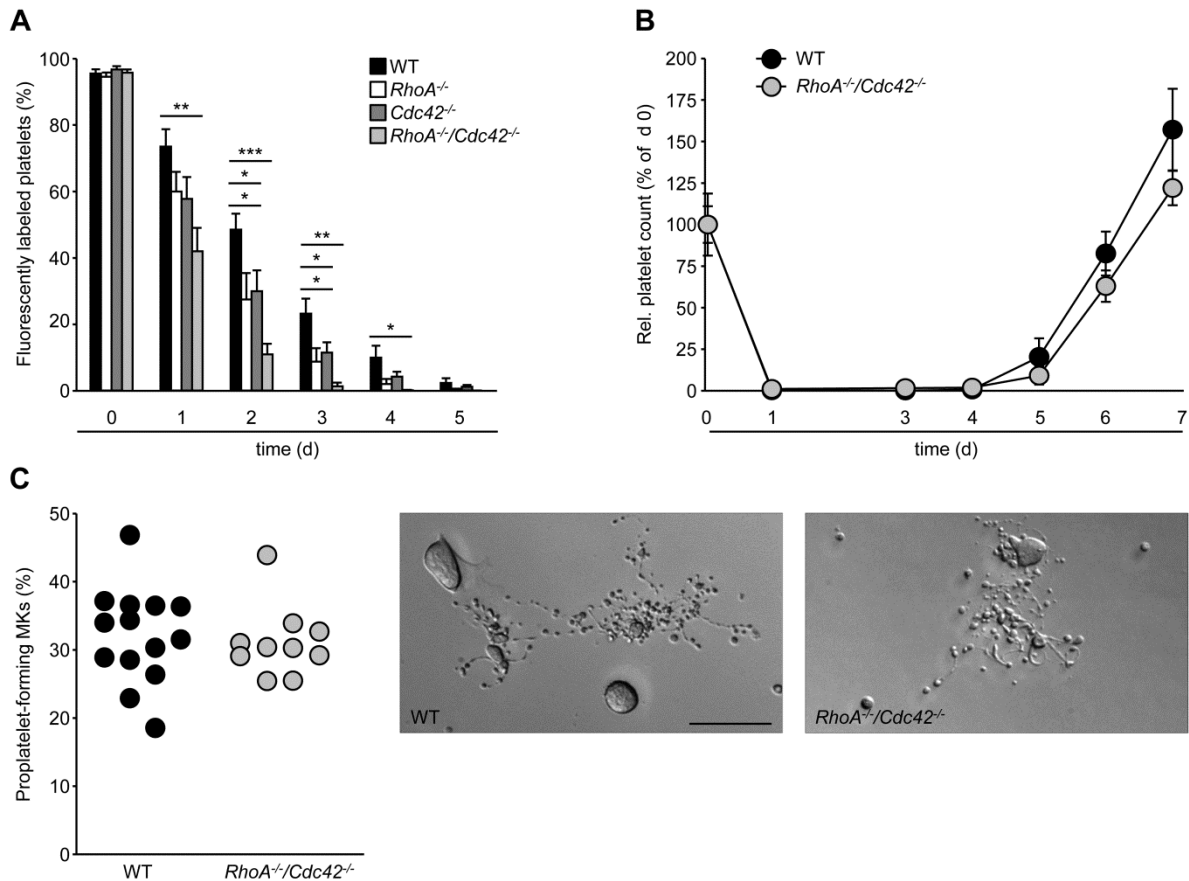

Figure 39. Rapid platelet clearance from the circulation, but unaltered platelet production upon platelet depletion in *RhoA⁻ᐟ⁻/Cdc42⁻ᐟ⁻* mice. (A) Life span of WT (black bars), *RhoA⁻ᐟ⁻* (white bars), *Cdc42⁻ᐟ⁻* (dark gray bars) and *RhoA⁻ᐟ⁻/Cdc42⁻ᐟ⁻* (light gray bars) platelets in the circulation was determined by flow cytometry by quantifying the percentage of fluorescently labeled GPIX⁺ platelets at the indicated time points after injection of a DyLight 488-conjugated anti-GPIX-derivative. Results are expressed as MFI ± SD and are representative of 3 independent experiments with n = 4 mice per genotype. (B) WT and *RhoA⁻ᐟ⁻/Cdc42⁻ᐟ⁻* mice were treated with a single bolus injection of platelet-depleting anti-GPIbα-antibodies and peripheral platelet counts were measured at the indicated time points until initial values were reached. Results are expressed as MFI ± SD and are representative of 2 independent experiments with n = 5 mice per genotype. (C) Determination of proplatelet formation in FLC-MK cultures (embryonic day 14.5, day 4 of culture). (Left panel) Each symbol represents the mean percentage of proplatelet-forming MKs per visual field (under 20-fold magnification of a light microscope) derived from 1 embryo. Visual fields (n ≥ 10) containing a minimum of 10 differentiated MKs without contact inhibition were analyzed and the mean percentage of proplatelet-forming MKs determined (n = 14 WT and n = 10 *RhoA⁻ᐟ⁻/Cdc42⁻ᐟ⁻* embryos from 4 females). (Right panel) Representative differential interference contrast images of proplatelet-forming MKs. Bar: 50 μm. Statistical analyses represent comparison to WT platelets. *$P < .05$; **$P < .01$; ***$P < .001$.

3.3.4. RhoA/Cdc42 deficiency results in severely altered ultrastructure of *bone-marrow megakaryocytes* (BM MKs)

Despite unaltered proplatelet production *in vitro* (Figure 39C), the observation that platelet counts were dramatically reduced in *RhoA⁻/⁻/Cdc42⁻/⁻* mice and the morphology of circulating platelets was severely altered implied the existence of functional defects in *RhoA⁻/⁻/Cdc42⁻/⁻* MKs *in vivo*. Therefore, maturation and ultrastructure of MKs *in situ* – i.e. in their natural microenvironment - were examined.

Hematoxylin and eosin-stained BM sections revealed increased numbers of BM MKs in *Cdc42⁻/⁻* and *RhoA⁻/⁻/Cdc42⁻/⁻* mice (Figure 40A-B). Importantly, however, it was difficult to unambiguously identify *RhoA⁻/⁻/Cdc42⁻/⁻* MKs in these sections because of altered morphology and decreased delineation from adjacent BM cells. To overcome this difficulty in analysis, *RhoA⁻/⁻/Cdc42⁻/⁻* MKs were visualized on cryosections stained with anti-GPIb antibodies. These analyses demonstrated a significant increase in BM MK numbers in the mutant mice (Figure 40C-D). Surprisingly, plasma Thpo levels, which are generally considered to be inversely related to platelet counts,[159,160] were only slightly elevated (Figure 40F), as measured by an ELISA system. Importantly, the ploidy of BM MKs was not affected by the combined deficiency of RhoA and Cdc42, thus ruling out a general defect in endomitosis in the absence of RhoA and Cdc42 (Figure 40E).

To examine the morphology of BM MKs, sections of femora from WT, *RhoA⁻/⁻*, *Cdc42⁻/⁻* and *RhoA⁻/⁻/Cdc42⁻/⁻* mice were analyzed by TEM (Figure 41A). Mature WT and *RhoA⁻/⁻* MKs displayed unaltered ultrastructural morphology with clearly visible *demarcation membrane system* (DMS), a reservoir for future proplatelet and platelet membranes,[100,101] and a peripheral zone, demarcating the MKs from surrounding cells. *Cdc42⁻/⁻* MKs exhibited slightly reduced membrane invaginations. In marked contrast, *RhoA⁻/⁻/Cdc42⁻/⁻* MKs showed a severely altered appearance with no membrane invaginations, increased numbers of vacuoles and no demarcation from surrounding cells which, similarly to the analysis of hematoxylin and eosin-stained BM sections, made it difficult to unambiguously identify BM MKs (Figure 41A). Detailed TEM analysis of *RhoA⁻/⁻/Cdc42⁻/⁻* BM MKs revealed aberrant membrane development (Figure 41Biv), highly disordered DMS (Figure 41Bi, iii) and structures reminiscent of empty granules which did not display the opacity of normal granules (Figure 41Bii). Together, these data demonstrated impaired membrane development and proplatelet formation in the absence of RhoA and Cdc42 and revealed critical overlapping functions of both Rho GTPases in the terminal stages of platelet production *in vivo*.
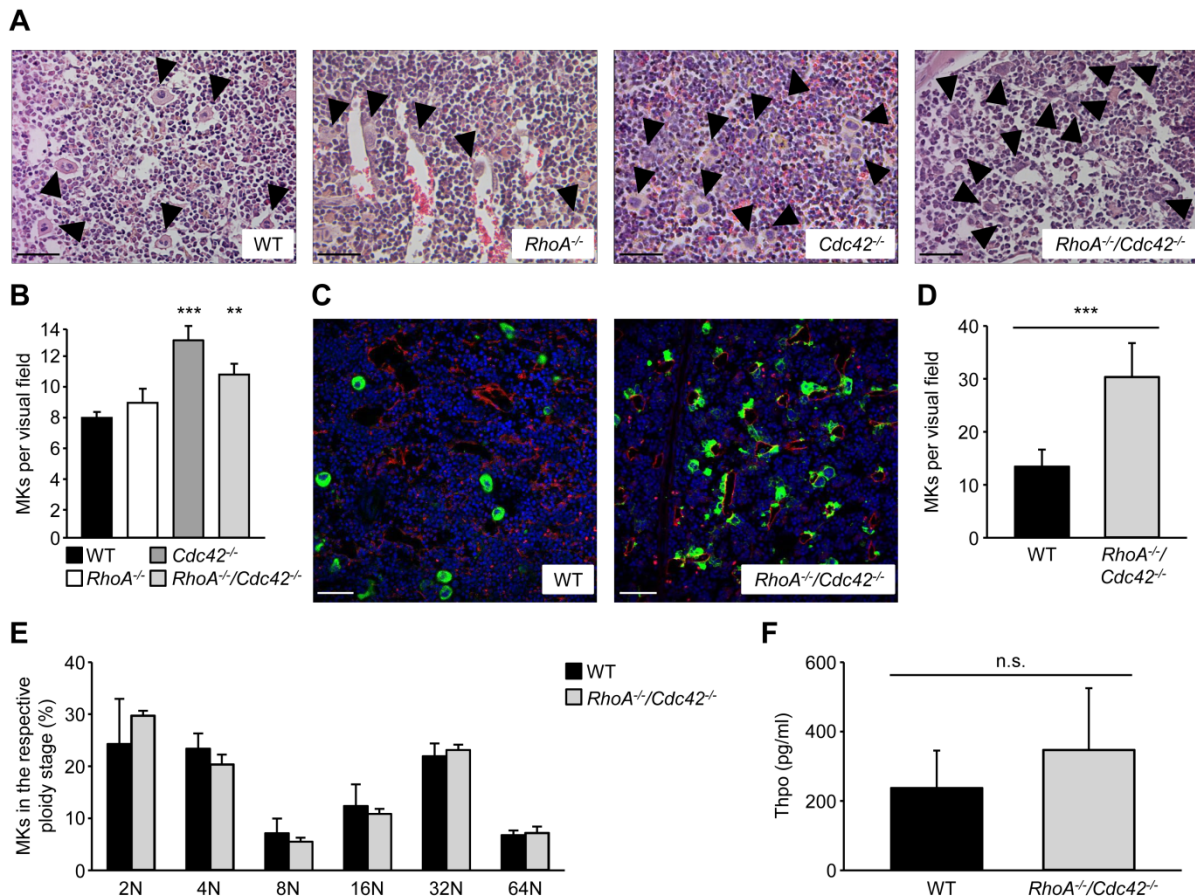
Figure 40. Increased BM MK numbers in *RhoA^-/-^/Cdc42^-/-^* mice. (A) Representative hematoxylin and eosin-stained BM sections of WT, *RhoA^-/-^*, *Cdc42^-/-^* [127] and *RhoA^-/-^/Cdc42^-/-^* mice. Arrowheads point at MKs. Bars: 50 μm. (B) Quantification of the number of BM MKs per visual field (328 x 246 μm) in WT (black bars), *RhoA^-/-^* (white bars), *Cdc42^-/-^* (dark gray bars) and *RhoA^-/-^/Cdc42^-/-^* (light gray bars) mice. Results are expressed as MFI ± SD (n = 7-8 mice per genotype). (C) Confocal images of immunostained BM of WT and *RhoA^-/-^/Cdc42^-/-^* femora. MKs, proplatelets and platelets were visualized by anti-GPIbα staining (green). Endothelial cells were labeled with an anti-CD105 antibody (red) and nuclei were counterstained with DAPI. Bars: 50 μm. (D) Quantification of the number of BM MKs per visual field in WT (black bars) and *RhoA^-/-^/Cdc42^-/-^* (light gray bars) mice. Results are expressed as MFI ± SD (n = 3 for WT and n = 7 for *RhoA^-/-^/Cdc42^-/-^* mice). (E) Functional endomitosis in *RhoA^-/-^/Cdc42^-/-^* mice. BM MK ploidy was assessed in whole BM single cell suspensions *in situ* (i.e. without further MK cultivation) by flow cytometry using an MK-/platelet-specific FITC-conjugated anti-GPIIb/IIIa-antibody in combination with propidium iodide staining to determine DNA content. Results are expressed as MFI ± SD and are representative of 3 independent experiments with n = 4 mice per genotype. (F) Plasma thrombopoietin levels in WT and *RhoA^-/-^/Cdc42^-/-^* mice were determined by an ELISA system. Results are expressed as MFI ± SD (n = 4 per genotype). Statistical analyses represent comparison to WT platelets. **$P < .01$; ***$P < .001$; n.s., not significant.

The aberrant morphology and the absence of characteristic membrane invaginations in BM MKs raised the possibility that extramedullary hematopoiesis may occur in *RhoA^-/-^/Cdc42^-/-^* mice. The spleen is a major site of platelet clearance as part of the reticulo-endothelial system, but may also contribute to platelet production in case of BM damage or dysfunction. Indeed, dramatically increased numbers of MKs forming clusters in the red pulp were identified in sections from spleens of *RhoA^-/-^/Cdc42^-/-^* mice, whereas splenic MK numbers were unaltered in *RhoA^-/-^* mice and only slightly elevated in *Cdc42^-/-^* mice (Figure

42). Of note, *RhoA^-/-/Cdc42^-/-* mice did not develop splenomegaly despite the marked increase in MK numbers in the spleen.
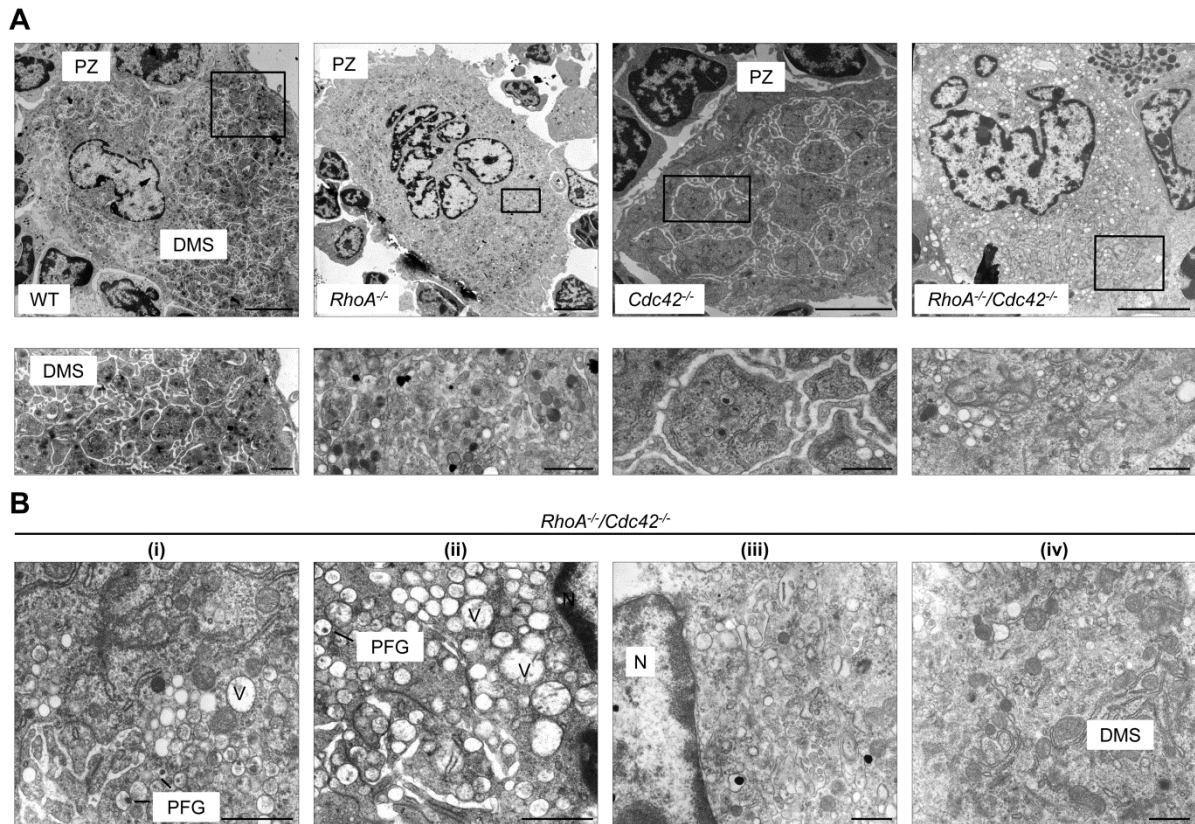
A

B

Figure 41. *RhoA^-/-/Cdc42^-/-* **BM MKs display severely altered ultrastructure.** (A) TEM analysis of BM MKs. (Upper panel) Overview. Bars: 5 μm. (Lower panel) Detailed view. Bars: 1 μm. Note loss of delineation to adjacent cells, aberrant DMS and increased vacuole numbers in *RhoA^-/-/Cdc42^-/-* BM MKs. *Cdc42^-/-* MK images from Pleines *et al.*[127] (B) Representative detailed images of different *RhoA^-/-/Cdc42^-/-* BM MKs. Bars: 1 μm. DMS: *demarcation membrane system*; N: *nucleus*; PFG: *partially filled granules*; PZ: *peripheral zone*; V: *vacuoles*.

A

B
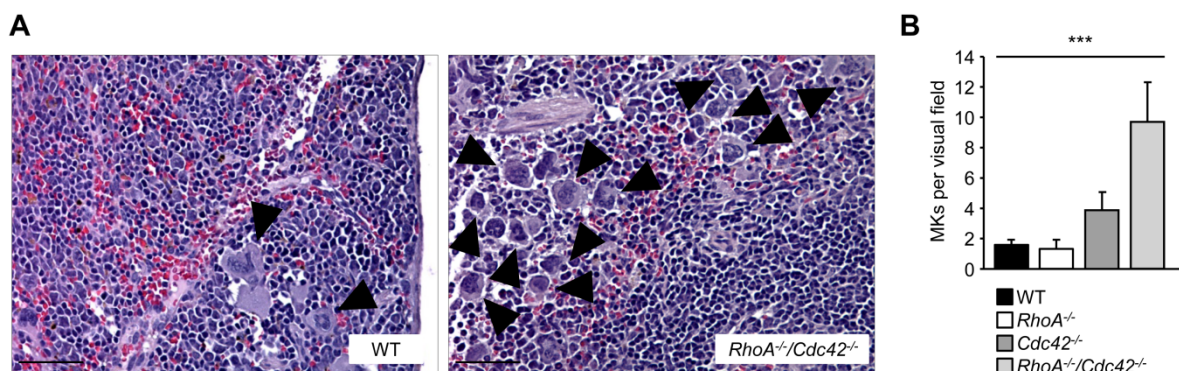
Figure 42. Increased numbers of splenic MKs in *RhoA^-/-/Cdc42^-/-* mice. (A) Representative hematoxylin and eosin-stained sections of the spleen of WT and *RhoA^-/-/Cdc42^-/-* mice. Arrowheads point at MKs. Bars: 50 μm. (B) Quantification of the number of BM MKs per visual field (328 x 246 μm) in WT (black bars), *RhoA^-/-* (white bars), *Cdc42^-/-* (dark gray bars) and *RhoA^-/-/Cdc42^-/-* (light gray bars) mice. Results are expressed as MFI ± SD (n = 7-8 mice per genotype). Statistical analyses represent comparison to WT platelets. ***P < .001.

3.3.5. Accelerated clearance of circulating platelets significantly contributes to the severe thrombocytopenia in *RhoA⁻/⁻/Cdc42⁻/⁻* mice

The significant elevation of MK numbers in the spleen suggested that the MKs residing there may be actively involved in thrombopoiesis. To test this directly, WT and *RhoA⁻/⁻/Cdc42⁻/⁻* mice (Figure 43A) were splenectomized and platelet count and size were subsequently monitored by flow cytometry (Figure 43B-C). Peripheral platelet counts slightly increased, whereas a mild reduction in platelet size was observed in WT mice, but otherwise splenectomy had no effect on platelet morphology (Figure 43B-C). Of note, splenectomy had no long-term effect on platelet counts, but the size of circulating platelets increased even further in *RhoA⁻/⁻/Cdc42⁻/⁻* mice (Figure 43B-D). Resting *RhoA⁻/⁻/Cdc42⁻/⁻* platelets still displayed a distinct appearance characterized by a predominantly roundish shape and large vacuoles (Figure 43D). However, TEM analysis revealed the presence of a few discoid-shaped platelets with normal granule content and distribution (Figure 43D).
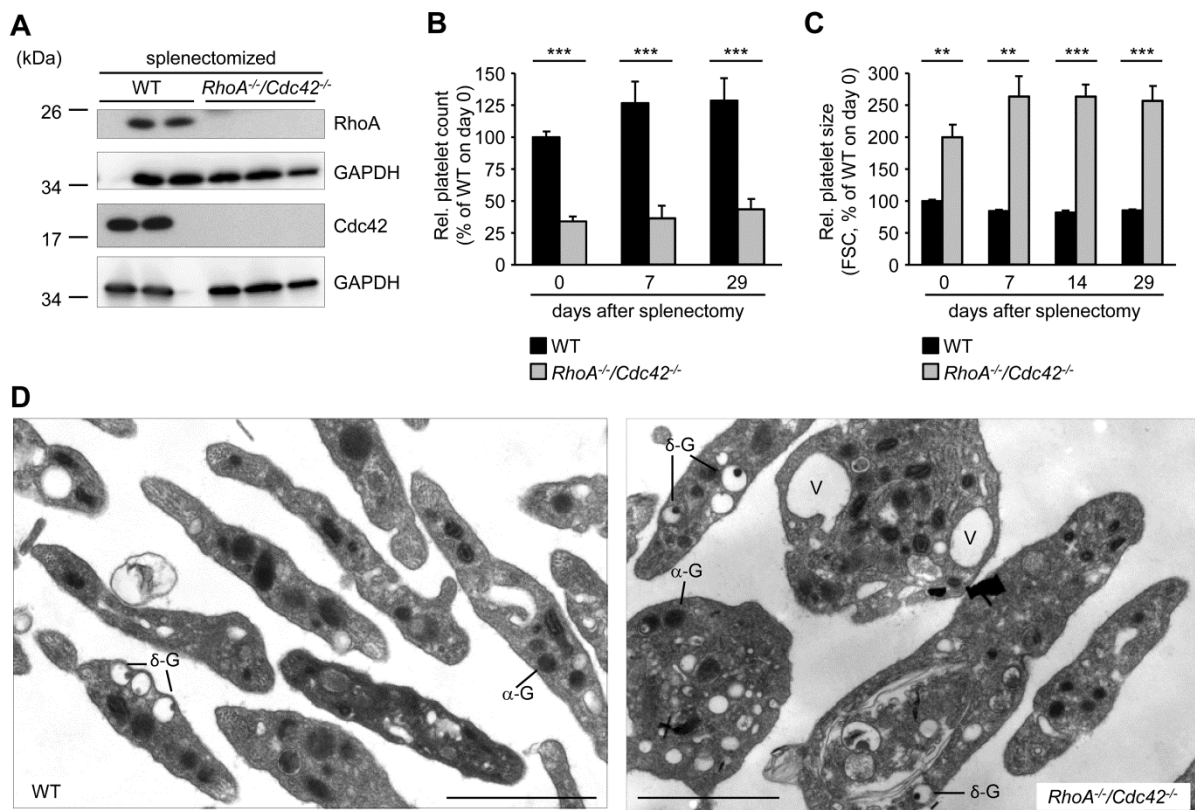
Figure 43. Splenectomy does not ameliorate the severe macrothrombocytopenia observed in *RhoA⁻/⁻/Cdc42⁻/⁻* mice. (A) Western blot analysis demonstrating absence of RhoA and Cdc42 in platelets from splenectomized MK-/platelet-specific RhoA/Cdc42-deficient mice. GAPDH expression was used as loading control. Peripheral platelet counts (B) and relative platelet size (C) of WT (black bars), and *RhoA⁻/⁻/Cdc42⁻/⁻* (light gray bars) mice were determined by flow cytometry at the indicated time points after splenectomy. Values were normalized to WT levels which were set to 100%. Results are expressed as MFI ± SD (n = 4 mice per group). (D) TEM analysis of resting WT and *RhoA⁻/⁻/Cdc42⁻/⁻* platelets isolated on d 29 after splenectomy. Bars: 1 μm. δ-G: *dense granule*; α-G: *α-granule*; V: *vacuoles*. **P < .01; ***P < .001.

Subsequently, circulating platelets were characterized with respect to surface glycoprotein expression and functional responses upon stimulation with different agonists. Expression levels of several prominent platelet surface receptors were slightly increased in *RhoA$^{-/-}$/Cdc42$^{-/-}$* platelets which was, however, probably due to the significantly increased platelet size in splenectomized *RhoA$^{-/-}$/Cdc42$^{-/-}$* mice (Table 3-5).

	WT	RhoA$^{-/-}$/Cdc42$^{-/-}$
GPIb	241 ± 8	227 ± 13
GPV	238 ± 11	272 ± 16*
GPIX	345 ± 6	370 ± 17
CD9	940 ± 12	1235 ± 106*
GPVI	48 ± 1	40 ± 2‡
CLEC-2	132 ± 6	164 ± 5‡
α2	40 ± 3	46 ± 2*
β1	98 ± 3	138 ± 12†
αIIbβ3	384 ± 9	476 ± 39*

Table 3-5. Analysis of surface expression of glycoproteins in WT and *RhoA$^{-/-}$/Cdc42$^{-/-}$* platelets in splenectomized mice. Diluted whole blood was collected from WT and *RhoA$^{-/-}$/Cdc42$^{-/-}$* mice 7 d after splenectomy and stained with saturating amounts of fluorophore-labeled antibodies. Platelets were analyzed by flow cytometry. Results express MFI ± SD (n = 4 mice per group) and were reproduced also at later time points after splenectomy (d 29 after surgery). * $P < .05$; $^{†} P < .01$; $^{‡} P < .001$.

Importantly, splenectomy essentially ameliorated defective integrin αIIbβ3 activation, specifically upon activation with GPCR-specific agonists (Figure 44A, left panel). Surprisingly, circulating platelets in *RhoA$^{-/-}$/Cdc42$^{-/-}$* mice displayed an overall increase in degranulation-dependent α-granule release, as demonstrated by analysis of P-selectin exposure by flow cytometry (Figure 44A, right panel). Removal of the spleen considerably improved the life span of *RhoA$^{-/-}$/Cdc42$^{-/-}$* platelets (Figure 44B), but had no effects on the severe bleeding diathesis (Figure 44C). Collectively, these results indicated that splenectomy significantly altered both morphology and functionality of *RhoA$^{-/-}$/Cdc42$^{-/-}$* platelets *ex vivo*, but this treatment did not yield any significant improvement of platelet counts or hemostatic function in the mutant mice.

In a final set of experiments, the effect of splenectomy on MK morphology was examined by TEM. Removal of the spleen did not have any major influence on BM MK development in WT mice (Figure 45i). Although the ultrastructure of a few *RhoA$^{-/-}$/Cdc42$^{-/-}$* MKs was still characterized by absence of DMS and granules and by an increased number of vacuoles (Figure 45ii), several *RhoA$^{-/-}$/Cdc42$^{-/-}$* BM MKs displayed key features of mature MKs, including clearly defined peripheral zone and membrane invaginations and normal distribution of granules (Figure 45iii). Furthermore, TEM analysis even revealed the presence

of terminally differentiated MKs in the process of proplatelet release in splenectomized *RhoA^-/-/Cdc42^-/-* mice (Figure 45iv). These findings were in accordance with the partially restored morphology of circulating *RhoA^-/-/Cdc42^-/-* platelets after spleen removal.
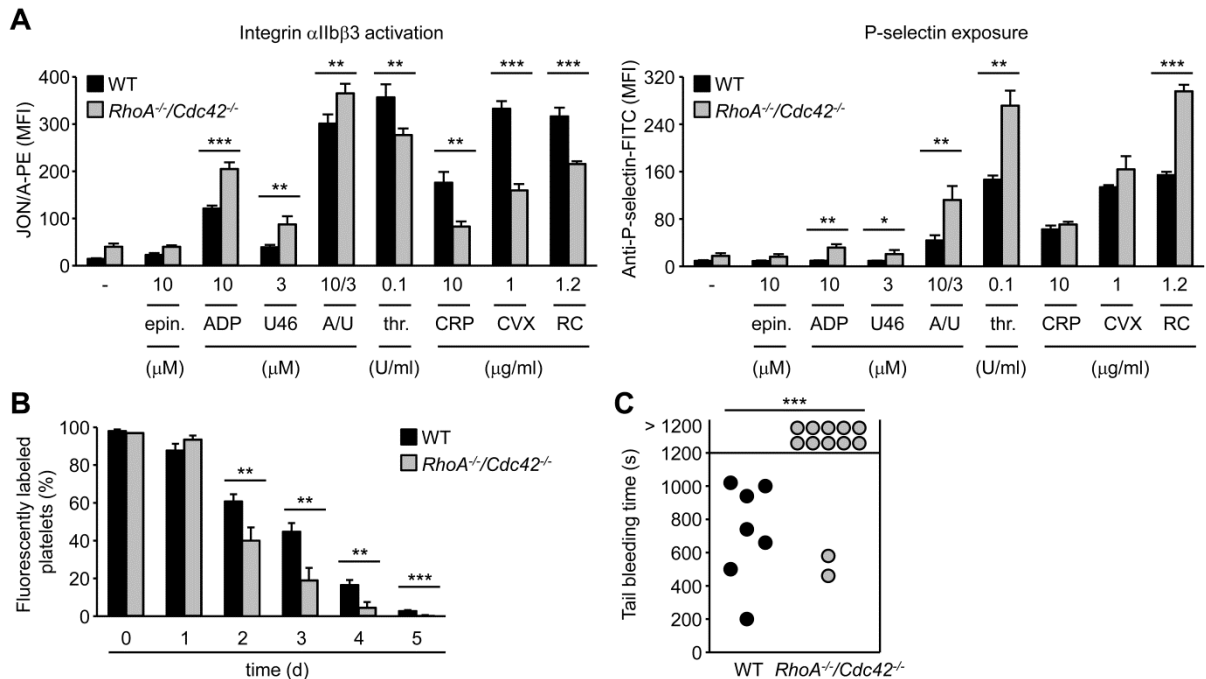

Figure 44. Splenectomy is associated with reduced platelet clearance, but does not ameliorate defective hemostatic function in *RhoA^-/-/Cdc42^-/-* mice. (A) Flow cytometric analysis of activated integrin αIIbβ3 (binding of JON/A-PE) (left panel) and degranulation-dependent P-selectin exposure (right panel) upon stimulation with the indicated agonists in WT (black bars) and *RhoA^-/-/Cdc42^-/-* (light gray bars) platelets. Results are expressed as MFI ± SD (n = 4 mice per group). Experiments were carried out on d 29 after splenectomy. (B) Life span of WT (black bars) and *RhoA^-/-/Cdc42^-/-* (light gray bars) platelets in the circulation was determined by quantifying the percentage of fluorescently labeled GPIX^+ platelets at the indicated time points after injection of a DyLight 488-conjugated anti-GPIX-derivative by flow cytometry. Results are expressed as MFI ± SD (n = 4 mice per group). Experiments started on d 14 after splenectomy. (C) Tail bleeding times in splenectomized WT and *RhoA^-/-/Cdc42^-/-* mice on d 7 after surgery. Each symbol represents 1 animal. *P < .05; **P < .01; ***P < .001.
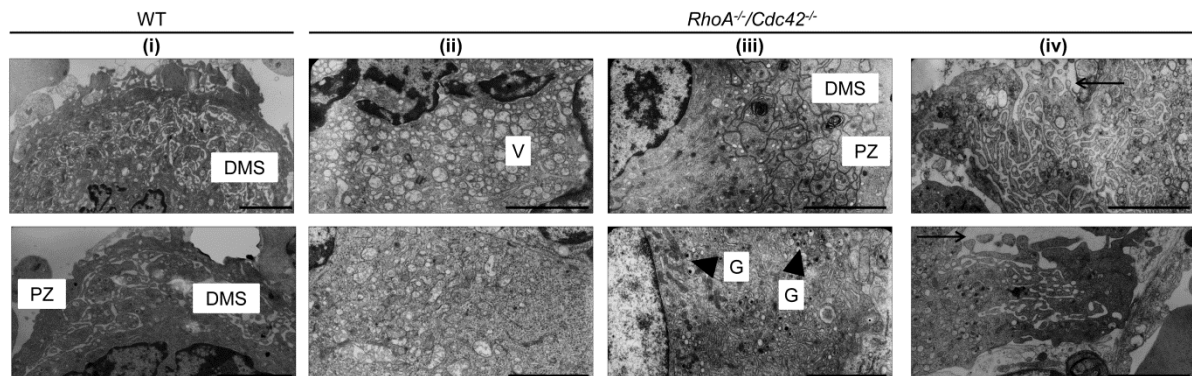
Figure 45. Splenectomy partially rescues ultrastructural defects of BM MKs in *RhoA^-/-/Cdc42^-/-* mice. TEM analysis of BM MKs of splenectomized WT and *RhoA^-/-/Cdc42^-/-* mice on d 29 after surgery. Bars: 2.5 μm. Note proplatelet formation and release (arrows) and presence of granules in *RhoA^-/-/Cdc42^-/-* BM MKs. DMS: *demarcation membrane system*; N: *nucleus*; G: *granules* (arrowheads); PZ: *peripheral zone*; V: *vacuoles*.

To further elucidate the mechanisms underlying rapid clearance of circulating platelets in *RhoA$^{-/-}$/Cdc42$^{-/-}$* mice, macrophages were selectively depleted in mutant and WT mice by clodronate treatment. Macrophage depletion led to a two-fold increase in peripheral platelet counts in *RhoA$^{-/-}$/Cdc42$^{-/-}$* mice compared to vehicle-treated littermate mutant mice which was accompanied by a significant reduction in platelet size (Figure 46A-B). These results suggested that the severe thrombocytopenia in *RhoA$^{-/-}$/Cdc42$^{-/-}$* mice was, at least partially, dependent on accelerated platelet clearing by macrophages.
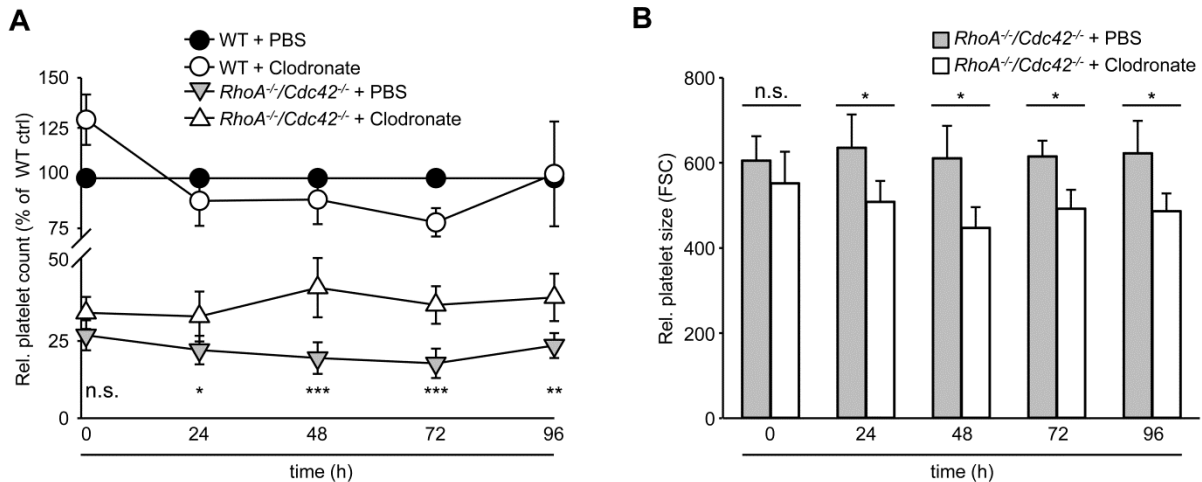
Figure 46. Macrophage depletion slightly ameliorates the severe macrothrombocytopenia in *RhoA$^{-/-}$/Cdc42$^{-/-}$* mice. Peripheral platelet counts (A) and size (B) were monitored over time after clodronate-encapsulated liposome-mediated macrophage depletion in WT and *RhoA$^{-/-}$/Cdc42$^{-/-}$* mice by flow cytometry. Values for platelet counts were normalized to WT control levels (WT mice treated with PBS liposomes) which were set to 100%. Values for platelet size were normalized to WT levels (WT mice treated with clodronate-liposomes) which were set to 100%. Results are expressed as MFI ± SD (n = 4-6 mice per group) and are representative of 2 independent experiments. Statistical significance solely indicates differences in clodronate-treated vs. vehicle-treated *RhoA$^{-/-}$/Cdc42$^{-/-}$* mice. *P < .05; **P < .01; ***P < .001; n.s., not significant.

Together, the results summarized in this part of the thesis indicated that RhoA and Cdc42 cooperatively control final steps of megakaryopoiesis and platelet hemostatic functions. However, both GTPases play opposing roles in the control of platelet degranulation and occlusive arterial thrombus formation.

4. Discussion

Platelets fulfill a vital function in hemostasis, as they form a hemostatic plug to stop posttraumatic blood loss. The platelet activation process at sites of vascular injury needs to be tightly controlled, since excessive platelet reactivity in the setting of pathological thrombus formation may lead to life-threatening vessel occlusion. Currently available treatment options in acute ischemic disease states are limited and antiplatelet agents are contraindicative in many cases because of increased incidence of bleeding complications that often outweighs therapeutic benefits. The adverse effects of clinically used platelet inhibitors on primary hemostasis emphasize the necessity to identify and characterize novel pharmacological targets for antiplatelet drugs with a powerful, yet safe antithrombotic profile.

In recent years, several major platelet surface receptors, including the (hem)ITAM-bearing receptors GPVI and CLEC-2, have been identified as critical regulators of platelet adhesion and activation and have emerged as promising novel targets in antiplatelet drug design due to their role in the initiation of thrombotic and thrombo-inflammatory signaling cascades. However, the role of GPVI and CLEC-2 is not restricted to their involvement in thrombosis and primary hemostasis. The past decade has witnessed significant progress in our understanding of the role of both platelet receptors in a plethora of (patho)physiological processes, including inflammation, atherosclerosis, lymphatic vessel development and tumor progression.[30,53,54] This knowledge raises awareness about the possibility of severe side-effects of therapeutic agents interfering with the (hem)ITAM signaling pathway. Furthermore, recent findings underscore the demand to better characterize the mechanisms by which platelet receptor signaling governs the initiation and progression of complex thrombotic and thrombo-inflammatory disease states.

Powerful platelet activation eventually culminates in substantial cytoskeletal rearrangements and secretion from α- and dense granules – processes that are strictly controlled by Rho GTPases, most notably RhoA, Cdc42 and Rac1. The tight regulation of the actin cytoskeleton, microtubule dynamics and degranulation is essential for maintenance of intact platelet function in hemostasis. In addition, cytoskeletal rearrangements are pivotal during critical steps of MK maturation which precede platelet generation. Therefore, there is an increasing demand to further investigate the contribution of Rho GTPases in the regulation of the above-mentioned processes and to unravel putative functional redundancies.

4.1. SLAP/SLAP2 prevent excessive platelet (hem)ITAM signaling in arterial thrombosis and ischemic stroke in mice

The results presented in the first part of this thesis establish SLAP and SLAP2 as negative regulators of surface expression and signaling of the ITAM receptor GPVI and the hemITAM receptor CLEC-2 in mouse platelets. However, single deficiency of either adapter protein had only a minor effect on platelet (hem)ITAM signaling (Figure 7, Figure 8), whereas the combined loss of SLAP and SLAP2 resulted in a marked platelet hyperreactivity to (hem)ITAM-coupled agonists *in vitro* (Figure 9, Figure 10). This powerful cellular activation translated into a significant prothrombotic phenotype (Figure 19) and dramatically increased susceptibility to focal cerebral ischemia *in vivo* (Figure 21). The results clearly demonstrate a functional redundancy of the two adapter proteins in the regulation of platelet (hem)ITAM signaling and reveal a crucial function of SLAP and SLAP2 in the control of thrombotic and thrombo-inflammatory events.

Involvement of SLAP in the regulation of surface expression levels of ITAM-coupled immune cell receptors, such as the TCR and BCR, is well-established.[75] *In vivo* studies have demonstrated an important role for SLAP in regulating TCR expression during a specific T lymphocyte developmental stage ($CD4^+CD8^+$) at which repertoire selection takes place.[86] Similarly, SLAP is required for the fine-tuning of BCR levels and signal strength during B cell development.[87] Importantly, increased GPVI receptor density did not significantly contribute to the marked hyperreactivity, as overshooting ITAM signaling was observed also in SLAP/SLAP2 deficient $Gp6^{+/-}$ platelets which express lower GPVI surface levels than WT control platelets (Figure 11). The experimental data summarized in this study suggest that the mechanism by which GPVI signaling is inhibited by SLAP proteins involves, at least in part, competition with *Src family kinases* (SFKs) for binding to the GPVI/FcRγ signaling complex. In support of this model, immunoprecipitations of the SFK Lyn contained substantially more GPVI in activated platelets in the absence of SLAP/SLAP2 (Figure 13) and tyrosine phosphorylation of downstream signaling proteins was also elevated (Figure 12). Collectively, these results establish SLAP/SLAP2 as negative regulators of ITAM signaling in platelets, presumably through competition with Lyn for binding to the GPVI cytosolic tail.

These results further implicate the existence of an important naturally occurring mechanism to dampen ITAM signaling in platelets to prevent excessive thrombotic activity which critically depends on the involvement of SLAP and SLAP2 and likely involves other adapter proteins. This assumption is supported by studies in mouse platelets lacking c-Cbl, an adapter protein that promotes protein ubiquitination, which showed increased aggregation in response to intermediate and low CRP concentrations that was associated with elevated

tyrosine phosphorylation of the FcRγ-chain, Syk, LAT and PLCγ2.[161] c-Cbl has been demonstrated to function as an E3 ligase mainly for activated protein tyrosine kinases of the Src and Syk family[162] and has been associated with Syk ubiquitination in platelets.[163] Given the fact that c-Cbl and SLAP function in intersecting biochemical pathways in immune cells, and their cooperation in a SLAP/c-Cbl complex mediating ubiquitination-dependent down-regulation of TCR and BCR levels is well-established,[74,81,82] it is tempting to speculate that interactions between members of both families of adapter proteins also exist in platelets and may be crucial for dampening of ITAM signaling. This inhibitory pathway functionally opposes another group of adapter proteins, including LAT, SLP-76, Grb2 and Gads, which are involved in the signal transduction cascade downstream of Syk and support platelet activation *in vitro* and *in vivo*.[147,164-167]

SLAP/SLAP2 also powerfully inhibit signaling downstream of the second (hem)ITAM-bearing receptor in mouse platelets CLEC-2 (Figure 14). Surprisingly, SLAP/SLAP2 deficiency resulted in LAT-independent enhanced PLCγ2 phosphorylation upon CLEC-2 stimulation (Figure 15) which demonstrates that SLAP/SLAP2 likely interfere with proximal molecules in the hemITAM signaling pathway. Although the exact molecular mechanisms remain elusive, SLAP/SLAP2 appear to attenuate the CLEC-2 signaling cascade by tight regulation of the signal strength required for the phosphorylation and activation of key effector molecules, including PLCγ2. Consequently, deficiency of both proteins substantially lowers the threshold[47,147] necessary for powerful cellular activation to occur. Modulation of CLEC-2 signaling by SLAP and SLAP2 may therefore have a major physiological significance in other processes beyond the obvious implications in thrombosis and hemostasis, but this assumption clearly needs further experimental proof.

Another set of experiments demonstrated that SLAP/SLAP2 significantly contribute to dampening collagen-induced procoagulant activity in platelets and ensuing thrombin generation (Figure 16, Figure 17, Figure 18). These results are in line with earlier studies indicating that key components of the GPVI/ITAM signaling cascade, including the FcR$\gamma-$chain, LAT, Syk and PLCγ2, as well as GPVI-induced increase in cytosolic Ca^{2+} concentration, are critically involved in collagen-dependent PS exposure.[14,139,149] Increasing evidence suggests that platelet procoagulant activity, in particular by propagation of the contact phase of coagulation, plays an important role in initiating arterial thrombus formation.[168] In agreement with their critical function for inhibiting PS exposure and thrombin generation *in vitro*, SLAP and SLAP2 are essential to prevent overshooting thrombotic and thrombo-inflammatory processes *in vivo* (Figure 19, Figure 21, Figure 22).

Although the exact mechanisms by which platelets contribute to the development of brain infarction are still poorly understood, compelling experimental evidence suggests that acute

ischemic stroke does not solely result from local thrombotic vessel occlusion. In fact, ischemic stroke has been increasingly recognized as a complex disease in which platelets orchestrate multiple molecular and cellular interactions, involving immune cells, endothelial cells and the contact activation system, finally leading to disruption of the blood-brain barrier and neurological damage.[12,169] Importantly, recent studies on the involvement of platelet-receptor interactions in acute experimental stroke have surprisingly demonstrated that interference with early steps of platelet adhesion and activation, but notably not aggregation, significantly reduces secondary infarct growth without adverse effects on intracerebral bleeding.[32] Unexpectedly, inhibition of final steps of platelet aggregation via blockade of GPIIb/IIIa was associated with increased mortality due to intracranial hemorrhage in mice[32] and humans.[170,171] By contrast, the importance of initial platelet adhesion and activation steps involving the GPIb-VWF axis in the progression of ischemic stroke is now well-established.[30,32,172-174] Likewise, GPVI also appears to play a crucial role in the pathophysiology of acute stroke, as shown by profound protection of GPVI-depleted mice in the tMCAO model of ischemic stroke[32] and indirect evidence indicating increased GPVI activity in acute stroke patients.[175,176] The mechanisms by which GPVI promotes stroke progression remain elusive. As demonstrated in other experimental models of disease, such as rheumatoid arthritis, GPVI triggers microparticle formation and thus promotes the release of pro-inflammatory cytokines, including IL-1α,[34] which has been demonstrated to contribute to inflammation-mediated brain injury.[177] Thus, GPVI likely initiates a thrombo-inflammatory signaling cascade in acute ischemic stroke. The findings in *Slap$^{-/-}$/Slap2$^{-/-}$* mice further corroborate the hypothesis that GPVI/ITAM-mediated activation processes are of central importance during stroke development.

Ischemic stroke triggers a profound local inflammatory reaction characterized by the recruitment of different immune cell types. Importantly, previously neglected players in stroke progression – T cells – have been recently identified as essential pathogenic factors in early experimental stroke development.[152-154] The use of constitutive SLAP/SLAP2-deficient mice in the initial stroke experiments (Figure 21) raised the possibility that the observed phenotype may at least partially depend on altered T cell activity. Due to the lack of conditional SLAP or SLAP2 knockout mice, an adoptive platelet transfer approach was developed which unambiguously attributed the detrimental role of SLAP/SLAP2 in ischemic stroke to their expression in platelets (Figure 22). Of note, the exact mechanisms by which SLAP/SLAP2 prevent excessive GPVI activation remain elusive and probably at least partially differ from those involved in classical thrombus formation. Further studies on the involvement of SLAP/SLAP2 in the control of platelet interactions with immune and/or endothelial cells and the coagulation cascade may help to better understand underlying (patho)mechanisms.

Together, these data emphasize a central role of GPVI in the course of acute ischemic disease states and thereby establish modulators of GPVI activity, such as SLAP/SLAP2, as central factors in the pathology of atherothrombosis and ischemic stroke.

4.2. Antibody-induced GPVI down-regulation is associated with prolonged severe thrombocytopenia in *Slap$^{-/-}$/Slap2$^{-/-}$* mice

GPVI has emerged as an attractive potential target for antithrombotic therapy, as its blockade, antibody-induced depletion, competitive inhibition or genetic deficiency provided powerful protection from experimental arterial thrombosis without affecting platelet hemostatic functions.[13,38,151,155] However, the mechanisms by which the targeted down-regulation of GPVI occurs *in vivo* are still incompletely understood and require further characterization. Because SLAP and SLAP2 are involved in the control of internalization and degradation of ITAM-containing receptor complexes on immune cells, especially TCR and BCR, it was hypothesized that SLAP family members may also be involved in the antibody-induced endocytosis of the GPVI/FcRγ receptor complex. The results summarized in the second part of this thesis demonstrated that SLAP and SLAP2 are dispensable for GPVI down-regulation following administration of the monoclonal antibody JAQ1 (Figure 24). Unexpectedly, treatment of *Slap$^{-/-}$/Slap2$^{-/-}$* mice with JAQ1 induced sustained severe thrombocytopenia (Figure 25, Figure 26). Importantly, administration of F(ab')$_2$ fragments induced thrombocytopenia in *Slap$^{-/-}$/Slap2$^{-/-}$* mice, but notably, not in WT animals, with the same intensity as the intact IgG (Figure 27). F(ab')$_2$ antibody fragments lack the Fc-part and thus exert their effects in an Fc-independent fashion. The results suggested that FcγR-bearing cells in the reticulo-endothelial system are not primarily involved in anti-GPVI-induced platelet destruction in *Slap$^{-/-}$/Slap2$^{-/-}$* mice.

Importantly, JAQ1 triggered sustained and irreversible aggregation of *Slap$^{-/-}$/Slap2$^{-/-}$* platelets (Figure 28). Of note, binding of JAQ1 to GPVI in WT platelets has been shown to induce subliminal signaling associated with phosphorylation of Syk and PLCγ2 which only slightly exceeds basal phosphorylation of both proteins and is not sufficient to induce powerful cellular activation.[178] Aggregation of WT platelets can be mediated only upon cross-linking of surface-bound JAQ1 by an anti-rat IgG secondary antibody.[22,157]

The *proline-rich region* (PRR) in the cytosolic part of GPVI mediates binding of the SFKs Lyn and Fyn.[25,26] Lyn is required for the rapid platelet activation upon ligand engagement of GPVI.[27,179] Interestingly, a recent study demonstrated that GPVI-bound Lyn is held in the active state.[27] Still, it remains enigmatic how GPVI is constitutively associated with active Lyn without tonic activation. It has been hypothesized the ITAM-containing FcRγ is sequestered

to the cell membrane which enables GPVI to keep activated Lyn in close proximity of the FcRγ-chain, but prevents initiation of signal transduction in the absence of a strong stimulus.[27] Importantly, functional cooperation between Lck-bound PRR on CD3ε and SLAP have been implicated in the control of TCR expression levels during the $CD4^+CD8^+$ stage of thymocyte development.[180] SLAP/SLAP2 deficiency enhanced interactions of Lyn and activated GPVI (Figure 13). It is conceivable that SLAP proteins compete with Lyn for binding to the GPVI/FcRγ complex and lack of SLAP/SLAP2 presumably alters Lyn activation state and localization and facilitates the SFK-dependent initiation of powerful cellular activation even upon binding of a weak GPVI activating agent, such as JAQ1.

In mice, JAQ1-induced GPVI down-regulation is thought to occur through two principal mechanisms – ectodomain shedding, leading to the generation of soluble GPVI, and internalization.[39,41,42] Both mechanisms require intact signaling via the ITAM on the FcRγ-chain.[41] Recent findings suggest that GPVI immunodepletion is not an entirely cell-autonomous process and imply that cell types other than platelets are involved in the removal of the receptor from the cell surface and the concomitantly occurring transient thrombocytopenia (Ref.[39,41,42] and David Stegner, unpublished). Antibody-opsonized platelets become temporarily sequestered to the liver and spleen where the actual loss of the receptor takes place (Ref.[39] and David Stegner, unpublished). In contrast to WT platelets, $Slap^{-/-}/Slap2^{-/-}$ platelets became activated upon JAQ1-binding and were immediately removed from the circulation. JAQ1 was detectable in the circulation for up to 10-14 days upon a single bolus injection of the antibody (Figure 28) and antibody concentration of 1-2 μg/ml were still sufficient to induce thrombocytopenia in SLAP/SLAP2-deficient mice (data not shown). Interestingly, similar pharmacokinetics and long-term unresponsiveness of circulating platelets to collagen were observed in cynomolgus monkeys treated with an anti-GPVI antibody purified from the plasma of a patient with auto-anti-GPVI antibodies.[43] Importantly, JAQ1 did not affect the ability of MKs to produce platelets *in vitro* and *in vivo* (data not shown). Taken together, these results support the hypothesis that powerful cellular activation and subsequent clearance of activated platelets from the circulation is the predominant mechanism by which the sustained thrombocytopenia in $Slap^{-/-}/Slap2^{-/-}$ mice occurs. Importantly, it cannot be ruled out that JAQ1 treatment and the ensuing persistent thrombocytopenia affect the function of FcRγ-bearing immune and endothelial cells which could further contribute to enhanced removal of circulating platelets, but this hypothesis needs to be tested by additional studies.

Remarkably, the phenomenon of prolonged severe thrombocytopenia was specific for antibody-induced GPVI down-regulation, as peripheral platelet counts returned with similar kinetics in WT and SLAP/SLAP2-deficient mice upon depletion of CLEC-2[49] and

GPIbα (which induces Fc-independent thrombocytopenia)[130] or GPIIb/IIIa(which induces Fc-dependent thrombocytopenia)[130] (Figure 29 and data not shown). Mechanistically, the JAQ1-induced thrombocytopenia occurred in a Syk-dependent manner (Figure 31). By contrast, transient thrombocytopenia was observed in LAT-deficient *Slap⁻/⁻/Slap2⁻/⁻* mice (Figure 30). Notably, downstream signaling and PLCγ2 phosphorylation were partially preserved in LAT-deficient *Slap⁻/⁻/Slap2⁻/⁻* platelets (Figure 15), but not in Syk-deficient *Slap⁻/⁻/Slap2⁻/⁻* platelets (data not shown) following GPVI activation, demonstrating that intact signaling downstream of GPVI is required for the JAQ1-induced thrombocytopenia to occur in *Slap⁻/⁻/Slap2⁻/⁻* platelets. However, GPVI down-regulation via receptor internalization still occurred in Syk-deficient *Slap⁻/⁻/Slap2⁻/⁻* platelets (Figure 32, Figure 33), albeit with slower kinetics than in WT platelets. Firstly, these findings demonstrate that Syk-independent GPVI internalization still occurs, although platelets are completely refractory to GPVI stimulation. Secondly, the critical signaling event during targeted down-regulation of GPVI presumably takes place further upstream of Syk, probably at the level of SFKs, as demonstrated for other (hem)ITAM-bearing receptors, including TCR and CLEC-2, for which SFKs, but not Syk family kinase members, are needed to down-regulate the respective (hem)ITAM-containing receptor.[59,81]

Interactions between SLAP/SLAP2 and Syk have been extensively studied in T and B cells. SLAP has been demonstrated to associate with the Syk family kinases ZAP-70 and Syk upon TCR activation.[79] Furthermore, co-expression of SLAP-2 and Syk or ZAP-70 induces the down-regulation of the kinase.[73,74] Functional cooperation between SLAP and ZAP-70 during thymocyte development has been shown to ensure that only cells with intact TCR signaling can survive in the periphery.[86] Similar mechanisms may apply to platelets in which SLAP is required to dampen Syk activity and prevent excessive GPVI signaling in different settings.

Collectively, these data emphasize the importance of evaluating the expression and function of proteins which modulate key steps of the GPVI signaling cascade prior to and during targeted down-regulation. This may help to avoid undesired side-effects of anti-GPVI treatment related to antibody-induced severe thrombocytopenia.

4.3. RhoA and Cdc42 have both distinct and overlapping functions in platelet production and action

Constitutive deficiency of RhoA, Cdc42 and Rac1 in mice resulted in early embryonic lethality which hampered studies in primary knockout cells.[109,181,182] Meanwhile, the lethal phenotype has been circumvented by the availability of tissue- and lineage-specific deletion of the three

ubiquitously expressed Rho GTPases without the danger of off-target effects related to the use of inhibitors, overexpression or knockdown approaches. Despite the new avenues which the conditional knockout systems have opened, little is known about specific functions of Rho GTPases during MK maturation and platelet generation. In this thesis, the role of the Rho GTPases RhoA and Cdc42 in platelet production and function has been investigated using conditional MK-/platelet-specific single- and double-deficient mice (Cre/loxP system).

The significantly decreased peripheral platelet counts in RhoA[112] and Cdc42[113] single deficient mice implicated important roles of both proteins in platelet production. Not surprisingly, double deficiency of RhoA and Cdc42 led to a further decrease in peripheral platelet counts (Figure 34). Importantly, thrombocytopenia in these mice was accompanied by a significant increase in platelet size and severely altered ultrastructure, characterized by a heterogeneous cell population with increased vacuole numbers and varying granule content (Figure 34, Figure 35). Of note, subcellular morphology and granule distribution were preserved in the single deficient platelets (Figure 34 and Pleines *et al.*, 2010,[113] 2012[112]). Unexpectedly, RhoA/Cdc42-deficient platelets were still largely functional in different experimental settings *in vitro* and *in vivo* (Figure 36, Figure 37, Figure 38B, C). Remarkably, $RhoA^{-/-}/Cdc42^{-/-}$ platelets were capable of granule secretion and concomitant deficiency of Cdc42 even compensated for the degranulation defect in $RhoA^{-/-}$ platelets after $G_{q/13}$ stimulation (Figure 36). RhoA likely facilitates degranulation, whereas Cdc42 appears to inhibit granule secretion in platelets, indicating that both GTPases may play opposing roles in exocytosis in platelets. However, the mechanisms by which Rho GTPases regulate exocytosis remain elusive and may be cell type-specific.[183] For instance, Cdc42 positively regulates exocytosis in tumor cells,[184] but reduces insulin secretion in pancreatic β-cells.[185] Central to the involvement of Rho GTPases in facilitating or inhibiting secretion processes is their role in the control of associations between the exocyst complex and IQGAP1.[183] IQGAP1 is a scaffold protein which has been established as a major regulator of actin dynamics and tubulin multimerization.[186,187] Importantly, Rac1/Cdc42-deficient MKs displayed decreased IQGAP1 expression,[127] whereas $RhoA^{-/-}/Cdc42^{-/-}$ MKs exhibited unaltered IQGAP1 expression compared to WT MKs (data not shown), suggesting that Rac1 and RhoA may differentially regulate IQGAP1 expression in the absence of Cdc42 in mature MKs, but clearly, exact mechanisms remain to be investigated.

Importantly, the largely unaltered α-granule release in RhoA/Cdc42-deficient platelets *in vitro* translated into preserved occlusive arterial thrombus formation *in vivo* (Figure 38B, C), despite severe thrombocytopenia (Table 3-3 and Figure 34B). This represents a further important difference between RhoA/Cdc42 double deficiency and combined Rac1/Cdc42 deficiency which was associated with a profound protection in a model of arterial thrombosis.[127] The data suggested distinct functions of Rho GTPases in the progression of

arterial thrombus formation. Notably, *RhoA$^{-/-}$/Cdc42$^{-/-}$* platelets displayed severely impaired hemostatic functions (Figure 38A). These findings implied that the formation of a hemostatic plug which prevents excessive blood loss and the formation of an occlusive thrombus may follow different mechanisms in the absence of RhoA and Cdc42. Furthermore, these data demonstrated overlapping functions of RhoA and Cdc42 in the maintenance of intact hemostasis and non-redundant roles in the development of pathological vessel occlusion.

RhoA/Cdc42-deficient proplatelets and platelets exhibited a profound defect in microtubule organization (Figure 35A, B). Microtubules are essentially involved in the transport of granules and organelles to the proplatelets[104] and in the determination of final platelet size in the blood.[188] Importantly, platelets isolated from mice lacking the hematopoietic-specific β1 tubulin isoform were characterized by reduced microtubule coils in the marginal band despite compensatory overexpression of two alternative tubulin isoforms - β2 and β5.[189] Furthermore, β1 tubulin-deficient mice suffered from thrombocytopenia due to defective proplatelet generation and platelets did not display the characteristic discoid shape.[189] Likewise, common downstream effector molecules of RhoA and Cdc42, such as the formin protein mDia1, are critically involved in the regulation of tubulin stabilization.[190] Only recently, it has been demonstrated that mDia1 knockdown mediates increased proplatelet production and reduced stress fiber formation.[191] Conversely, expression of constitutively active mDia1 inhibited proplatelet formation and overexpression of mDia1 induced loss of microtubule stability.[191] Similar to the phenotype observed in RhoA/Cdc42-deficient proplatelet-forming MKs (Figure 35B), proplatelet tips of *Rac1$^{-/-}$/Cdc42$^{-/-}$* MKs were virtually devoid of tubulin, but interestingly, Rac1/Cdc42-deficient platelets displayed increased microtubule coil numbers.[127] Collectively, increasing experimental evidence suggests that besides the well-documented role of Rho GTPases in actin remodeling and stress fiber formation, converging pathways downstream of RhoA, Cdc42 and Rac1 which involve key effector molecules, such as mDia1, have a major contribution to the stabilization of microtubules in MKs and platelets. Clearly, the cross-talk between Rho GTPases, effector molecules and critical modulators of their activity needs to be better characterized in the course of future studies.

RhoA/Cdc42 deficiency was associated with markedly altered morphology of BM MKs (Figure 41). Single deficiency of RhoA or Cdc42 had no or only minor alterations in the ultrastructure, suggesting that RhoA and Cdc42 have redundant functions in the regulation of MK morphology, granule distribution and development of DMS or compensatory mechanisms circumvent the mutation. Indeed, little is known about the specific roles of RhoA and Cdc42 during late steps of megakaryopoiesis. It has been suggested that Cdc42 may positively regulate proplatelet formation during late MK maturation.[99] Importantly, the DMS was dilated in Cdc42-deficient MKs, resulting in bigger proplatelet territories (Figure 41 and Pleines *et al.*,

2013[127]). A more direct piece of evidence for this assumption came from a study in GPIbβ-deficient mice.[192] Of note, Cdc42 has been demonstrated to be a key regulator of filopodia formation downstream of the VWF-GPIb axis in platelets.[113] *GPIbb*^{-/-} MKs displayed larger proplatelet territories which resembles the phenotype of Cdc42-deficient MKs.[127,192] In addition, GPIbβ deficiency was associated with reduced proplatelet formation *in vitro*, elevated BM MKs counts *in vivo* and numbers of microtubule coils in the marginal band of circulating platelets were increased.[192] By contrast, several studies suggested that RhoA inhibits proplatelet formation, presumably by two independent signaling cascades: the above mentioned RhoA/mDia1 pathway[191] and the RhoA/ROCK/myosin IIA pathway which has been demonstrated to inhibit *in vitro* proplatelet formation.[121-123,125] These findings have been controversially discussed because of the discrepancy to the fact that RhoA-deficient mice displayed moderately decreased platelet counts.[112,126] Since increased platelet clearance in *RhoA*^{-/-} mice did not significantly contribute to the phenotype,[112,126] an alternative explanation could be that premature platelet release and/or mislocalization of MKs may contribute to the observed thrombocytopenia, but this hypothesis needs to be tested. The data presented in this thesis support the notion that RhoA and Cdc42 cooperatively regulate late steps of megakaryopoiesis.

The severe thrombocytopenia and the constant pressure to produce and rapidly release platelets may provide an alternative explanation for the profound ultrastructural alterations in RhoA/Cdc42-deficient BM MKs. Interestingly, the ultrastructure of *RhoA*^{-/-}*/Cdc42*^{-/-} BM MKs (Figure 41) strongly resembles typical features of the morphology of MKs of patients suffering from chronic thrombocytopenia. The ultrastructure of BM MKs of such patients is characterized by cytoplasmic vacuolization and dilation of the DMS, leading to the production of large platelets devoid of granules.[193,194] The severe thrombocytopenia in RhoA/Cdc42-deficient mice likely resulted from both increased recycling of circulating platelets (Figure 39A) and decreased *in vivo* platelet production. Paradoxically, *in vitro* proplatelet formation was unaltered in RhoA/Cdc42-deficient MKs derived from fetal liver cells (Figure 39C). *In vitro* proplatelet production systems have been instrumental for studies on MK differentiation, proplatelet extension and proplatelet formation,[3] but one significant limitation of this assay is that it does not reproduce the natural environment of the MKs with all its activating and inhibitory clues. Unexpectedly, platelet production following a strong challenge introduced by depletion of circulating platelets followed similar kinetics in WT and *RhoA*^{-/-}*/Cdc42*^{-/-} mice (Figure 39B), indicating that platelet production is not inhibited in general manner in the knockout mice.

The assumption that increased platelet recycling significantly contributed to the severe thrombocytopenia observed in *RhoA*^{-/-}*/Cdc42*^{-/-} mice was supported by the fact that macrophage depletion improved peripheral platelet counts (Figure 46). Remarkably, removal

of the spleen - a site of platelet clearance – did not lead to further platelet count drop (Figure 43B). These findings indicated that extramedullary thrombopoiesis probably does not take place in *RhoA*^{-/-}*/Cdc42*^{-/-} mice. However, splenectomy improved the life span (Figure 44B) and the ultrastructure of BM MKs (Figure 45) and circulating platelets (Figure 43D). These unexpected effects on morphology may be due to the fact that decreased platelet removal lowers the pressure for BM MKs to produce platelets. However, this hypothesis requires further investigation. For instance, the effects of chronic thrombocytopenia on the development of WT BM MKs need to be assessed in the future in order to be able to discriminate between a phenotype derived from the actual mutation and more general effects of thrombocytopenia.

Taken together, these data emphasize important overlapping functions of RhoA and Cdc42 in platelet biogenesis and reveal redundant and non-redundant roles of both proteins in granule secretion and hemostasis. Additional studies will be required to better characterize distinct and overlapping pathways, the cross-talk between them and the involvement of downstream effector molecules.

4.4. Concluding remarks and future plans

The findings summarized in this thesis shed new light on the mechanisms involved in the regulation of the (hem)ITAM signaling cascade in platelets. SLAP/SLAP2 negatively regulate GPVI and CLEC-2 expression and signaling, possibly by interacting with common proximal key signaling molecules. These putative interactions have important implications in the modulation of platelet reactivity and prevent excessive cell activation in the pathological settings of experimental occlusive arterial thrombosis and ischemic stroke. Although caution is required with regard to the direct translation of findings obtained in knockout mouse models to the human system, the data presented in this thesis suggest that down-regulation or inactivation of SLAP proteins may significantly contribute to the progression of ischemic cardiovascular and cerebrovascular syndromes in patients. Conversely, approaches to enhance SLAP/SLAP2 activity or to avoid their inactivation might be beneficial in the prevention of thrombotic and thrombo-inflammatory disease conditions. However, further studies are required to better characterize the mechanisms regulating SLAP/SLAP2 activity and to evaluate the suitability of both adapter proteins as pharmacological targets. Notably, such modulation of SLAP/SLAP2 expression and activity may have important implications also during targeted down-regulation of (hem)ITAM receptors. In particular, tightly controlled regulation of downstream signaling by SLAP proteins appears to be essential to prevent thrombocytopenia after targeting GPVI for immunodepletion.

Platelet adhesion receptors, including GPIb and GPVI, have only recently been identified as key players in the development of ischemic stroke. The findings obtained in $Slap^{-/-}/Slap2^{-/-}$ mice are the first to provide more direct evidence for the role of GPVI expression and the downstream signaling cascade in stroke progression. However, further experimental data are required to elucidate the principal pathomechanisms that govern secondary infarct growth in conditions of hyperreactive GPVI signaling. Furthermore, SLAP/SLAP2 might be critically involved in the modulation of (hem)ITAM receptor signaling in more classical inflammatory settings, including for instance, inflammation-induced hemorrhage. Importantly, one obvious limitation of experimental data obtained in SLAP/SLAP2-deficient mice used in the present thesis is the fact that these animals are constitutive knockout mice. This impairs conclusions about the exact contribution of different cell types in the progression of complex thrombo-inflammatory diseases. Generation of conditional knockout mice would help to determine how expression of SLAP/SLAP2 in different cells affects the severity of (thrombo-)inflammatory disorders.

Rho GTPases have been established as critical regulators of cytoskeletal rearrangements. More recently, these proteins have been increasingly recognized as important modulators of the final steps of megakaryopoiesis. Data summarized in this thesis demonstrate that the Rho GTPases RhoA and Cdc42 have several overlapping, but also unexpected non-redundant functions in the control of platelet production and function. The most widely accepted current model of thrombopoiesis suggests that mature MKs reside in the vicinity of vascular sinusoids in which they extend and release proplatelets.[91] However, what remains elusive are the mechanisms that are responsible for the final localization of the MKs close to the blood vessels in the BM and how interactions between differentiated MKs and sinusoidal endothelial cells are regulated. Work in our laboratory has only recently led to the hypothesis that RhoA may act as a negative regulator of MK migration, polarization and directed proplatelet formation *in vivo*. These functions of RhoA appear to be critically counterbalanced by the GPIb-Cdc42 axis. These findings assign a critical role for RhoA and Cdc42 as master regulators of efficient thrombopoiesis *in vivo* and the underlying molecular pathways of the interdependence between both GTPases are the current subject of intensive research.

Furthermore, studies on the role of RhoB in platelet production and function are planned. RhoB is a Rho GTPase which is highly homologous to and shares many common effector molecules with RhoA.[106] RhoB is involved in vesicle trafficking and studies in cell types other than MKs and platelets suggested functional redundancies between RhoA and RhoB in cell polarization and motality.[106,195] Initial experiments in our laboratory demonstrated that the expression of RhoB is upregulated in RhoA-deficient platelets, but the functional consequences of this upregulation are still unknown and form the aim of future studies.

5. References

1. Grozovsky R, Hoffmeister KM, Falet H. Novel clearance mechanisms of platelets. *Curr Opin Hematol*. 2010;17(6):585-589.

2. Lozano R, Naghavi M, Foreman K, et al. Global and regional mortality from 235 causes of death for 20 age groups in 1990 and 2010: a systematic analysis for the Global Burden of Disease Study 2010. *Lancet*. 2012;380(9859):2095-2128.

3. Machlus KR, Thon JN, Italiano JE, Jr. Interpreting the developmental dance of the megakaryocyte: a review of the cellular and molecular processes mediating platelet formation. *Br J Haematol*. 2014;165(2):227-236.

4. Thon JN, Peters CG, Machlus KR, et al. T granules in human platelets function in TLR9 organization and signaling. *J Cell Biol*. 2012;198(4):561-574.

5. Thon JN, Italiano JE. Platelets: production, morphology and ultrastructure. *Handb Exp Pharmacol*. 2012;10.1007/978-3-642-29423-5_1(210):3-22.

6. Varga-Szabo D, Pleines I, Nieswandt B. Cell adhesion mechanisms in platelets. *Arterioscler Thromb Vasc Biol*. 2008;28(3):403-412.

7. Savage B, Almus-Jacobs F, Ruggeri ZM. Specific synergy of multiple substrate-receptor interactions in platelet thrombus formation under flow. *Cell*. 1998;94(5):657-666.

8. Ruggeri ZM, Orje JN, Habermann R, Federici AB, Reininger AJ. Activation-independent platelet adhesion and aggregation under elevated shear stress. *Blood*. 2006;108(6):1903-1910.

9. Maxwell MJ, Westein E, Nesbitt WS, Giuliano S, Dopheide SM, Jackson SP. Identification of a 2-stage platelet aggregation process mediating shear-dependent thrombus formation. *Blood*. 2007;109(2):566-576.

10. Nesbitt WS, Westein E, Tovar-Lopez FJ, et al. A shear gradient-dependent platelet aggregation mechanism drives thrombus formation. *Nat Med*. 2009;15(6):665-673.

11. Nieswandt B, Watson SP. Platelet-collagen interaction: is GPVI the central receptor? *Blood*. 2003;102(2):449-461.

12. Nieswandt B, Pleines I, Bender M. Platelet adhesion and activation mechanisms in arterial thrombosis and ischaemic stroke. *J Thromb Haemost*. 2011;9 Suppl 1:92-104.

13. Dutting S, Bender M, Nieswandt B. Platelet GPVI: a target for antithrombotic therapy?! *Trends Pharmacol Sci*. 2012;33(11):583-590.

14. Heemskerk JW, Mattheij NJ, Cosemans JM. Platelet-based coagulation: different populations, different functions. *J Thromb Haemost*. 2013;11(1):2-16.

15. Muller F, Mutch NJ, Schenk WA, et al. Platelet polyphosphates are proinflammatory and procoagulant mediators in vivo. *Cell*. 2009;139(6):1143-1156.

16. Shattil SJ, Newman PJ. Integrins: dynamic scaffolds for adhesion and signaling in platelets. *Blood*. 2004;104(6):1606-1615.

17. Bergmeier W, Hynes RO. Extracellular matrix proteins in hemostasis and thrombosis. *Cold Spring Harb Perspect Biol*. 2012;4(2).

18. Offermanns S. Activation of platelet function through G protein-coupled receptors. *Circ Res*. 2006;99(12):1293-1304.

19. Stegner D, Nieswandt B. Platelet receptor signaling in thrombus formation. *J Mol Med (Berl)*. 2011;89(2):109-121.

20. Underhill DM, Goodridge HS. The many faces of ITAMs. *Trends Immunol*. 2007;28(2):66-73.

21. Clemetson JM, Polgar J, Magnenat E, Wells TN, Clemetson KJ. The platelet collagen receptor glycoprotein VI is a member of the immunoglobulin superfamily closely related to FcalphaR and the natural killer receptors. *J Biol Chem*. 1999;274(41):29019-29024.

22. Nieswandt B, Bergmeier W, Schulte V, Rackebrandt K, Gessner JE, Zirngibl H. Expression and function of the mouse collagen receptor glycoprotein VI is strictly dependent on its association with the FcRgamma chain. *J Biol Chem*. 2000;275(31):23998-24002.

23. Berlanga O, Bori-Sanz T, James JR, et al. Glycoprotein VI oligomerization in cell lines and platelets. *J Thromb Haemost*. 2007;5(5):1026-1033.

24. Miura Y, Takahashi T, Jung SM, Moroi M. Analysis of the interaction of platelet collagen receptor glycoprotein VI (GPVI) with collagen. A dimeric form of GPVI, but not the monomeric form, shows affinity to fibrous collagen. *J Biol Chem*. 2002;277(48):46197-46204.

25. Suzuki-Inoue K, Tulasne D, Shen Y, et al. Association of Fyn and Lyn with the proline-rich domain of glycoprotein VI regulates intracellular signaling. *J Biol Chem*. 2002;277(24):21561-21566.

26. Ezumi Y, Shindoh K, Tsuji M, Takayama H. Physical and functional association of the Src family kinases Fyn and Lyn with the collagen receptor glycoprotein VI-Fc receptor gamma chain complex on human platelets. *J Exp Med*. 1998;188(2):267-276.

27. Schmaier AA, Zou Z, Kazlauskas A, et al. Molecular priming of Lyn by GPVI enables an immune receptor to adopt a hemostatic role. *Proc Natl Acad Sci U S A*. 2009;106(50):21167-21172.

28. Severin S, Nash CA, Mori J, et al. Distinct and overlapping functional roles of Src family kinases in mouse platelets. *J Thromb Haemost*. 2012;10(8):1631-1645.

29. Watson SP, Herbert JM, Pollitt AY. GPVI and CLEC-2 in hemostasis and vascular integrity. *J Thromb Haemost*. 2010;8(7):1456-1467.

30. Vogtle T, Cherpokova D, Bender M, Nieswandt B. Targeting platelet receptors in thrombotic and thrombo-inflammatory disorders. *Hamostaseologie*. 2015;35(2).

31. Arthur JF, Dunkley S, Andrews RK. Platelet glycoprotein VI-related clinical defects. *Br J Haematol*. 2007;139(3):363-372.

32. Kleinschnitz C, Pozgajova M, Pham M, Bendszus M, Nieswandt B, Stoll G. Targeting platelets in acute experimental stroke: impact of glycoprotein Ib, VI, and IIb/IIIa blockade on infarct size, functional outcome, and intracranial bleeding. *Circulation*. 2007;115(17):2323-2330.

33. Boulaftali Y, Hess PR, Getz TM, et al. Platelet ITAM signaling is critical for vascular integrity in inflammation. *J Clin Invest*. 2013;123(2):908-916.

34. Boilard E, Nigrovic PA, Larabee K, et al. Platelets amplify inflammation in arthritis via collagen-dependent microparticle production. *Science*. 2010;327(5965):580-583.

35. Devi S, Kuligowski MP, Kwan RY, et al. Platelet recruitment to the inflamed glomerulus occurs via an alphaIIbbeta3/GPVI-dependent pathway. *Am J Pathol*. 2010;177(3):1131-1142.

36. Schonberger T, Siegel-Axel D, Bussl R, et al. The immunoadhesin glycoprotein VI-Fc regulates arterial remodelling after mechanical injury in ApoE-/- mice. *Cardiovasc Res*. 2008;80(1):131-137.

37. Bultmann A, Li Z, Wagner S, et al. Impact of glycoprotein VI and platelet adhesion on atherosclerosis--a possible role of fibronectin. *J Mol Cell Cardiol*. 2010;49(3):532-542.

38. Stegner D, Haining EJ, Nieswandt B. Targeting glycoprotein VI and the immunoreceptor tyrosine-based activation motif signaling pathway. *Arterioscler Thromb Vasc Biol*. 2014;34(8):1615-1620.

39. Nieswandt B, Schulte V, Bergmeier W, et al. Long-term antithrombotic protection by in vivo depletion of platelet glycoprotein VI in mice. *J Exp Med*. 2001;193(4):459-469.

40. Schulte V, Rabie T, Prostredna M, Aktas B, Gruner S, Nieswandt B. Targeting of the collagen-binding site on glycoprotein VI is not essential for in vivo depletion of the receptor. *Blood*. 2003;101(10):3948-3952.

41. Rabie T, Varga-Szabo D, Bender M, et al. Diverging signaling events control the pathway of GPVI down-regulation in vivo. *Blood*. 2007;110(2):529-535.

42. Bender M, Hofmann S, Stegner D, et al. Differentially regulated GPVI ectodomain shedding by multiple platelet-expressed proteinases. *Blood*. 2010;116(17):3347-3355.

43. Takayama H, Hosaka Y, Nakayama K, et al. A novel antiplatelet antibody therapy that induces cAMP-dependent endocytosis of the GPVI/Fc receptor gamma-chain complex. *J Clin Invest*. 2008;118(5):1785-1795.

44. Bender M, May F, Lorenz V, et al. Combined in vivo depletion of glycoprotein VI and C-type lectin-like receptor 2 severely compromises hemostasis and abrogates arterial thrombosis in mice. *Arterioscler Thromb Vasc Biol*. 2013;33(5):926-934.

45. Gruner S, Prostredna M, Aktas B, et al. Anti-glycoprotein VI treatment severely compromises hemostasis in mice with reduced alpha2beta1 levels or concomitant aspirin therapy. *Circulation*. 2004;110(18):2946-2951.

46. Gitz E, Pollitt AY, Gitz-Francois JJ, et al. CLEC-2 expression is maintained on activated platelets and on platelet microparticles. *Blood*. 2014;124(14):2262-2270.

47. Suzuki-Inoue K, Fuller GL, Garcia A, et al. A novel Syk-dependent mechanism of platelet activation by the C-type lectin receptor CLEC-2. *Blood*. 2006;107(2):542-549.

48. Suzuki-Inoue K, Kato Y, Inoue O, et al. Involvement of the snake toxin receptor CLEC-2, in podoplanin-mediated platelet activation, by cancer cells. *J Biol Chem*. 2007;282(36):25993-26001.

49. May F, Hagedorn I, Pleines I, et al. CLEC-2 is an essential platelet-activating receptor in hemostasis and thrombosis. *Blood*. 2009;114(16):3464-3472.

50. Hughes CE, Pollitt AY, Mori J, et al. CLEC-2 activates Syk through dimerization. *Blood*. 2010;115(14):2947-2955.

51. Severin S, Pollitt AY, Navarro-Nunez L, et al. Syk-dependent phosphorylation of CLEC-2: a novel mechanism of hem-immunoreceptor tyrosine-based activation motif signaling. *J Biol Chem*. 2011;286(6):4107-4116.

52. Suzuki-Inoue K, Inoue O, Ding G, et al. Essential in vivo roles of the C-type lectin receptor CLEC-2: embryonic/neonatal lethality of CLEC-2-deficient mice by blood/lymphatic misconnections and impaired thrombus formation of CLEC-2-deficient platelets. *J Biol Chem*. 2010;285(32):24494-24507.

53. Suzuki-Inoue K, Inoue O, Ozaki Y. Novel platelet activation receptor CLEC-2: from discovery to prospects. *J Thromb Haemost*. 2011;9 Suppl 1:44-55.

54. Boulaftali Y, Hess PR, Kahn ML, Bergmeier W. Platelet immunoreceptor tyrosine-based activation motif (ITAM) signaling and vascular integrity. *Circ Res*. 2014;114(7):1174-1184.

55. Herzog BH, Fu J, Wilson SJ, et al. Podoplanin maintains high endothelial venule integrity by interacting with platelet CLEC-2. *Nature*. 2013;502(7469):105-109.

56. Hess PR, Rawnsley DR, Jakus Z, et al. Platelets mediate lymphovenous hemostasis to maintain blood-lymphatic separation throughout life. *J Clin Invest*. 2014;124(1):273-284.

57. Bertozzi CC, Schmaier AA, Mericko P, et al. Platelets regulate lymphatic vascular development through CLEC-2-SLP-76 signaling. *Blood*. 2010;116(4):661-670.

58. Finney BA, Schweighoffer E, Navarro-Nunez L, et al. CLEC-2 and Syk in the megakaryocytic/platelet lineage are essential for development. *Blood*. 2012;119(7):1747-1756.

59. Lorenz V, Stegner D, Stritt S, et al. Targeted downregulation of platelet CLEC-2 occurs through Syk-independent internalization. *Blood*. 2015;10.1182/blood-2014-11-611905.

60. Jones CI, Barrett NE, Moraes LA, Gibbins JM, Jackson DE. Endogenous inhibitory mechanisms and the regulation of platelet function. *Methods Mol Biol*. 2012;788:341-366.

61. Gibbins JM. The negative regulation of platelet function: extending the role of the ITIM. *Trends Cardiovasc Med*. 2002;12(5):213-219.

62. Alshahrani MM, Yang E, Yip J, et al. CEACAM2 negatively regulates hemi (ITAM-bearing) GPVI and CLEC-2 pathways and thrombus growth in vitro and in vivo. *Blood*. 2014;124(15):2431-2441.

63. Senis YA, Mazharian A, Mori J. Src family kinases: at the forefront of platelet activation. *Blood*. 2014;124(13):2013-2024.

64. Sidorenko SP, Clark EA. The dual-function CD150 receptor subfamily: the viral attraction. *Nat Immunol*. 2003;4(1):19-24.

65. Patil S, Newman DK, Newman PJ. Platelet endothelial cell adhesion molecule-1 serves as an inhibitory receptor that modulates platelet responses to collagen. *Blood*. 2001;97(6):1727-1732.

66. Dhanjal TS, Ross EA, Auger JM, et al. Minimal regulation of platelet activity by PECAM-1. *Platelets*. 2007;18(1):56-67.

67. Wong C, Liu Y, Yip J, et al. CEACAM1 negatively regulates platelet-collagen interactions and thrombus growth in vitro and in vivo. *Blood*. 2009;113(8):1818-1828.

68. Washington AV, Gibot S, Acevedo I, et al. TREM-like transcript-1 protects against inflammation-associated hemorrhage by facilitating platelet aggregation in mice and humans. *J Clin Invest*. 2009;119(6):1489-1501.

69. Mazharian A, Wang YJ, Mori J, et al. Mice lacking the ITIM-containing receptor G6b-B exhibit macrothrombocytopenia and aberrant platelet function. *Sci Signal*. 2012;5(248):ra78.

70. Angrist M, Wells DE, Chakravarti A, Pandey A. Chromosomal localization of the mouse Src-like adapter protein (Slap) gene and its putative human homolog SLA. *Genomics*. 1995;30(3):623-625.

71. Meijerink PH, Yanakiev P, Zorn I, et al. The gene for the human Src-like adaptor protein (hSLAP) is located within the 64-kb intron of the thyroglobulin gene. *Eur J Biochem*. 1998;254(2):297-303.

72. Loreto MP, McGlade CJ. Cloning and characterization of human Src-like adaptor protein 2 and a novel splice isoform, SLAP-2-v. *Oncogene*. 2003;22(2):266-273.

73. Pandey A, Ibarrola N, Kratchmarova I, et al. A novel Src homology 2 domain-containing molecule, Src-like adapter protein-2 (SLAP-2), which negatively regulates T cell receptor signaling. *J Biol Chem*. 2002;277(21):19131-19138.

74. Loreto MP, Berry DM, McGlade CJ. Functional cooperation between c-Cbl and Src-like adaptor protein 2 in the negative regulation of T-cell receptor signaling. *Mol Cell Biol*. 2002;22(12):4241-4255.

75. Dragone LL, Shaw LA, Myers MD, Weiss A. SLAP, a regulator of immunoreceptor ubiquitination, signaling, and trafficking. *Immunol Rev*. 2009;232(1):218-228.

76. Pandey A, Duan H, Dixit VM. Characterization of a novel Src-like adapter protein that associates with the Eck receptor tyrosine kinase. *J Biol Chem*. 1995;270(33):19201-19204.

77. Kim HJ, Zou W, Ito Y, et al. Src-like adaptor protein regulates osteoclast generation and survival. *J Cell Biochem*. 2010;110(1):201-209.

78. Sosinowski T, Pandey A, Dixit VM, Weiss A. Src-like adaptor protein (SLAP) is a negative regulator of T cell receptor signaling. *J Exp Med*. 2000;191(3):463-474.

79. Tang J, Sawasdikosol S, Chang JH, Burakoff SJ. SLAP, a dimeric adapter protein, plays a functional role in T cell receptor signaling. *Proc Natl Acad Sci U S A*. 1999;96(17):9775-9780.

80. Myers MD, Dragone LL, Weiss A. Src-like adaptor protein down-regulates T cell receptor (TCR)-CD3 expression by targeting TCRzeta for degradation. *J Cell Biol*. 2005;170(2):285-294.

81. Myers MD, Sosinowski T, Dragone LL, et al. Src-like adaptor protein regulates TCR expression on thymocytes by linking the ubiquitin ligase c-Cbl to the TCR complex. *Nat Immunol*. 2006;7(1):57-66.

82. Dragone LL, Myers MD, White C, et al. Src-like adaptor protein (SLAP) regulates B cell receptor levels in a c-Cbl-dependent manner. *Proc Natl Acad Sci U S A*. 2006;103(48):18202-18207.

83. Holland SJ, Liao XC, Mendenhall MK, et al. Functional cloning of Src-like adapter protein-2 (SLAP-2), a novel inhibitor of antigen receptor signaling. *J Exp Med*. 2001;194(9):1263-1276.

84. Pakuts B, Debonneville C, Liontos LM, Loreto MP, McGlade CJ. The Src-like adaptor protein 2 regulates colony-stimulating factor-1 receptor signaling and down-regulation. *J Biol Chem*. 2007;282(25):17953-17963.

85. Manes GA, Masendycz P, Nguyen T, et al. A potential role for the Src-like adapter protein SLAP-2 in signaling by the colony stimulating factor-1 receptor. *FEBS J*. 2006;273(8):1791-1804.

86. Sosinowski T, Killeen N, Weiss A. The Src-like adaptor protein downregulates the T cell receptor on CD4+CD8+ thymocytes and regulates positive selection. *Immunity*. 2001;15(3):457-466.

87. Dragone LL, Myers MD, White C, Sosinowski T, Weiss A. SRC-like adaptor protein regulates B cell development and function. *J Immunol*. 2006;176(1):335-345.

88. Kazi JU, Ronnstrand L. Src-Like adaptor protein (SLAP) binds to the receptor tyrosine kinase Flt3 and modulates receptor stability and downstream signaling. *PLoS One*. 2012;7(12):e53509.

89. Naudin C, Sirvent A, Leroy C, et al. SLAP displays tumour suppressor functions in colorectal cancer via destabilization of the SRC substrate EPHA2. *Nat Commun*. 2014;5:3159.

90. Sugihara S, Katsutani S, Deckmyn H, Fujimura K, Kimura A. Roles of Src-like adaptor protein 2 (SLAP-2) in GPVI-mediated platelet activation SLAP-2 and GPVI signaling. *Thromb Res*. 2010;126(4):e276-285.

91. Machlus KR, Italiano JE, Jr. The incredible journey: From megakaryocyte development to platelet formation. *J Cell Biol*. 2013;201(6):785-796.

92. Junt T, Schulze H, Chen Z, et al. Dynamic visualization of thrombopoiesis within bone marrow. *Science*. 2007;317(5845):1767-1770.

93. Zhang L, Orban M, Lorenz M, et al. A novel role of sphingosine 1-phosphate receptor S1pr1 in mouse thrombopoiesis. *J Exp Med*. 2012;209(12):2165-2181.

94. Pang L, Weiss MJ, Poncz M. Megakaryocyte biology and related disorders. *J Clin Invest*. 2005;115(12):3332-3338.

95. Kaushansky K, Lok S, Holly RD, et al. Promotion of megakaryocyte progenitor expansion and differentiation by the c-Mpl ligand thrombopoietin. *Nature*. 1994;369(6481):568-571.

96. Grozovsky R, Begonja AJ, Liu K, et al. The Ashwell-Morell receptor regulates hepatic thrombopoietin production via JAK2-STAT3 signaling. *Nat Med*. 2015;21(1):47-54.

97. Ng AP, Kauppi M, Metcalf D, et al. Mpl expression on megakaryocytes and platelets is dispensable for thrombopoiesis but essential to prevent myeloproliferation. *Proc Natl Acad Sci U S A*. 2014;111(16):5884-5889.

98. Nishimura S, Nagasaki M, Kunishima S, et al. IL-1alpha induces thrombopoiesis through megakaryocyte rupture in response to acute platelet needs. *J Cell Biol*. 2015;209(3):453-466.

99. Bluteau D, Lordier L, Di Stefano A, et al. Regulation of megakaryocyte maturation and platelet formation. *J Thromb Haemost*. 2009;7 Suppl 1:227-234.

100. Schulze H, Korpal M, Hurov J, et al. Characterization of the megakaryocyte demarcation membrane system and its role in thrombopoiesis. *Blood*. 2006;107(10):3868-3875.

101. Eckly A, Heijnen H, Pertuy F, et al. Biogenesis of the demarcation membrane system (DMS) in megakaryocytes. *Blood*. 2014;123(6):921-930.

102. Patel SR, Richardson JL, Schulze H, et al. Differential roles of microtubule assembly and sliding in proplatelet formation by megakaryocytes. *Blood*. 2005;106(13):4076-4085.

103. Bender M, Thon JN, Ehrlicher AJ, et al. Microtubule sliding drives proplatelet elongation and is dependent on cytoplasmic dynein. *Blood*. 2015;125(5):860-868.

104. Richardson JL, Shivdasani RA, Boers C, Hartwig JH, Italiano JE, Jr. Mechanisms of organelle transport and capture along proplatelets during platelet production. *Blood*. 2005;106(13):4066-4075.

105. Italiano JE, Jr., Lecine P, Shivdasani RA, Hartwig JH. Blood platelets are assembled principally at the ends of proplatelet processes produced by differentiated megakaryocytes. *J Cell Biol*. 1999;147(6):1299-1312.

106. Heasman SJ, Ridley AJ. Mammalian Rho GTPases: new insights into their functions from in vivo studies. *Nat Rev Mol Cell Biol*. 2008;9(9):690-701.

107. Jaffe AB, Hall A. Rho GTPases: biochemistry and biology. *Annu Rev Cell Dev Biol*. 2005;21:247-269.

108. Aslan JE, McCarty OJ. Rho GTPases in platelet function. *J Thromb Haemost*. 2013;11(1):35-46.

109. Pedersen E, Brakebusch C. Rho GTPase function in development: how in vivo models change our view. *Exp Cell Res*. 2012;318(14):1779-1787.

110. Hart MJ, Jiang X, Kozasa T, et al. Direct stimulation of the guanine nucleotide exchange activity of p115 RhoGEF by Galpha13. *Science*. 1998;280(5372):2112-2114.

111. Klages B, Brandt U, Simon MI, Schultz G, Offermanns S. Activation of G12/G13 results in shape change and Rho/Rho-kinase-mediated myosin light chain phosphorylation in mouse platelets. *J Cell Biol*. 1999;144(4):745-754.

112. Pleines I, Hagedorn I, Gupta S, et al. Megakaryocyte-specific RhoA deficiency causes macrothrombocytopenia and defective platelet activation in hemostasis and thrombosis. *Blood*. 2012;119(4):1054-1063.

113. Pleines I, Eckly A, Elvers M, et al. Multiple alterations of platelet functions dominated by increased secretion in mice lacking Cdc42 in platelets. *Blood*. 2010;115(16):3364-3373.

114. Akbar H, Shang X, Perveen R, et al. Gene targeting implicates Cdc42 GTPase in GPVI and non-GPVI mediated platelet filopodia formation, secretion and aggregation. *PLoS One*. 2011;6(7):e22117.

115.   Goggs R, Savage JS, Mellor H, Poole AW. The small GTPase Rif is dispensable for platelet filopodia generation in mice. *PLoS One*. 2013;8(1):e54663.

116.   Dutting S, Heidenreich J, Cherpokova D, et al. Critical off-target effects of the widely used Rac1 inhibitors NSC23766 and EHT1864 in mouse platelets. *J Thromb Haemost*. 2015;13(5):827-838.

117.   McCarty OJ, Larson MK, Auger JM, et al. Rac1 is essential for platelet lamellipodia formation and aggregate stability under flow. *J Biol Chem*. 2005;280(47):39474-39484.

118.   Pleines I, Elvers M, Strehl A, et al. Rac1 is essential for phospholipase C-gamma2 activation in platelets. *Pflugers Arch*. 2009;457(5):1173-1185.

119.   Goggs R, Harper MT, Pope RJ, et al. RhoG protein regulates platelet granule secretion and thrombus formation in mice. *J Biol Chem*. 2013;288(47):34217-34229.

120.   Kim S, Dangelmaier C, Bhavanasi D, et al. RhoG protein regulates glycoprotein VI-Fc receptor gamma-chain complex-mediated platelet activation and thrombus formation. *J Biol Chem*. 2013;288(47):34230-34238.

121.   Chang Y, Aurade F, Larbret F, et al. Proplatelet formation is regulated by the Rho/ROCK pathway. *Blood*. 2007;109(10):4229-4236.

122.   Chen Z, Naveiras O, Balduini A, et al. The May-Hegglin anomaly gene MYH9 is a negative regulator of platelet biogenesis modulated by the Rho-ROCK pathway. *Blood*. 2007;110(1):171-179.

123.   Eckly A, Strassel C, Freund M, et al. Abnormal megakaryocyte morphology and proplatelet formation in mice with megakaryocyte-restricted MYH9 inactivation. *Blood*. 2009;113(14):3182-3189.

124.   Kunishima S, Saito H. Advances in the understanding of MYH9 disorders. *Curr Opin Hematol*. 2010;17(5):405-410.

125.   Shi DS, Smith MC, Campbell RA, et al. Proteasome function is required for platelet production. *J Clin Invest*. 2014;124(9):3757-3766.

126.   Suzuki A, Shin JW, Wang Y, et al. RhoA is essential for maintaining normal megakaryocyte ploidy and platelet generation. *PLoS One*. 2013;8(7):e69315.

127.   Pleines I, Dutting S, Cherpokova D, et al. Defective tubulin organization and proplatelet formation in murine megakaryocytes lacking Rac1 and Cdc42. *Blood*. 2013;122(18):3178-3187.

128.   Villeval JL, Cohen-Solal K, Tulliez M, et al. High thrombopoietin production by hematopoietic cells induces a fatal myeloproliferative syndrome in mice. *Blood*. 1997;90(11):4369-4383.

129.   Bergmeier W, Rackebrandt K, Schroder W, Zirngibl H, Nieswandt B. Structural and functional characterization of the mouse von Willebrand factor receptor GPIb-IX with novel monoclonal antibodies. *Blood*. 2000;95(3):886-893.

130.   Nieswandt B, Bergmeier W, Rackebrandt K, Gessner JE, Zirngibl H. Identification of critical antigen-specific mechanisms in the development of immune thrombocytopenic purpura in mice. *Blood*. 2000;96(7):2520-2527.

131.   Bergmeier W, Schulte V, Brockhoff G, Bier U, Zirngibl H, Nieswandt B. Flow cytometric detection of activated mouse integrin alphaIIbbeta3 with a novel monoclonal antibody. *Cytometry*. 2002;48(2):80-86.

132.   Nieswandt B, Echtenacher B, Wachs FP, et al. Acute systemic reaction and lung alterations induced by an antiplatelet integrin gpIIb/IIIa antibody in mice. *Blood*. 1999;94(2):684-693.

133. Liontos LM, Dissanayake D, Ohashi PS, Weiss A, Dragone LL, McGlade CJ. The Src-like adaptor protein regulates GM-CSFR signaling and monocytic dendritic cell maturation. *J Immunol*. 2011;186(4):1923-1933.

134. Zhang W, Sommers CL, Burshtyn DN, et al. Essential role of LAT in T cell development. *Immunity*. 1999;10(3):323-332.

135. Jackson B, Peyrollier K, Pedersen E, et al. RhoA is dispensable for skin development, but crucial for contraction and directed migration of keratinocytes. *Mol Biol Cell*. 2011;22(5):593-605.

136. Wu X, Quondamatteo F, Lefever T, et al. Cdc42 controls progenitor cell differentiation and beta-catenin turnover in skin. *Genes Dev*. 2006;20(5):571-585.

137. Tiedt R, Schomber T, Hao-Shen H, Skoda RC. Pf4-Cre transgenic mice allow the generation of lineage-restricted gene knockouts for studying megakaryocyte and platelet function in vivo. *Blood*. 2007;109(4):1503-1506.

138. Morowski M, Vogtle T, Kraft P, Kleinschnitz C, Stoll G, Nieswandt B. Only severe thrombocytopenia results in bleeding and defective thrombus formation in mice. *Blood*. 2013;121(24):4938-4947.

139. Gilio K, van Kruchten R, Braun A, et al. Roles of platelet STIM1 and Orai1 in glycoprotein VI- and thrombin-dependent procoagulant activity and thrombus formation. *J Biol Chem*. 2010;285(31):23629-23638.

140. Dirnagl U. Bench to bedside: the quest for quality in experimental stroke research. *J Cereb Blood Flow Metab*. 2006;26(12):1465-1478.

141. Braeuninger S, Kleinschnitz C, Nieswandt B, Stoll G. Focal cerebral ischemia. *Methods Mol Biol*. 2012;788:29-42.

142. Bederson JB, Pitts LH, Tsuji M, Nishimura MC, Davis RL, Bartkowski H. Rat middle cerebral artery occlusion: evaluation of the model and development of a neurologic examination. *Stroke*. 1986;17(3):472-476.

143. Moran PM, Higgins LS, Cordell B, Moser PC. Age-related learning deficits in transgenic mice expressing the 751-amino acid isoform of human beta-amyloid precursor protein. *Proc Natl Acad Sci U S A*. 1995;92(12):5341-5345.

144. Swanson RA, Morton MT, Tsao-Wu G, Savalos RA, Davidson C, Sharp FR. A semiautomated method for measuring brain infarct volume. *J Cereb Blood Flow Metab*. 1990;10(2):290-293.

145. Gajewski A, Krohne G. Subcellular distribution of the Xenopus p58/lamin B receptor in oocytes and eggs. *J Cell Sci*. 1999;112 (Pt 15):2583-2596.

146. Cherpokova D, Bender M, Morowski M, et al. SLAP/SLAP2 prevent excessive platelet (hem)ITAM signaling in thrombosis and ischemic stroke in mice. *Blood*. 2015;125(1):185-194.

147. Judd BA, Myung PS, Obergfell A, et al. Differential requirement for LAT and SLP-76 in GPVI versus T cell receptor signaling. *J Exp Med*. 2002;195(6):705-717.

148. Zwaal RF, Schroit AJ. Pathophysiologic implications of membrane phospholipid asymmetry in blood cells. *Blood*. 1997;89(4):1121-1132.

149. Munnix IC, Strehl A, Kuijpers MJ, et al. The glycoprotein VI-phospholipase Cgamma2 signaling pathway controls thrombus formation induced by collagen and tissue factor in vitro and in vivo. *Arterioscler Thromb Vasc Biol*. 2005;25(12):2673-2678.

150. Kuijpers MJ, Munnix IC, Cosemans JM, et al. Key role of platelet procoagulant activity in tissue factor-and collagen-dependent thrombus formation in arterioles and venules in vivo differential sensitivity to thrombin inhibition. *Microcirculation*. 2008;15(4):269-282.

151. Bender M, Hagedorn I, Nieswandt B. Genetic and antibody-induced glycoprotein VI deficiency equally protects mice from mechanically and FeCl(3) -induced thrombosis. *J Thromb Haemost*. 2011;9(7):1423-1426.

152. Yilmaz G, Arumugam TV, Stokes KY, Granger DN. Role of T lymphocytes and interferon-gamma in ischemic stroke. *Circulation*. 2006;113(17):2105-2112.

153. Kleinschnitz C, Schwab N, Kraft P, et al. Early detrimental T-cell effects in experimental cerebral ischemia are neither related to adaptive immunity nor thrombus formation. *Blood*. 2010;115(18):3835-3842.

154. Shichita T, Sugiyama Y, Ooboshi H, et al. Pivotal role of cerebral interleukin-17-producing gammadeltaT cells in the delayed phase of ischemic brain injury. *Nat Med*. 2009;15(8):946-950.

155. Massberg S, Gawaz M, Gruner S, et al. A crucial role of glycoprotein VI for platelet recruitment to the injured arterial wall in vivo. *J Exp Med*. 2003;197(1):41-49.

156. Schulte V, Reusch HP, Pozgajova M, Varga-Szabo D, Gachet C, Nieswandt B. Two-phase antithrombotic protection after anti-glycoprotein VI treatment in mice. *Arterioscler Thromb Vasc Biol*. 2006;26(7):1640-1647.

157. Nieswandt B, Bergmeier W, Eckly A, et al. Evidence for cross-talk between glycoprotein VI and Gi-coupled receptors during collagen-induced platelet aggregation. *Blood*. 2001;97(12):3829-3835.

158. Snell DC, Schulte V, Jarvis GE, et al. Differential effects of reduced glycoprotein VI levels on activation of murine platelets by glycoprotein VI ligands. *Biochem J*. 2002;368(Pt 1):293-300.

159. Kuter DJ, Rosenberg RD. The reciprocal relationship of thrombopoietin (c-Mpl ligand) to changes in the platelet mass during busulfan-induced thrombocytopenia in the rabbit. *Blood*. 1995;85(10):2720-2730.

160. Kaushansky K. Determinants of platelet number and regulation of thrombopoiesis. *Hematology Am Soc Hematol Educ Program*. 2009;10.1182/asheducation-2009.1.147:147-152.

161. Auger JM, Best D, Snell DC, Wilde JI, Watson SP. c-Cbl negatively regulates platelet activation by glycoprotein VI. *J Thromb Haemost*. 2003;1(11):2419-2426.

162. Duan L, Reddi AL, Ghosh A, Dimri M, Band H. The Cbl family and other ubiquitin ligases: destructive forces in control of antigen receptor signaling. *Immunity*. 2004;21(1):7-17.

163. Dangelmaier CA, Quinter PG, Jin J, Tsygankov AY, Kunapuli SP, Daniel JL. Rapid ubiquitination of Syk following GPVI activation in platelets. *Blood*. 2005;105(10):3918-3924.

164. Watson SP, Auger JM, McCarty OJ, Pearce AC. GPVI and integrin alphaIIb beta3 signaling in platelets. *J Thromb Haemost*. 2005;3(8):1752-1762.

165. Bezman NA, Lian L, Abrams CS, et al. Requirements of SLP76 tyrosines in ITAM and integrin receptor signaling and in platelet function in vivo. *J Exp Med*. 2008;205(8):1775-1788.

166. Hughes CE, Auger JM, McGlade J, Eble JA, Pearce AC, Watson SP. Differential roles for the adapters Gads and LAT in platelet activation by GPVI and CLEC-2. *J Thromb Haemost*. 2008;6(12):2152-2159.

167. Dutting S, Vogtle T, Morowski M, et al. Growth factor receptor-bound protein 2 contributes to (hem)immunoreceptor tyrosine-based activation motif-mediated signaling in platelets. *Circ Res*. 2014;114(3):444-453.

168. Jackson SP. Arterial thrombosis--insidious, unpredictable and deadly. *Nat Med*. 2011;17(11):1423-1436.

169.   Stoll G, Kleinschnitz C, Nieswandt B. Molecular mechanisms of thrombus formation in ischemic stroke: novel insights and targets for treatment. *Blood*. 2008;112(9):3555-3562.

170.   Adams HP, Jr., Effron MB, Torner J, et al. Emergency administration of abciximab for treatment of patients with acute ischemic stroke: results of an international phase III trial: Abciximab in Emergency Treatment of Stroke Trial (AbESTT-II). *Stroke*. 2008;39(1):87-99.

171.   Kellert L, Hametner C, Rohde S, et al. Endovascular stroke therapy: tirofiban is associated with risk of fatal intracerebral hemorrhage and poor outcome. *Stroke*. 2013;44(5):1453-1455.

172.   Kleinschnitz C, De Meyer SF, Schwarz T, et al. Deficiency of von Willebrand factor protects mice from ischemic stroke. *Blood*. 2009;113(15):3600-3603.

173.   Zhao BQ, Chauhan AK, Canault M, et al. von Willebrand factor-cleaving protease ADAMTS13 reduces ischemic brain injury in experimental stroke. *Blood*. 2009;114(15):3329-3334.

174.   Fujioka M, Hayakawa K, Mishima K, et al. ADAMTS13 gene deletion aggravates ischemic brain damage: a possible neuroprotective role of ADAMTS13 by ameliorating postischemic hypoperfusion. *Blood*. 2010;115(8):1650-1653.

175.   Bigalke B, Stellos K, Geisler T, et al. Expression of platelet glycoprotein VI is associated with transient ischemic attack and stroke. *Eur J Neurol*. 2010;17(1):111-117.

176.   Al-Tamimi M, Gardiner EE, Thom JY, et al. Soluble glycoprotein VI is raised in the plasma of patients with acute ischemic stroke. *Stroke*. 2011;42(2):498-500.

177.   Thornton P, McColl BW, Greenhalgh A, Denes A, Allan SM, Rothwell NJ. Platelet interleukin-1alpha drives cerebrovascular inflammation. *Blood*. 2010;115(17):3632-3639.

178.   Schulte V, Snell D, Bergmeier W, Zirngibl H, Watson SP, Nieswandt B. Evidence for two distinct epitopes within collagen for activation of murine platelets. *J Biol Chem*. 2001;276(1):364-368.

179.   Quek LS, Pasquet JM, Hers I, et al. Fyn and Lyn phosphorylate the Fc receptor gamma chain downstream of glycoprotein VI in murine platelets, and Lyn regulates a novel feedback pathway. *Blood*. 2000;96(13):4246-4253.

180.   Mingueneau M, Sansoni A, Gregoire C, et al. The proline-rich sequence of CD3epsilon controls T cell antigen receptor expression on and signaling potency in preselection CD4+CD8+ thymocytes. *Nat Immunol*. 2008;9(5):522-532.

181.   Chen F, Ma L, Parrini MC, et al. Cdc42 is required for PIP(2)-induced actin polymerization and early development but not for cell viability. *Curr Biol*. 2000;10(13):758-765.

182.   Sugihara K, Nakatsuji N, Nakamura K, et al. Rac1 is required for the formation of three germ layers during gastrulation. *Oncogene*. 1998;17(26):3427-3433.

183.   Ory S, Gasman S. Rho GTPases and exocytosis: what are the molecular links? *Semin Cell Dev Biol*. 2011;22(1):27-32.

184.   Sakurai-Yageta M, Recchi C, Le Dez G, et al. The interaction of IQGAP1 with the exocyst complex is required for tumor cell invasion downstream of Cdc42 and RhoA. *J Cell Biol*. 2008;181(6):985-998.

185.   Rittmeyer EN, Daniel S, Hsu SC, Osman MA. A dual role for IQGAP1 in regulating exocytosis. *J Cell Sci*. 2008;121(Pt 3):391-403.

186.   Malarkannan S, Awasthi A, Rajasekaran K, et al. IQGAP1: a regulator of intracellular spacetime relativity. *J Immunol*. 2012;188(5):2057-2063.

187.   Watanabe T, Wang S, Kaibuchi K. IQGAPs as key regulators of actin-cytoskeleton dynamics. *Cell Struct Funct*. 2015;10.1247/csf.15003.

188. Thon JN, Macleod H, Begonja AJ, et al. Microtubule and cortical forces determine platelet size during vascular platelet production. *Nat Commun*. 2012;3:852.

189. Schwer HD, Lecine P, Tiwari S, Italiano JE, Jr., Hartwig JH, Shivdasani RA. A lineage-restricted and divergent beta-tubulin isoform is essential for the biogenesis, structure and function of blood platelets. *Curr Biol*. 2001;11(8):579-586.

190. Palazzo AF, Cook TA, Alberts AS, Gundersen GG. mDia mediates Rho-regulated formation and orientation of stable microtubules. *Nat Cell Biol*. 2001;3(8):723-729.

191. Pan J, Lordier L, Meyran D, et al. The formin DIAPH1 (mDia1) regulates megakaryocyte proplatelet formation by remodeling the actin and microtubule cytoskeletons. *Blood*. 2014;124(26):3967-3977.

192. Strassel C, Eckly A, Leon C, et al. Intrinsic impaired proplatelet formation and microtubule coil assembly of megakaryocytes in a mouse model of Bernard-Soulier syndrome. *Haematologica*. 2009;94(6):800-810.

193. Dameshek W, Miller EB. The megakaryocytes in idiopathic thrombocytopenic purpura, a form of hypersplenism. *Blood*. 1946;1:27-50.

194. Houwerzijl EJ, Blom NR, van der Want JJ, et al. Ultrastructural study shows morphologic features of apoptosis and para-apoptosis in megakaryocytes from patients with idiopathic thrombocytopenic purpura. *Blood*. 2004;103(2):500-506.

195. Konigs V, Jennings R, Vogl T, et al. Mouse macrophages completely lacking Rho subfamily GTPases (RhoA, RhoB, and RhoC) have severe lamellipodial retraction defects, but robust chemotactic navigation and altered motility. *J Biol Chem*. 2014;289(44):30772-30784.

6. Appendix

6.1. Abbreviations

ADAM	a disintegrin and metalloproteinase
ADP	adenosine diphosphate
ATP	adenosine triphosphate
AU	arbitrary units
BCR	B cell receptor
BFU	burst-forming unit
BM	bone marrow
BSA	bovine serum albumin
BW	body weight
CD	cluster of differentiation
Cdc42	cell division control protein 42 homolog
CEACAM1	carcino-embryonic antigen-related cell adhesion molecule-1
CFU	colony-forming unit
CLEC-2	C-type lectin-like receptor 2
CRP	collagen-related peptide
CSF-1R	colony-stimulating factor-1 receptor
ctrl	control
d	day
DAG	diacyl glycerol
DAPI	4',6-diamidino-2-phenylindole
DIC	differential interference contrast
DKO	double knockout
DMS	demarcation membrane system
DNA	deoxyribonucleic acid
ECL	enhanced chemiluminescence
ECM	extracellular matrix
EDTA	ethylenediaminetetraacetate
EGTA	ethylene glycol tetraacetate
ELISA	enzyme-linked immunosorbent assay
FcR	Fc receptors
FCS	fetal calf (bovine) serum
FITC	fluorescein isothiocyanate
FLC	fetal liver cells
g	gravity
GAP	GTPase-activating proteins
GDI	guanine nucleotide-dissociation inhibitor
GDP	guanosine diphosphate
GEF	guanine nucleotide-exchange factor
GP	glycoprotein
GPCR	G protein-coupled receptor
GTP	guanosine-5'-triphosphate
GTPase	guanosine 5'-triphosphatase
h	hour
HCT	hematocrit
HGB	hemoglobin
HRP	horseradish peroxidase
HSC	hematopoietic stem cells
i.p.	intraperitoneal(ly)
i.v.	intravenous(ly)

Ig	immunoglobulin
IL	interleukin
IMDM	Iscove's Modified Dulbecco's Medium
IP	immunoprecipitation
IP$_3$	inositol-3,4,5-trisphosphate
ITAM	immunoreceptor tyrosine-based activation motif
ITIM	immunoreceptor tyrosine-based inhibitory motif
ITSM	immunoreceptor tyrosine-based switch motif
kDa	kilodalton
KO	knockout
LAT	linker for activation of T cells
MCA	middle cerebral artery
MFI	mean fluorescence intensity
min	minute
MK	megakaryocyte(s)
MLC	myosin light chain
MOPS	3-(N-morpholino)propanesulfonic
MPV	mean platelet volume
n.d.	not detectable
n.s.	not significant
NA	numerical aperture
o/n	overnight
OCS	open canalicular system
PBS	phosphate-buffered saline
PCR	polymerase chain reaction
PE	phycoerythrin
PECAM-1	platelet endothelial cell adhesion molecule-1
PF4	platelet factor 4
PFA	paraformaldehyde
PGI$_2$	prostaglandin I$_2$, prostacyclin
PIP$_2$	phosphatidylinositol-4,5-bisphosphate
PKC	protein kinase C
PLC	phospholipase C
PRP	platelet-rich plasma
PRR	proline-rich region
PS	phosphatidylserine
PVDF	polyvinylidene difluoride
Rac1	Ras-related C3 botulinum toxin substrate 1
RBC	red blood cells
RhoA	Ras homolog gene family, member A
ROCK	Rho-associated protein kinase
RT	room temperature
RTK	receptor tyrosine kinase
s	seconds
SDS	sodium dodecyl sulfate
SDS-PAGE	sodium dodecyl sulfate polyacrylamide gel electrophoresis
SFKs	Src family kinases
sGPVI	soluble GPVI
SH	Src homology
SHIP	SH2 domain-containing inositol 5-phosphatase
SHP	SH2 domain-containing protein tyrosine phosphatase
SLAP	Src-like adapter protein
SLP-76	SH2-containing leukocyte protein 76
Syk	spleen tyrosine kinase
TBS	Tris-buffered saline
TCR	T cell receptor

TEM	transmission electron microscopy
TF	tissue factor
Thpo	thrombopoietin
TLT-1	TREM-like transcript-1
TMB	3,3,5,5-tetramethylbenzidine
tMCAO	transient middle cerebral artery occlusion
TTC	2,3,5-triphenyltetrazolium chloride
VWF	von Willebrand factor
WB	Western blot
WBC	white blood cells
WT	wild-type

6.2. Acknowledgements

Judith van Eeuwijk, Simon Stritt and Carsten Deppermann for their constant support and encouragement throughout the years, for fruitful discussions, useful suggestions and the constructive criticism.

Juliana Goldmann, Stefanie Hartmann and Jonas Müller for excellent technical support, preparation of antibodies and sample preparation for TEM analyses, respectively.

Dr. Sabine Herterich for determination of activated partial thromboplastin time and prothrombin time.

Dr. Elizabeth Haining, Dr. Sebastian Dütting, Judith van Eeuwijk, Sarah Schießl, Viola Lorenz, Ayesha Baig, Inga Birkholz and Dominic Faber for carefully proofreading my thesis.

All current and former members of the Department of Experimental Biomedicine – Vascular Medicine for their contribution to this thesis by technical or other support, for the inspiring research environment and the incredible working atmosphere.

All animal caretakers in the animal facilities in the RVZ and ZEMM for their help. Special thanks to Dr. Katharina Remer and Dr. Heike Wagner for excellent supervision of the animal facilities.

Elke Hauck and Kerstin Siegmann for the outstanding organization and coordination within the Department and the SFB688.

The team of the Graduate School of Life Sciences for the organization of the transferable skills program and the coordination of the PhD study program.

The Bioimaging Centre (Rudolf Virchow Center) for providing technical infrastructure and support.

Last but not least, my deepest gratitude to my family for their support, help, encouragement and affectionate love.

6.3. Publications

6.3.1. Original articles

Cherpokova D, Bender M, Morowski M, Kraft P, Schuhmann MK, Akbar SM, Sultan CS, Hughes CE, Kleinschnitz C, Stoll G, Dragone LL, Watson SP, Tomlinson MG, Nieswandt B. SLAP/SLAP2 prevent excessive platelet (hem)ITAM signaling in thrombosis and ischemic stroke in mice. *Blood*. 2015;125(1):185-94.

Dütting S, Heidenreich J, **Cherpokova D**, Amin E, Zhang SC, Ahmadian MR, Brakebusch C, Nieswandt B. Critical off-target effects of the widely used Rac1 inhibitors NSC23766 and EHT1864 in mouse platelets. *J Thromb Haemost*. 2015; 13(5):827-38.

Devanathan V, Hagedorn I, Köhler D, Pexa K, **Cherpokova D**, Kraft P, Singh M, Rosenberger P, Stoll G, Birnbaumer L, Piekorz RP, Beer-Hammer S, Nieswandt B, Nürnberg B. Platelet Gi protein Gαi2 is an essential mediator of thrombo-inflammatory organ damage in mice. *Proc Natl Acad Sci U S A*. 2015;doi: 10.1073/pnas.1505887112.

Deppermann C, **Cherpokova D**, Nurden P, Schulz JN, Thielmann I, Kraft P, Vögtle T, Kleinschnitz C, Dütting S, Krohne G, Eming SA, Nurden AT, Eckes B, Stoll G, Stegner D, Nieswandt B. Gray platelet syndrome and defective thrombo-inflammation in Nbeal2-deficient mice. *J Clin Invest*. 2013;123(8):3331-42.

Pleines I, Dütting S, **Cherpokova D**, Eckly A, Meyer I, Morowski M, Krohne G, Schulze H, Gachet C, Debili N, Brakebusch C, Nieswandt B. Defective tubulin organization and proplatelet formation in murine megakaryocytes lacking Rac1 and Cdc42. *Blood*. 2013;122(18):3178-87.

6.3.2. Reviews

Vögtle T, **Cherpokova D**, Bender M, Nieswandt B. Targeting platelet receptors in thrombotic and thrombo-inflammatory disorders. *Hamostaseologie*. 2015;35(2).

6.3.3. Oral presentations

SLAP/SLAP2 are critical negative regulators of platelet (hem)ITAM signaling in arterial thrombosis and ischemic stroke. 8th International Symposium Platelets 2014, Ma'ale Hachamisha (Israel)

Src-like adapter proteins (SLAPs) are critical negative regulators of GPVI/ITAM signaling in arterial thrombosis and ischemic stroke. XXIVth congress of the International Society on Thrombosis and Hemostasis, 2013, Amsterdam (The Netherlands) (Winner of the Young Investigator Award; prize money 500 €)

6.3.4. Posters

Src-like adapter proteins (SLAPs) are critical negative regulators of GPVI/ITAM-signalling in arterial thrombosis and ischaemic stroke. 8th International Symposium of the Graduate School of Life Science, 2013, Würzburg (Germany)

Src-like adapter proteins are negative regulators of GPVI/ITAM-signaling in platelets. 7th International Symposium of the Graduate School of Life Science, 2012, Würzburg (Germany)

Src-like adapter proteins are negative regulators of GPVI/ITAM-signaling in platelets. Joint Symposium of the Collaborative Research Center (SFB) 688 and the Comprehensive Heart Failure Center Würzburg, 2012, Würzburg (Germany)

Src-like adapter proteins are negative regulators of GPVI/ITAM-signaling in platelets. 17th International Vascular Biology Meeting 2012, Wiesbaden (Germany)

6.4. Curriculum vitae

Name   Deya Cherpokova

Date of birth   18.11.1987

Place of birth Plovdiv, Bulgaria

Nationality   Bulgarian

Education

2011 – present PhD student in the group of Prof. Dr. Bernhard Nieswandt, Department of Experimental Biomedicine, University Hospital and Rudolf Virchow Center for Experimental Biomedicine, Julius-Maximilians-Universität Würzburg

2011   Graduation – Master of Science in Biomedicine, Julius-Maximilians-Universität Würzburg

2009 – 2011   Master studies in Biomedicine, Julius-Maximilians-Universität Würzburg

2009   Graduation – Bachelor of Science in Biomedicine, Julius-Maximilians-Universität Würzburg

2006 – 2009   Bachelor studies in Biomedicine, Julius-Maximilians-Universität Würzburg

2006   Bulgarian high school diploma

1994 – 2006   Primary, secondary and high school in Plovdiv, Bulgaria

Würzburg, June 2015   _____

Deya Cherpokova

6.5. Affidavit

I hereby declare that my thesis entitled, "Studies on modulators of platelet (hem)ITAM signaling and platelet production in genetically modified mice", is the result of my own work. I did not receive any help or support from commercial consultants. All sources and/or materials applied are listed and specified in the thesis.

Furthermore, I confirm that this thesis has not yet been submitted as part of another examination process neither in identical nor in similar form.

Würzburg, June 2015 _____

Deya Cherpokova

6.6. Eidesstattliche Erklärung

Hiermit erkläre ich an Eides statt, die Dissertation „Untersuchungen an Modulatoren des thrombozytären (hem)ITAM-Signalwegs und der Thrombozytenbildung in genetisch veränderten Mäusen" eigenständig, d.h. insbesondere selbstständig und ohne Hilfe eines kommerziellen Promotionsberaters, angefertigt und keine anderen als die von mir angegebenen Quellen und Hilfsmittel verwendet zu haben.

Ich erkläre außerdem, dass die Dissertation weder in gleicher noch in ähnlicher Form bereits in einem anderen Prüfungsverfahren vorgelegen hat.

Würzburg, Juni 2015_____

Deya Cherpokova